SPATIAL VARIABILITY OF DESERT LOESS ON THE CARRIZOZO LAVA FLOW, SOUTH-CENTRAL NEW MEXICO

Shari L. Bauman

Department of Earth and Environmental Science
New Mexico Institute of Mining and Technology
Socorro, New Mexico

Submitted in partial fulfillment of the requirements for the degree of
Master of Science in Geochemistry

March 1999

TABLE OF CONTENTS

LIST OF FIGURES

LIST OF TABLES

LIST OF APPENDICES

ACKNOWLEDGEMENTS

There are many people that I owe special thanks to for helping me obtain this ultimate goal of a Master of Science degree in Geochemistry.

I would first like to acknowledge my committee. Special thanks to my advisor, Dr. Philip Kyle, who has given me support, guidance, and encouragement throughout this project and my career as a graduate student at New Mexico Institute of Mining and Technology. I would also like to acknowledge Dr. Bruce Harrison, my secondary advisor, for his valuable support and input during this project. And thanks go to Dr. Peter Mozley for his input and interest in this research.

I would like to acknowledge the X- Ray Fluorescence Spectrometry Laboratory for supporting my research through a Research Assistantship and the New Mexico Geological Society for partially funding this project. Samples were irradiated at the University of Missouri under Reactor Sharing research, supported in part by the US Department of Energy Grant DE-FG02-95NE38135. And thanks to the XRF, XRD, Electron Microprobe, and Soil Laboratories at New Mexico Institute of Mining and Technology and the New Mexico Bureau of Mines and Mineral Resources for allowing me to analyze my samples. I would also like to acknowledge Bob Myers of the National Environment and Safety Directorate at White Sands Missile Range for permitting me to access and finish my field work on the highly restricted White Sands Missile Range.

Special thanks to a few budding scientists and great friends: Erik Munroe, Christopher Young, Tanya Tansley, Shannon Lindaas, Peter Rinkleff, and Sarah and Steve Lundberg. I appreciate all that you have done throughout the years. Best of luck to everyone in the future!!!! Special thanks to Steve and Sarah Lundberg for putting up with me over the last few month. And ultimate thanks to Sarah Lundberg and Peter Rinkeff who contributed more than they probably wanted to, by helping make my field work bearable and productive.

I would especially like to thank my family- Mom, Dad, Alan, and Karen for their encouragement, support and guidance before, during and after this journey. And to Grandpa Shugar for his inspiration, enthusiasm and words of wisdom. Grandpa, I am flying with the eagles. I love you all very much!!!

1. ABSTRACT

The Carrizozo lava flow is an ideal isochronous (5ka) surface to examine the influences of climate, provenance, and surface cover types on the abundance, physical and chemical composition of loess deposits and early pedogenic process occurring within the deposits. The Carrizozo lava flow is 75 km long with complex surface topography, which provides catchments for eolian material accumulation, as well as the development of a range of surface cover types (i.e. desert pavement, grasses and cacti, and juniper trees). The Carrizozo lava flow is also geologically surrounded by various lithologies within the Tularosa Basin and dust transport is by southwestern prevailing winds.

Surface cover type influences the loess composition in two ways: (1) by influencing the moisture content and thus the accumulation of chemical constituents in the soil profile during pedogenesis and (2) by preferentially trapping material. In general, higher concentrations of CaO, MgO, S, soluble salts, chloride and calcium carbonate are found in the south and are indicative of provenance effects. Strong correlations in chemistry coupled with the prevailing wind direction suggests that the evaporite gypsum dune deposit of White Sands and the dolomitic rocks from the San Andres Mountains influence the dust composition.

The Carrizozo dust flux average of 0.54 g/cm^2/ka is very comparable to those found in the southwestern United States and in similar desert environments around the world. The non-pedogenic calcium carbonate chemical composition of the Carrizozo loess is similar to the regional shale standard (NASC), local crustal composition and to soils developing on the Potrillo volcanic field in southern New Mexico. As expected, high

deviation in chemistry is observed when compared to the Carrizozo basalt composition, indicating that the soils are indeed of eolian origin and not basalt weathering products.

Furthermore, surface cover type, provenance, and wind direction affect the abundance, physical and chemical composition of the Carrizozo lava flow loess deposits and the early developmental stages of pedogenesis. The Carrizozo lava flow has provided an opportunity to investigate the spatial variability associated with these factors, as well as the remarkable uniformity of the eolian material and accumulation over the last 5,000 years.

2. INTRODUCTION

In semi-arid and arid regions, eolian material has been recognized as an important component of geomorphic and pedologic processes (Yaalon and Ganor, 1973; McFadden et al., 1986). In desert landscapes, many geomorphic surfaces, such as rocky hillslopes (Wells et al., 1985), alluvial piedmonts (Gile and Grossman, 1979), and lava flows (Eppes, 1996; McFadden et al., 1986) trap eolian sediment (dust), altering the surface geomorphology. In the southwestern United States, dust is an important component in pedogenesis (Yaalon and Ganor, 1973; Machette, 1985; Reheis, 1990). It is a major source of secondary carbonate (Lattman, 1973; Gile, 1975; Bachman and Machette, 1977; McFadden and Tinsley, 1985) and clay (Yaalon and Ganor, 1973; Gile et al., 1981) in soils.

Reheis and Kihl (1995) provided the first regional source of information on modern rates of dust deposition and the composition of eolian dust in Southern Nevada and California over a five-year period. They related rate of deposition and composition of dust to climate, lithology of the dust source, and geomorphic setting. Climatic factors such as precipitation and temperature affect dust flux. The average dust flux increases with mean annual temperature, however the annual dust flux mostly reflects changes in annual precipitation. In addition, playa and alluvial sources produced the same amount of dust per unit area, however the total volume of dust is larger from alluvial sources. Source also influences the chemistry of the dust, as playas tend to produce dust richer in soluble salts and carbonates than alluvial sources (except carbonate-rich alluvium).

Reheis et al. (1995) related the rates of deposition and composition of the dust, to influx rates and soil properties within a southern Nevada and California field area.

Shallow-surface horizons in soils, developing on alluvial fans, are nearly identical in chemical composition to that of modern dust, however the composition of progressively deeper horizons approaches the composition of the parent material. Dust deposition rates and soil accumulation rates yielded information on the interplay of paleoclimate, dust supply and soil-forming processes. The results indicated that modern dust-deposition rates (1) account for the mid to late Holocene soil-accumulation rates, and (2) are lower than the early Holocene soil-accumulation rates which can be attributed to dust-deflation and dust-deposition events occurring near former pluvial lakes.

The paleoenvironmental significance of eolian dust is that it is preserved as terrestrial loess deposits. Loess is a terrestrial wind blown silt deposit, which can be described by its physical and mineralogical properties. Unweathered loess is typically homogeneous, well-sorted, non- or weakly stratified and highly porous. Loess consists chiefly of quartz, feldspar, mica, clay minerals and carbonate grains (Pye, 1987). Loess is typically composed of particles between 10 and 50 μm in size (Tsoar and Pye, 1987), and usually has a prominent mode between 20 and 30 μm. Several stages are involved in the formation of loess deposits (Smalley, 1966): (1) formation of loess- size particles; (2) transport of this material; (3) deposition; and (4) post-depositional modifications (pedogenesis). Dust is typically transported to surfaces predominantly as suspended loads, and pedogenesis is dependent on the rate of deposition and the amount of moisture available for leaching.

Numerous studies have been conducted on the formation of soils in the extensive loess deposits of the North American mid-continent (Ruhe, 1984). However, there are

limited studies on the formation of soils in desert loess (Wells et al., 1985; McFadden et al., 1986; Eppes, 1996).

Isochronous lava flows in desert regions provide an excellent landscape to study geomorphic processes and pedogenesis in desert loess, as the lava flow surface acts as a time-stratigraphic unit. Geomorphic and soil studies conducted on the basalt flows of the Cima volcanic field in California (Wells et al., 1985; McFadden et al., 1986), the Pinacate volcanic fields in Mexico (Slate et al., 1991) and the Potrillo volcanic field in New Mexico (Eppes, 1996), showed that basalt flow topography evolves dramatically with time. The surface of young basalt flows is extremely irregular with high relief. The topography of pahoehoe lava flows is primarily due to the collapse of lava tubes, which form abundant depressions ranging in size from meters to hundreds of meters in circumference. Surrounding these depressions are fractured, smooth or undulating surfaces. These topographic variations provide depressions or catchments for dust to accumulate in.

On the Cima, Pinacate and Potrillo volcanic fields, accretionary mantles of coarse cobbles and fine eolian deposits are trapped by the irregular flow surfaces (Wells et al., 1985; McFadden et al., 1986; Slate et al., 1991; Eppes, 1996). The accretionary mantles record episodic, climatically induced influxes of eolian fines and material derived from local sources, such as playa floors and distal piedmont regions (Wells et al., 1985). Soils developed on these lava flows, vary in age from Pliocene to late Pleistocene, and exhibit systematic changes as a function of age and surface morphology of the lava flow (Wells et al., 1985; McFadden et al., 1986; Eppes, 1996). The older the lava flow surface, the more developed the soils are.

The Carrizozo lava flow, in south-central New Mexico, provides an excellent setting for evaluating the processes of desert loess deposition. The 5 ka Carrizozo lava flow acts as a time stratigraphic unit in which the accumulated loess is of younger age. The Carrizozo lava flow has been used to examine the effects of surface cover, source areas and local climate on dust accumulation rates, composition and pedogenic processes. The objectives of this study are to: (1) determine dust flux over the last 5,000 years; (2) investigate the physical and chemical composition of the desert loess and its spatial variability with surface cover type and location; (3) evaluate provenance and source effects and (4) determine pedogenic influences.

3. PHYSICAL SETTING

3.1. Geology

3.1.1. Carrizozo Lava Flow

The Carrizozo lava flow is located in Lincoln and Otero Counties, south- central New Mexico, between north latitudes 33^0 15' and 34^0 00' and west longitudes $105^0$45' and 106^0 30' (Figure 1). The flow consists of two lava flows, the Upper Carrizozo lava flow (UCLF) and the Lower Carrizozo lava flow (LCLF) (Renault, 1970). Both flows originated from the 27-m-tall cinder cone, Little Black Peak and flowed northeast-southwest along the floor of the Tularosa Basin. The UCLF extends approximately 25 km from the vent, whereas the LCLF extends for a total distance of 75 km (47 miles) into White Sands Missile Range where access is restricted by the U.S. Army. At the contact between the UCLF and the LCLF, brecciation is evident, however no erosion or soil development is apparent (Faris, 1980).

The lava flows range in width from 0.8 km (0.5 miles) to 8 km (5 miles), in thickness from 3 to 21 m (10 to 70 ft), and covers approximately 330 km^2 (127mi^2) in area (Allen, 1951). The lava is a dense gray to black, vesicular olivine basalt with a fine grained to aphanitic texture, and contains plagioclase laths and small olivine phenocrysts (Faris, 1980). The rock is typically unaltered and although some compositional trends are observed within the two lava flows, the chemical composition of the two flows on average is indistinguishable (Faris, 1980; Renault, 1970).

The compound, tube-fed, pahoehoe flow exhibits a variety of surface features (Keszthelyi and Pieri, 1993). The surface morphology is composed of ropy textures, smooth sheets, flow banding, toes, inflation features (i.e. tumuli and pressure ridges), and

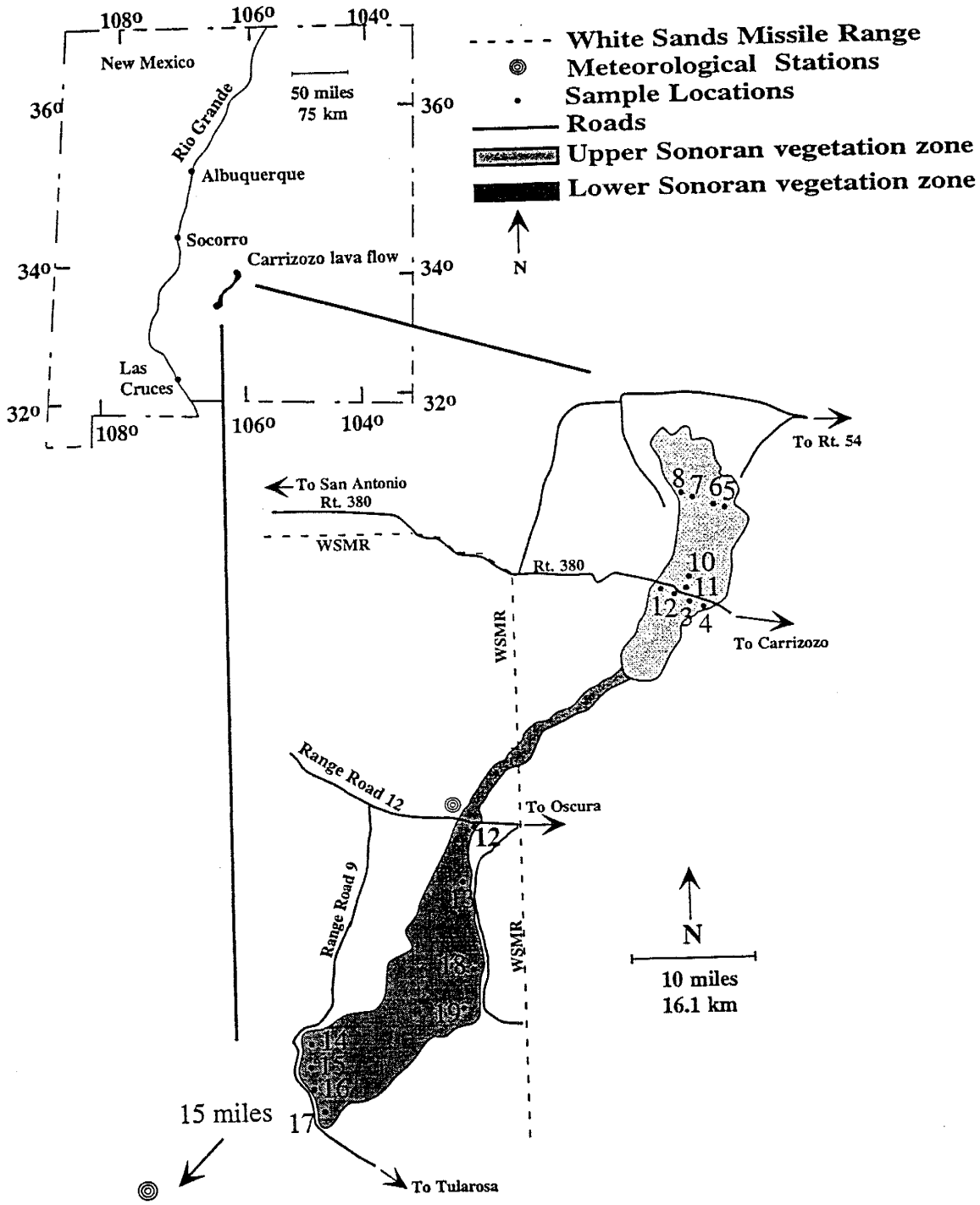

Figure 1. Sample locations, vegetation zones, wind stations and the surrounding Carrizozo lava flow boundaries, south-central- New Mexico.

lava tubes with fissure and collapse openings. The natural topographic variations in flow morphology provide depressions or catchments for dust accumulation (Figure 2).

The age of the Carrizozo lava flow has been under investigation since the 1950's. In the 1950's and 60's, the age of the Carrizozo lava flow was estimated to be 1.0 to 1.5 ka using flow morphology characteristics (Allen, 1951; Weber, 1964). However, this age is not considered to be an absolute age. In the 1970's, Weber (1979) searched for charcoal to date using the carbon-14 method, but was unsuccessful.

In the 1990's, Salyards (1991) used secular variation magnetostratigraphy, and suggested an age of 5,000 years. In the late 1990's, cosmogenic nuclide surface-exposure dating methods provided alternatives. Phillips et al. (1997) and Dunbar (in press) dated the Carrizozo lava flows using cosmogenic ^{36}Cl. ^{36}Cl dates of 4.9 +/- 0.5 to 5.4+/- 1.0 and 5.6 +/- 0.9 ka, yielded an average of 5.3 +/- 0.8 ka (Phillips et al., 1997, Dunbar in press). This average is considerably older than the original estimates of 1.0 to 1.5 ka (Allen, 1951), but is in close agreement to the estimates of Salyards (1991). Cosmogenic ^{3}He surface-exposure dating has given an average date of 4.8 ka (Anthony et al., 1998) which is similar to the magnetostratigraphy and ^{36}Cl dates.

The ^{36}Cl dating also indicates that the UCLF and the LCLF were erupted with no significant time break, at least none >1 ka (Dunbar, in press). This interpretation is consistent with the field observations of Faris (1980), with the continuous geochemical nature and the lack of soil development or erosion. From the 1950's until just recently the accepted age of the Carrizozo lava flow has been considered to be 1.0 to 1.5 ka. For this study, an average of the recent determination of 5 ka is used.

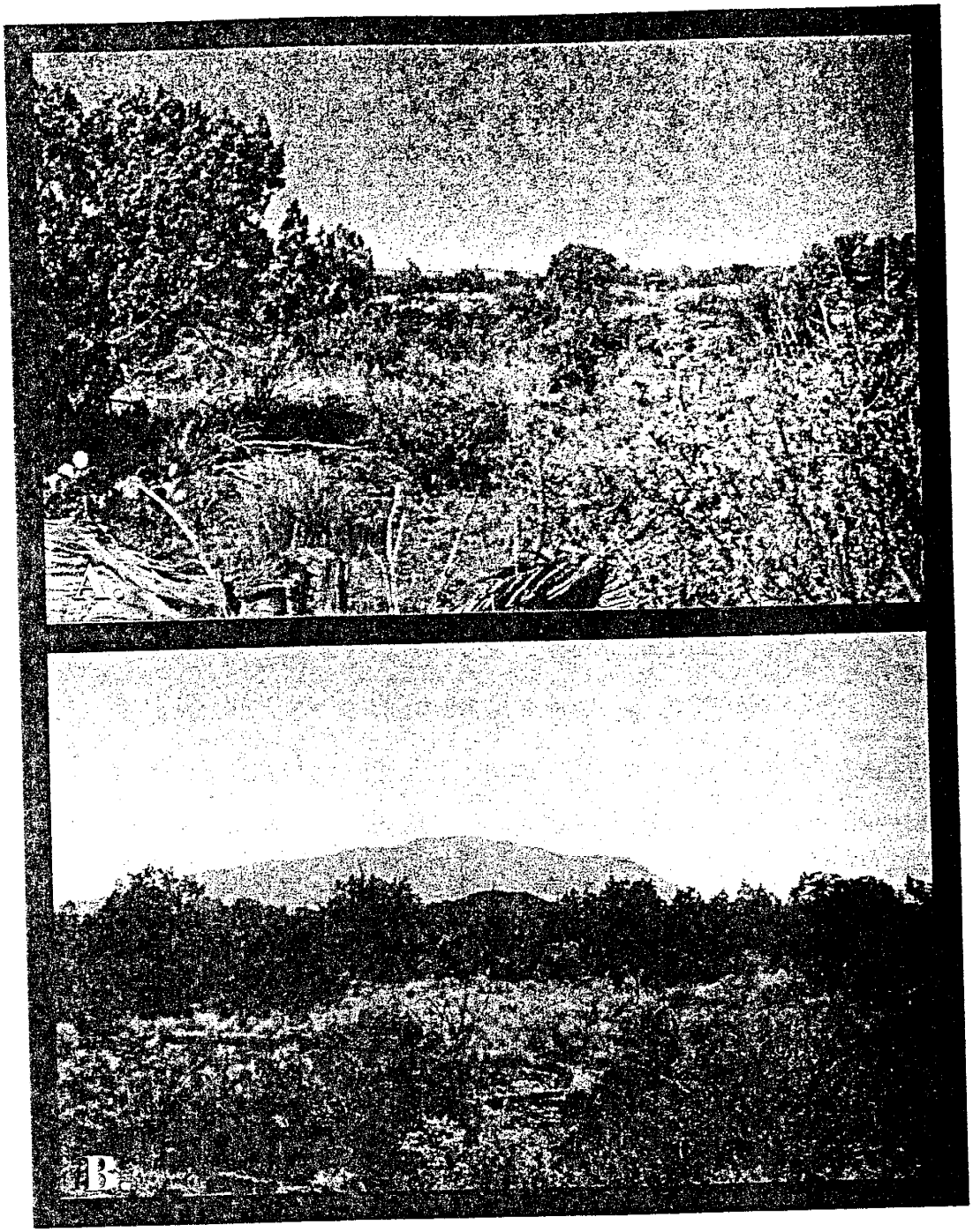

Figure 2. Photographs of the Carrizozo lava flow morphology in the northern region. High density of juniper trees are present. A.) General lava flow morphology. B.) Looking east, Little Black Peak cinder cone in the foreground and Sierra Blanca Pluton in the background.

3.1.2. Regional Geology

The Carrizozo lava flow is surrounded by many geologic formations with strong lithologic variations (Figure 3, modified from, NMMBR, 1982). In the north and east, mountainous landforms are predominantly composed of Tertiary igneous intrusives. The significant mountains and lithologies in this area include the Gallinas Mountains (granite to gneiss) (Perhac, 1964), Jicarilla Mountains (syenite to monzonite) (Budding, 1964), Carrizo Mountain (quartz syenite to alkali granite) (Weber, 1964), Patos Mountain (rhyolite), Capitan Pluton (granite), and Sierra Blanca (andesite and volcanic conglomerates) (Thompson, 1964). A blanket of Cretaceous sandstones and shales (Mesaverde Formation and Mancos Shale) cover the region between the prominent geologic features stated above.

The San Andres Mountains and Oscura Mountains are located to the southwest and west. Both consist of Pre-Cambrian granites overlain by Pennsylvanian Madera Limestone, Permian Abo (sandstones and shales) and Yeso (siltstones, limestones, sandstones and gypsum) Formations, Glorieta Sandstone, and the San Andres Limestone (limestones, dolomites, siltstones and gypsum) (Kottlowski, 1955). In the southern region, approximately 15 miles south of the Carrizozo lava flow, is the drifting Quaternary gypsum evaporite dune deposit, White Sands (Shields, 1956). These various lithologies provide an opportunity to examine provenance effects on the eolian material.

3.2. Climate

Precipitation varies along the 75 km length of the Carrizozo lava flow. The northern portion of the flow has an average altitude of 1,646 m (5,400 ft) which decreases

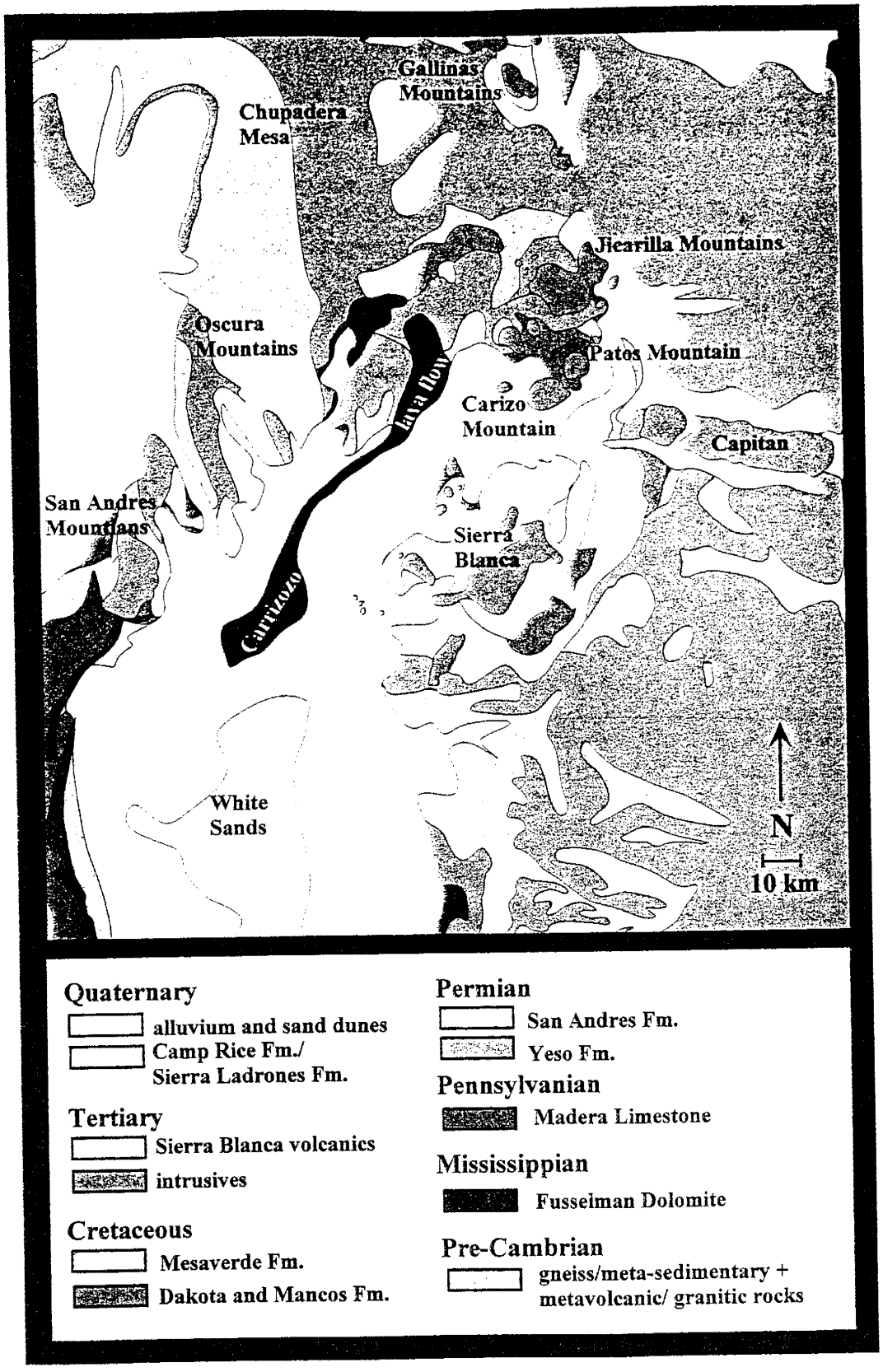

Figure 3. Geologic map of the Carrizozo lava flow and the surrounding area. Map modified from the NMBMMR highway geologic map, 1982. Standard geologic colors are presented for the lithologies.

to 1,280 m (4,200 ft) in the southern region. In the north, at an elevation of 1,657 m (5,438 ft), the average annual precipitation is 289 mm (11.37 in), and near the southern tip of the flow (elevation 1,352 m), the average annual precipitation is 226 mm (8.93 in) (U.S.D.A. Weather Bureau Climatic Summary of U.S. Section 29).

Climatological summaries were obtained from the White Sands Meterological Team-Forecast Station located at White Sands Missile Range. Average monthly vector wind direction data for five years were obtained from two locations on the White Sands Missile Range: (1) five miles south of the southern tip of the lava flow, and (2) the Oscura range station (Figure 1). Results indicate a prevailing southwestern wind direction (Eschrich, pers.comm.) (Figure 4).

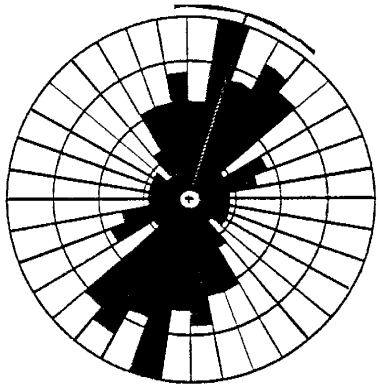

Figure 4. Rose diagram of the wind directions. Data from two locations was received from the White Sands Meteorological Team-Forecast Station located at White Sands Missile Range (Eschrich, personal communication). The diagram indicates the prevailing wind direction is southwestern.

3.3. Vegetation

The density of vegetation and species zonation varies from the north to the south and are influenced by the 365 m in elevation differences and the approximately 62 mm in average annual precipitation. Vegetation studies conducted by Shields (1956) and Shields and Crispin (1956) have provided information on species diversity.

The Carrizozo lava flow lies within two vegetation zones (Figure 1). The northern third lies approximately within the Upper Sonoran zone and the lower two-thirds within the Lower Sonoran zone. The vegetation zones correlate with the two lava flows, UCLF and LCLF.

Depressions on the lava surface provide support for many diversified floras. In the northern region (Upper Sonoran zone), the lava surface is forested by *Juniperus monosperma* (one-seeded juniper), which extends south to approximately 32 km from the northern edge of the lava flow. At this location, species characteristic of both zones extend into this overlap area where *J. monosperma*, an Upper Sonoran indicator, occurs sporadically among scattered growth of *Prosopis juliflora* var. *glandulosa* (mesquite) and *Larrea tridentata* (creosote bush), two Lower Sonoran indicators.

In the Upper Sonoran zone, plant species other than grasses are: *Juniperus monosperma* (one-seeded juniper), *Dasylirion wheeleri* (sotol), *Nolina microcarpa* (beargrass), *Yucca baccata* (banana yucca), *Berberis haematocarpa* (red hollygrape), *Opuntia leptocaulis* (rattail cactus), *Brickellia californica* (California brickell bush), and *Dalea formosa* (feather plume) (Shields, 1956; Shields and Crispin, 1956).

The vegetation types prominent in the Lower Sonoran Zone are: *Prosopis juliflora* var. *glandulosa* (mesquite) and *Larrrea tridentata* (creosote bush). Ubiquitous throughout the volcanic field are: *Atriplex canescens* (Four-wing saltbush), *Celtis reticulata* (hackberry), *Fallugia paradoxa* (Apache plume), *Opuntia engelmannii* (Engelmann prickly pear), *Opuntia imbricata* (staghorn cholla), *Rhus trilobata* (three-leaf sumac, skunkbush), and *Senecio longilobus* (woody groundsel) (Shields, 1956; Shields and Crispin, 1956).

4. METHODS

4.1. Field Technique

This study was designed to provide data on dust flux, the relationship of dust to local source lithologies and surface cover type, and to evaluate soil development. The method determined for field measurements and sample collection of loess deposits was based on previous chronosequence studies conducted by Harrison et al. (1990) and Eppes (1996). Harrison et al. (1990) observed soil variability on terrace trends in the Cajon Pass, where soils developing in swales are distinct from those developing on bars. Eppes (1996) concluded that soil properties observed in samples collected from the original topographic high of the lava flow surface were less variable indicating a more stable depositional environment, which is a better site for sampling.

Selection of sites for this study was based on accessibility, surface cover type, and size (Figure 1; Appendix 9.3.1). All samples were collected within 0.5 km of the flow perimeter, as soil development may vary as a function of distance from the perimeter of the lava flow (Slate et al., 1991).

In the northern third of the lava flow, three distinct surface cover types characterized the catchments: (1) desert pavement, (2) grasses and cacti, and (3) juniper trees, whereas only (1) desert pavement and (2) grasses and cacti catchments were found in the south. Eppes (1996) showed that catchment size and shape significantly influenced dust accumulation. Therefore, catchments were also chosen on the basis of size, ranging from 2-6 square meters, in order to constrain the variability. At each sample location, all surface cover type catchments were sampled and measured.

All samples were labeled based on the following criteria: (1) field area (CLF), (2) location number (1,2, etc.), (3) surface cover type (D= desert pavement, G= grasses and cacti, and J= juniper tree), and (4) increment with depth (0-4). The following example illustrates the system.

CLF-1-D (0-4)

where field area : CLF (Carrizozo Lava Flow)

location number :1

surface cover type : D= desert pavement

increment with depth : (0-4)= 0 cm to 4 cm

As catchment size and shape can influence runoff and consequently influx rates and rate of soil development, the catchment area and volume of loess accumulation were measured for each site using measuring tapes and a wooden dowel. Loess samples were collected incrementally with depth, in 2-3 cm increments, at each location with a garden trowel and the sample was stored in quart size storage bags. In-field bulk density samples were collected from the composite profile using a known volume container. All samples were described using the methods summarized by the Soil Survey staff (1951, 1975) (Appendix 9.3.2).

4.2. Laboratory Technique

Dust flux (Appendix 9.2.1) was calculated using field measurements of bulk density, catchment area and loess volume. Samples were analyzed at New Mexico Institute of Mining and Technology for physical and chemical properties. Physical analysis included: particle size analysis by the settling tube method (Appendix 9.2.2) and

grain morphology was examined using the electron microprobe (Appendix 9.2.3). Chemical analysis included: x-ray diffraction identification of clay mineralogy (Appendix 9.2.4), electrical conductivity determinations of soluble salt concentrations (Appendix 9.2.5), chloride concentrations (Appendix 9.2.6), calcium carbonate concentration by the Chittick method (Appendix 9.2.7), wave-length x-ray fluorescence spectrometry analyses for trace and major element concentration (Appendix 9.2.8), and trace and rare earth element composition by instrumental neutron activation analysis (Appendix 9.2.9).

Samples were initially dried at 50 ^{0}C for two days to remove moisture. The samples were sieved with a standard 2 mm sieve to remove the > 2 mm fraction. The < 2 mm samples were used for all analyses and were split using an aluminum table splitter.

5. RESULTS

5.1. Field Observations

The greater portion of the Carrizozo lava flow surface is barren and consists of exposed lava. The lava flow is in the accretionary stage of the geomorphic cycles described by Wells et al. (1985). Vegetation and loess are found in catchments of varying size, shape, and location and along cracks and fractures on the flow. In the northern region, juniper trees are abundant, growing in catchments and along cracked lava surfaces. Catchments vary in size (0.5 to 4,000 meters^2), shape (oblong to round), location (original topographic high to collapse features), and surface cover (variable vegetation and desert pavement). Typically, the loess accumulations are highly variable, being greatest in collapse features and lowest in depressions on the higher topographic surfaces of the flow.

The three surface cover types have distinct characteristics. The desert pavement catchments typically consist of a layer of closely packed, angular to subrounded gravels, with no vegetation. The grasses and cacti catchments include cacti (prickly pear, cholla, and hedgehog) and various grasses (black gramma and bristle grass); the juniper tree catchments contain a solo, one-seeded juniper tree.

In the northern region, catchments containing a juniper tree exhibit a thick accumulation of plant litter as well as greater accumulation of organic matter in the near surface horizons. The pedogenic organic material is apparent only in juniper tree catchments. In the southern region, minor amounts of pedogenesis are observed only in the desert pavement catchments. Very weakly developed soils containing a weak

vesicular A horizon was observed. Calcium carbonate or salts were noticeable on the undersides of some clasts in the southern region.

5.2. Bulk Density and Dust flux

Bulk density (Appendix 9.2.1) was measured on seven composite samples (Table 1). Results indicate variability with location on the flow. Higher bulk densities are observed in the north, averaging 1.25 g/cm^3 and decreased to the south to 0.94 g/cm^3 (Figure 5). Bulk density calculations were used in dust flux and chloride determinations.

Dust flux determined at thirty locations varies with surface cover type on the lava flow (Table 2; Appendix 9.2.1.). The highest flux is found in juniper tree catchments, averaging 0.78 g/cm^2/ka. The flux associated with desert pavement and grasses and cacti catchments remains the same throughout the extent of the flow with averages of 0.36 and 0.54 g/cm^2/ka, respectively (Figure 6). The overall average dust flux on the Carrizozo lava flow is 0.54 g/cm^2/ka.

5.3. Physical Properties

5.3.1. Grain Size

Grain size analysis was determined on twenty-four bulk samples (Appendix 9.2.2.), twelve from the north and twelve from the south (Table 3). The northern samples were digested with hydrogen peroxide (H_2O_2) to remove any organic matter. Sand abundance remained the same throughout the flow, averaging 28%. However, a slightly

Table 1. Bulk density estimates of the loess deposits on the Carrizozo lava flow. Bulk density was determined from in-field sampling using an known volume container.

Sample #	Bulk Density (g/cm^3)
CLF-5	1.25
CLF-6	1.25
CLF-7	1.25
CLF-8	1.25
CLF-10	1.25
CLF-11	1.25
CLF-12	1.16
CLF-13	1.31
CLF-14	0.92
CLF-15	1.08
CLF-16	0.94
CLF-17	0.94
CLF-18	0.94

Table 2. Dust flux estimates on the the Carrizozo lava flow, New Mexico. Calculations are based on field measurements. Averages and standard deviations are provided.

Sample	Flux ($g/cm^2/ka^1$)
CLF-8-D	0.27
CLF-8-G	0.59
CLF-8-J	0.86
CLF-7-D	0.60
CLF-7-G	0.64
CLF-7-J	0.94
CLF-6-D	0.26
CLF-6-G	0.69
CLF-6-J	0.78
CLF-5-D	n.m.
CLF-5-G	0.57
CLF-5-J	0.56
CLF-11-D	0.48
CLF-11-G	0.77
CLF-11-J	0.91
CLF-10-D	0.19
CLF-10-G	0.61
CLF-10-J	0.65
CLF-12-D	0.19
CLF-12-G	0.74
CLF-13-D	0.71
CLF-13-G	0.74
CLF-18-D	0.22
CLF-18-G	0.32
CLF-19-D	n.m.
CLF-19-G	n.m.
CLF-14-D	0.32
CLF-14-G	0.35
CLF-15-D	0.53
CLF-15-G	n.m.
CLF-16-D	0.25
CLF-16-G	0.65
CLF-17-D	0.32
CLF-17-G	0.47

	n=	Flux ($g/cm^2/ka^1$) average	std dev
A	30	0.54	0.22
AN	17	0.61	0.22
AS	13	0.45	0.20
ND	5	0.36	0.17
SD	7	0.36	0.19
NG	6	0.64	0.07
SG	6	0.54	0.19
NJ	6	0.78	0.15

A=	all samples
AN=	all northern samples
AS=	all southern samples
ND=	northern desert pavement
SD=	southern desert pavement
NG=	northern grasses and cacti
SG=	southern grasses and cacti
NJ=	northern juniper tree

D= desert pavement
G= grasses and cacti
J= juniper tree
n.m.= no measurement

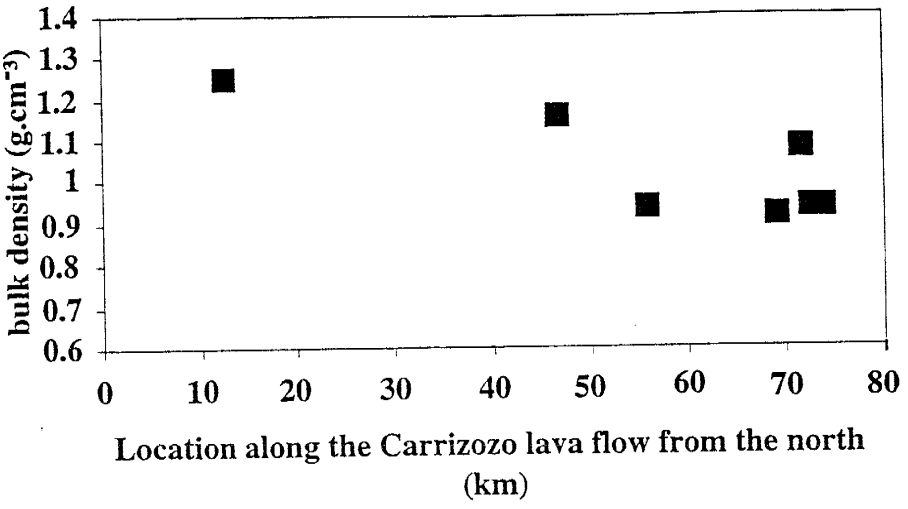

Figure 5. Average bulk density (g/cm3) with location (km) from the northern extreme of the lava flow. Zero represents the northern-most edge of the the flow and seventy-five represents the southern-most edge. Higher bulk density is observed in the soils in the northern region.

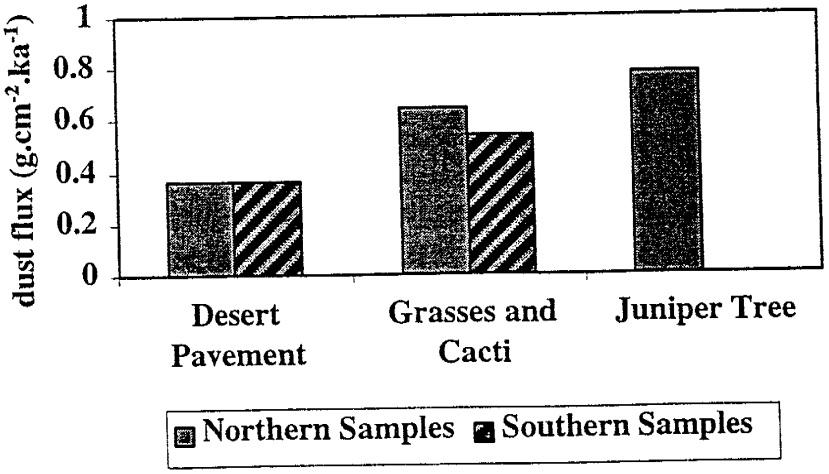

Figure 6. The average dust flux (g/cm2/ka) varies with surface cover type on the Carrizozo lava flow. Greatest flux associated with the northern juniper tree catchments and decreases with less vegetation.

greater abundance of sand is found in catchments containing juniper trees, averaging 36% compared to the grasses and cacti catchments and the desert pavement catchments, both averaging 25% (Figure 7a). The silt and clay abundance in the loess also remains constant throughout the extent of the flow, with no variability with surface cover type, averaging 62% silt and 11% clay (Figure 7b and c).

5.3.2. Grain Morphology

Grain shape, basic mineralogy and weathering features were examined on fourteen samples, six from the north and eight from the south (Table 4) using an electron microprobe (Appendix 9.2.3.). Of the fourteen samples analyzed, seven were sand fraction splits and seven were silt fraction splits. Samples examined from the north were obtained from the particle size analysis and therefore were previously washed and cleaned with di-ionized water (DI-H_2O) and hydrogen peroxide (H_2O_2). The southern splits were obtained by sieving the samples using an 80 μm sieve.

In all samples analyzed, the grain size is uniform throughout the sample mount (Figure 8a). The average grain size of the coarse fraction is 80 μm, and 50 μm for the fine split. Grain shape (Figure 8a) is subangular to subrounded and is similar in all locations and surface cover types.

The mineralogy includes quartz and potassium feldspar, with minor amounts of olivine, mica, zircon, and gypsum. High abundance of zircon is observed in the northern samples, and gypsum is detected only in southern samples (Figure 8b).

Surface features on the grains vary from coatings to weathering features. Undifferentiated iron, magnesium, and alumina coatings are found on a variety of grains

Table 3. Grain size analysis of loess on the Carrizozo lava flow, New Mexico. Samples were analyzed using the pipette method. Averages and standard deviations are provided.

Sample	Sand (%)	Silt (%)	Clay (%)
CLF-1-D	21	64	15
CLF-1-G	27	62	11
CLF-1-J	32	57	11
CLF-2-D	23	69	8
CLF-2-G	29	63	8
CLF-2-J	37	48	15
CLF-3-D	24	68	8
CLF-3-G	24	64	12
CLF-3-J	39	53	8
CLF-4-D	14	71	15
CLF-4-G	19	65	16
CLF-4-J	34	59	7
CLF-12-D	27	69	4
CLF-12-G	22	67	11
CLF-19-D	21	67	12
CLF-19-G	28	63	8
CLF-14-D	26	61	13
CLF-14-G	27	62	11
CLF-15-D	23	61	15
CLF-15-G	30	64	6
CLF-16-D	29	57	14
CLF-16-G	53	42	5
CLF-17-D	26	64	10
CLF-17-G	28	62	9

	n=	sand average	sand std dev	silt average	silt std dev	clay average	clay std dev
A	24	28	8	62	7	11	3
AN	12	27	8	62	7	11	3
AS	12	28	8	62	7	10	4
ND	4	21	4	68	3	11	4
SD	6	25	3	63	4	12	4
NG	4	25	4	63	1	12	3
SG	6	32	11	60	9	8	3
SG w/o CLF-16-G	5	27	3	64	2	9	2
NJ	4	36	3	54	5	10	4

A=	all samples
AN=	all northern samples
AS=	all southern samples
ND=	northern desert pavement
SD=	southern desert pavement
NG=	northern grasses and cacti
SG=	southern grasses and cacti
NJ=	northern juniper tree

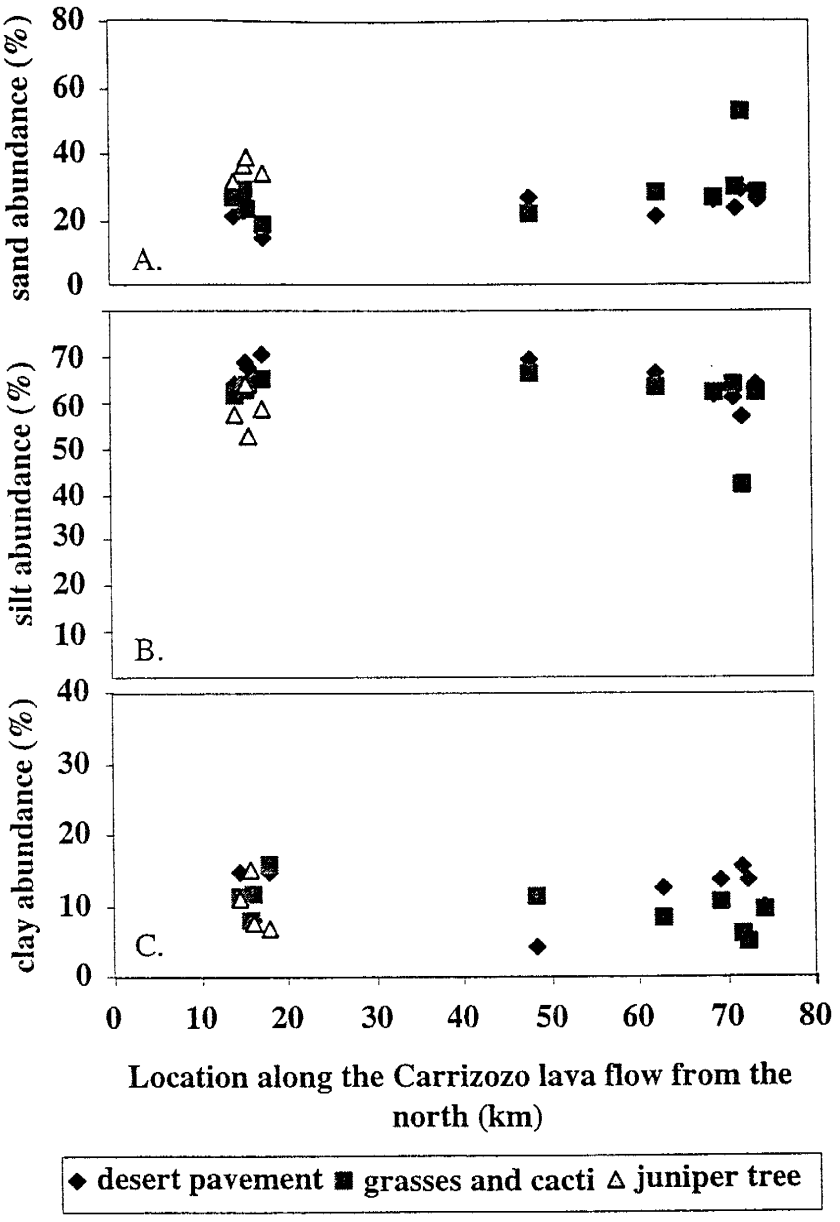

Figure 7 a,b, and c. (a) Sand abundance (%), (b) silt abundance (%), and (c) clay abundance (%) in the loess deposits along the Carrizozo lava flow from the north. Zero represents the northernmost edge of the flow and seventy-five represents the southernmost edge. Sand abundance remains the same throughout the extent of the lava flow, with slightly greater amounts in the juniper tree catchments. Silt and clay abundance remains constant throughout the extent of the lava flow. The overall texture of the loess deposits is uniform.

in most samples from both locations. Only the southern samples also contained undifferentiated coatings of clays and microcrystalline calcite, possible due to the lack of washing (Figure 8c and d). Digested samples exhibit little or no pitting on quartz grains giving a smooth surface appearance (Figure 8e). In all samples, weathered feldspar grains are found with visible etchings on the grain surface (Figure 8f). These etching are considered to be along crystal lattice dislocations (Berner and Holdren, 1977).

5.3.3. Mineralogy

Mineralogy of five bulk samples, three from the north and two from the south (Table 5), was determined using x- ray diffractometry (Appendix 9.2.4). Diffractograms indicates the presence of primarily quartz with minor amounts of albite in all samples (Appendix 9.3.3.). Clay mineralogy (Appendix 9.2.4) on the same samples also (Table 5) indicates abundant illite and kaolinite with traces of smectite found only in southern samples (Appendix 9.3.4.). One sample from the southern region contains chlorite.

5.4. Chemical Properties

5.4.1. Soluble Salts

Soluble salt concentration was measured on seventy-four incremental samples (Table 6; Appendix 9.3.5.) using electrical conductivity (Appendix 9.2.5.). Soluble salt concentrations vary with depth in each catchment. In northern juniper tree catchments, the greatest concentrations of soluble salts are found in near surface samples. However, in desert pavement catchments, the greatest concentration is found deeper in the soil profile (Figure 9 a, b). In the southern catchments, most surface cover types exhibit the greatest concentration of soluble salts in the near surface samples (Figures 9 c, d). The

Table 4. Grain morphology of loess samples from the Carrizozo lava flow, New Mexico. Samples were analyzed using an electron microprobe in the backscattered electron and scanning electron modes.

Sample #	Grain size range (um)	Grain size average (um)	Grain shape average	Basic mineralogy	Special mineralogy	Surface morphology	Surface features	Extra notes
CLF-4-D sand	50-100	100	subspherical, subangular	quartz, feldspar	zircon	smooth	undifferentiated Fe and Al coatings	uniform size and shape
CLF-4-D silt	25-100	25	subspherical, subrounded	quartz, feldspar	zircon	smooth	undifferentiated coatings	less uniform size and shape than 4-H sand
CLF-4-G sand	50-100	50	subspherical, subrounded	quartz, feldspar	zircon	smooth	undifferentiated Fe, Mg, and Al coatings	less uniform size than 4-H sand
CLF-4-G silt	50-100	50	subspherical, subangular	quartz, feldspar	zircon, microcrystalline calcite	smooth	undifferentiated Fe, Mg, and Al coatings	similar size and shape as 4-H fine
CLF-4-J sand	75-100	75	subspherical, subangular	quartz, feldspar	zircon	grain etching	undifferentiated coatings	less uniform than 4-H and L sand.
CLF-4-J silt	50-100	50	subspherical, subangular	quartz, feldspar		grain etching and pitting	undifferentiated coatings.	similar size and shape ti 4-L fine
CLF-15-D sand	50-100	50	subspherical, subrounded	quartz, feldspar		grain etching	undifferentiated Fe and Mg coatings	
CLF-15-D silt	50-75	50	subspherical, subangular	quartz, feldspar			less coatings present than 15-H coarse	
CLF-15-G sand	50-100	100	subspherical, subrounded	quartz, feldspar	gypsum		undifferentiated Fe, Mg and Al coatings	less uniform size and shape than northern samples
CLF-15-G silt	50-100	75	spherical, subrounded	quartz, feldspar	gypsum, zircon		undifferentiated coatings	
CLF-17-D sand	50-100	100	subspherical, subangular	quartz, feldspar	gypsum, zircon	grain etching	undifferentiated Fe, Mg, and Al coatings	
CLF-17-D silt	50-100	50	spherical, subrounded	quartz, feldspar	gypsum, barite, microcrystalline calcite		undifferentiated coatings	
CLF-17-G sand	75-100	100	spherical, subrounded	quartz, felspar				
CLF-17-G silt	50-75	50	spherical, subrounded	quartz, feldspar	gypsum	grain etching (trace)	undifferentiated coatings	

D= desert pavement
G= grasses and cacti
J= juniper tree

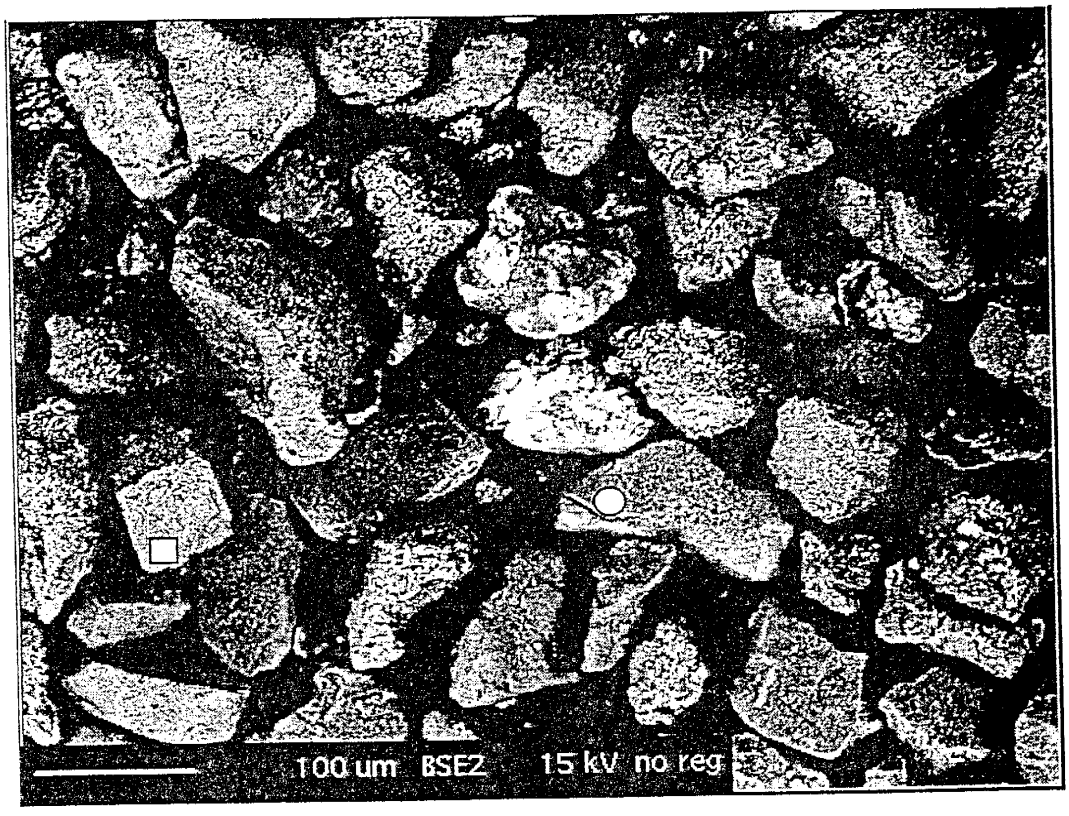

Figure 8a. Backscatter electron image of the coarse split (80um) of a northern desert pavement sample (CLF-4-D). Grain size and shape exhibit homogeneity. ◯=quartz □= feldspar.

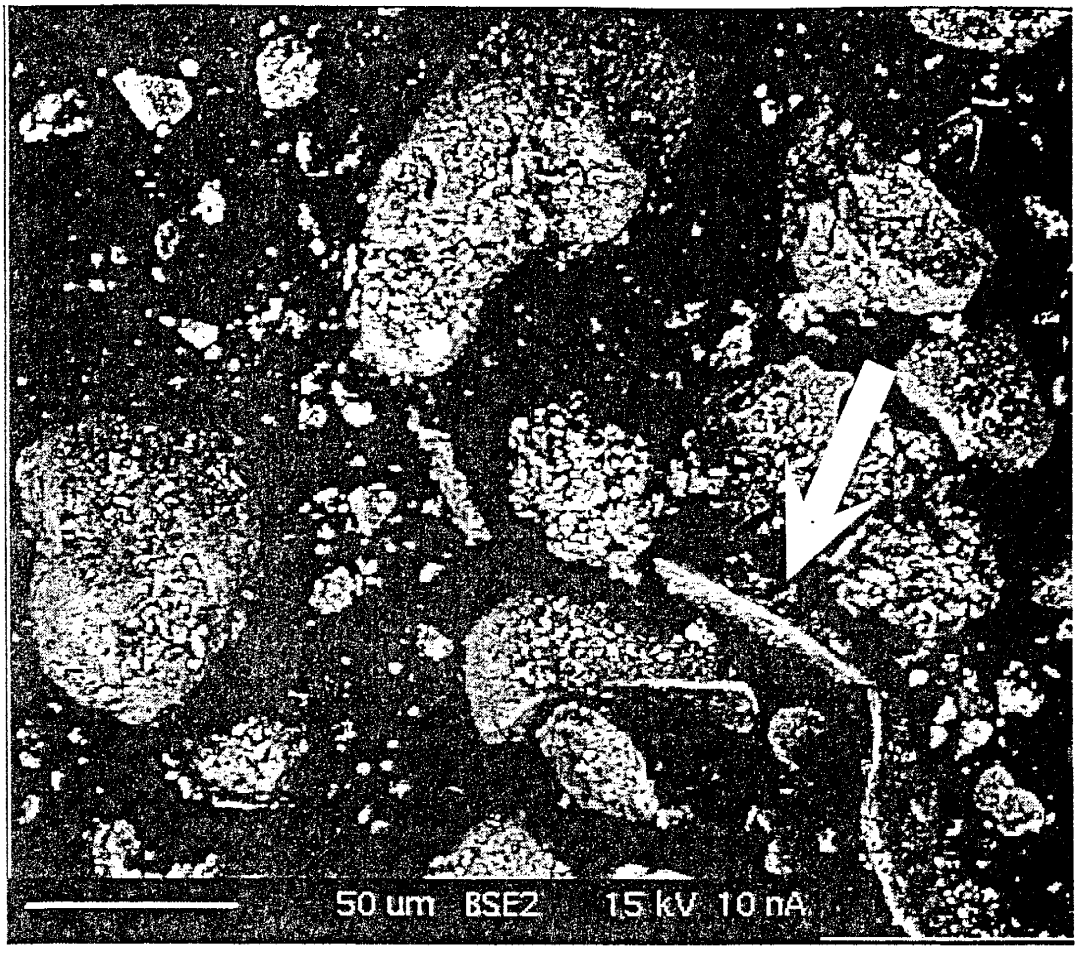

Figure 8b. Backscatter electron image of the fine split of a southern grasses and cacti catchment sample (CLF-15-G). ↑ denote a gypsum grain typically found only in southern catchments.

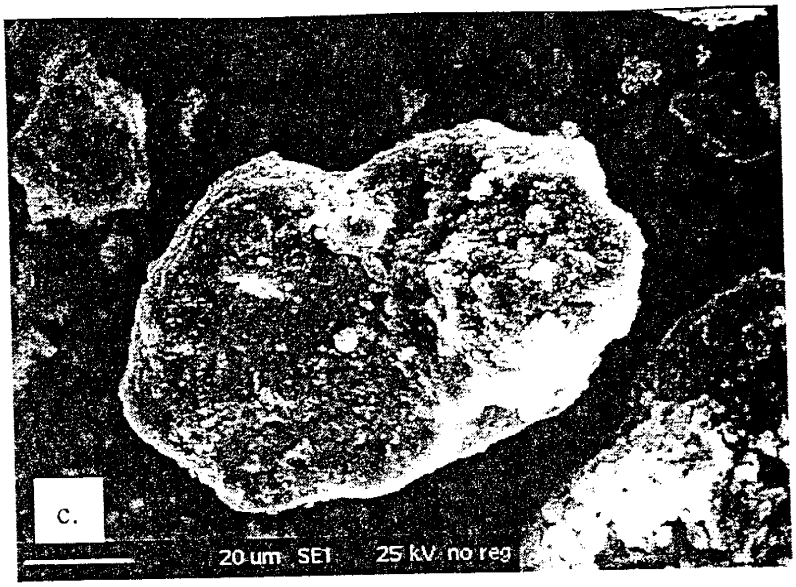

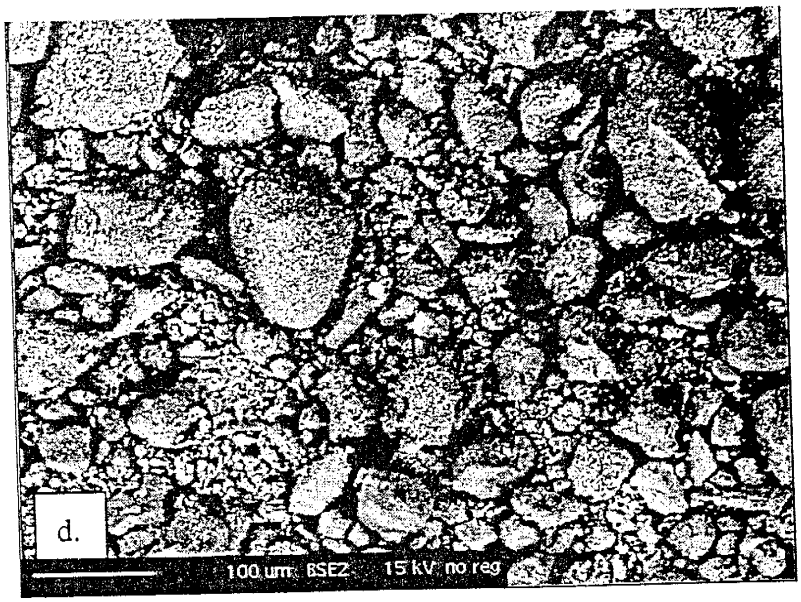

Figure 8c and d. (c) Scanning electron image of a grain surface from the fine split of a southern desert pavement catchment sample (CLF-15-D). This sample was not previously washed with hydrogen peroxide. Undifferentiated clay and microcrystalline calcite coatings are present. (d) Backscatter electron image of undifferentiated clay coatings on the grain surfaces of the fine split of the same southern desert pavement catchment sample as in c. (CLF-15-D). This sample was also not previously washed with hydrogen peroxide. Coatings primarily contain clays and microcrystalline calcite.

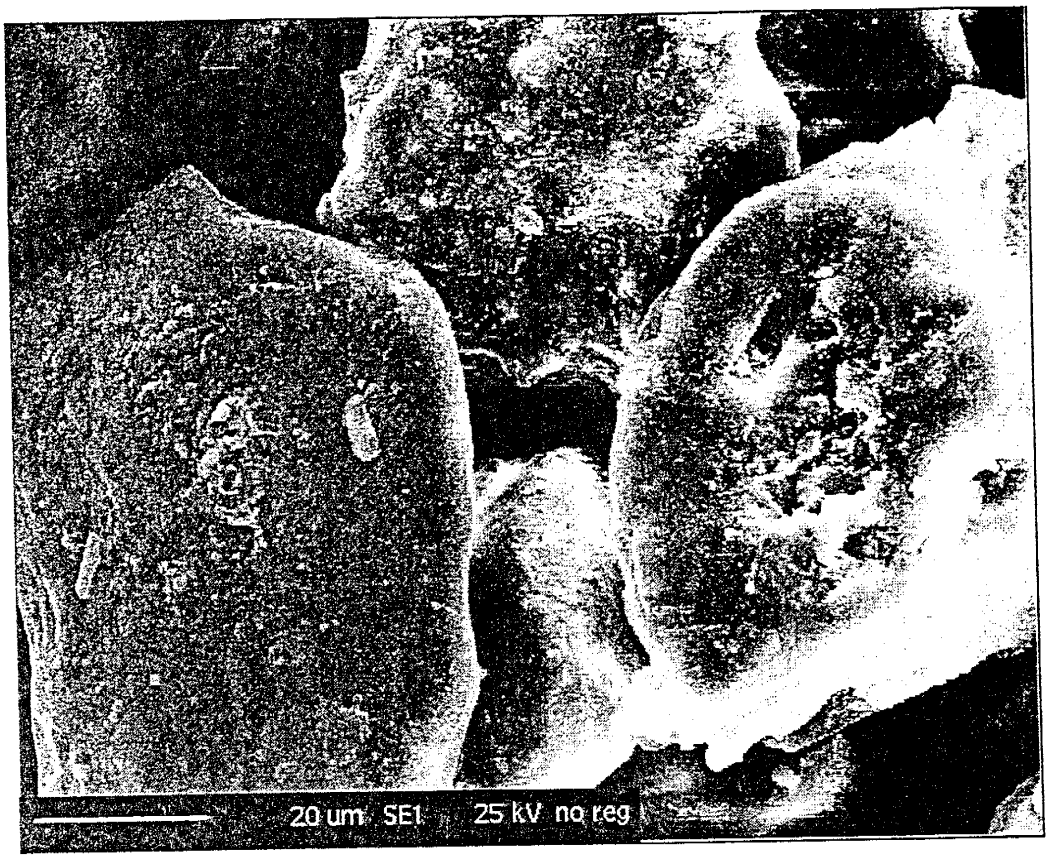

Figure 8e. Scanning electron image of a grain surface from the fine split of a northern desert pavement catchment sample (CLF-4-D). This sample was cleaned with hydrogen peroxide during the particle size analysis. Minor pitting and abrasion is observed.

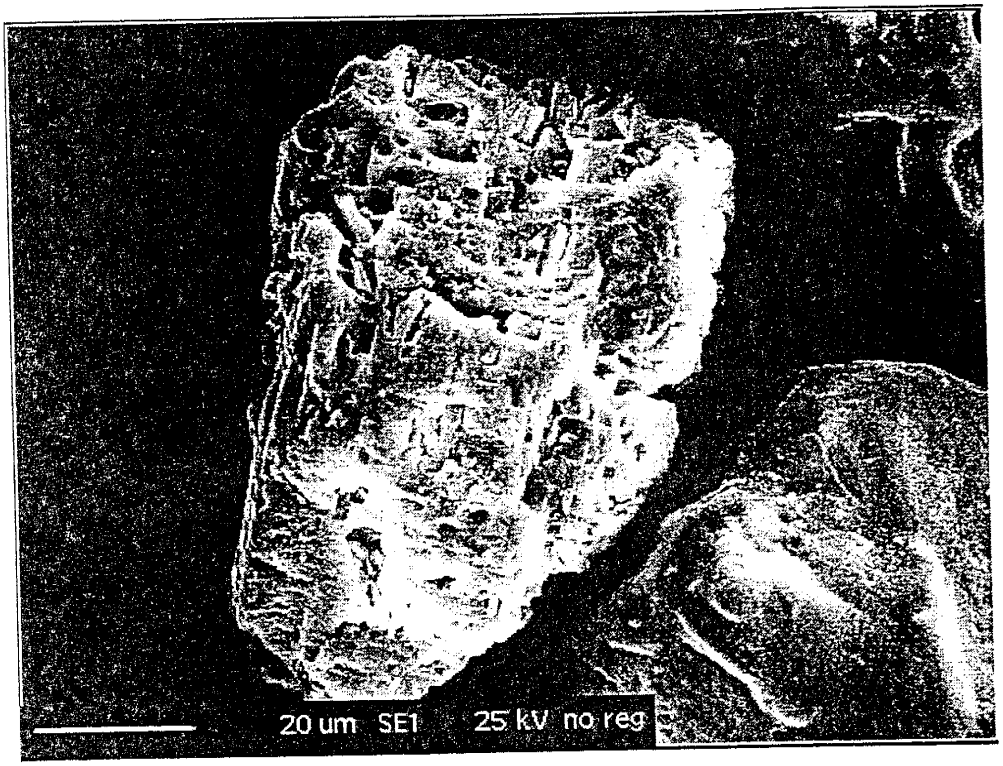

Figure 8f. Scanning electron image of a weathered feldspar from a northern juniper tree catchment (CLF-4-J). Etchings are selective along the crystal lattice dislocations as also observed by Berner and Holdren (1977). These etching features were observed on a variety of samples from both locations.

Table 5. Bulk mineralogy and clay mineralogy of loess samples from the Carrizozo lava flow, New Mexico. Samples were analyzed using x-ray diffractometry.

Sample #	Bulk Mineralogy	Clay Mineralogy (parts of ten)				
		Illite	Kaolinite	Smectite	Illite/Smectite	Chlorite
CLF-3-D	quartz, albite	3.5	3.5	0	2.9	0
CLF-3-G	quartz, albite, anorthoclase	5.7	3.2	0	1	0
CLF-3-J	quartz, albite, calcite	3.9	3.7	0	2.3	0
CLF-14-D	quartz, albite, anorthoclase	3.2	1.7	0.3	2.2	2.7
CLF-14-G	quartz, albite	5.1	4.8	0.4	0	0

D= desert pavement
G= grasses and cacti
J= juniper tree

exception are in catchments CLF-17-D and CLF-17-G, where the greatest concentrations and the most extreme values are found in the deepest sample.

The soluble salt concentration also varies with surface cover type. It is greatest in the juniper tree catchments (average 0.23%) compared to an average of 0.09% for both the grasses and cacti and desert pavement catchments in the north. In the south, the concentration of soluble salts statistically remains the same in both the desert pavement and grasses and cacti catchments, with averages of 0.15% and 0.13%, respectively (Table 6). Excluding the juniper tree catchments, there are significant differences between the north and the south catchments (Figure 10) with increased concentrations to the south.

5.4.2. Chloride

Chloride concentration was measured (Appendix 9.2.6.) on forty-eight incremental samples in order to evaluate moisture influxes within the soil profiles (Table 7; Appendix 9.3.6.). Chloride concentration varies with depth and with surface cover type. In northern and southern desert pavement catchments, chloride concentration is the highest in near surface samples and gradually decreases with depth in the profile, increasing slightly in the deepest sample, producing a bulge (Figure 11 a,b). However, the chloride concentrations differ with depth in the grasses and cacti catchments from the north to the south. In northern grasses and cacti catchments, the highest concentration is deepest in the soil profile (Figure 11c), whereas in the southern grasses and cacti catchments, the highest concentrations are found in the near surface samples (Figure 11d). In the northern juniper tree catchments, the highest concentrations are found in near surface samples (Figure 11e). Chloride concentration slightly varies in the loess

Table 6. Soluble salt concentration in the loess deposits on the Carrizozo lava flow, New Mexico. Samples were analyzed using electrical conductivity. Averages and standard deviations are provided. Analytical data is presented in Appendix 9.3.5.

	n=	Soluble salts (%)	
		average	std dev
A	71	0.14	0.08
AN	46	0.14	0.09
AS	25	0.14	0.06
ND	12	0.08	0.02
SD	11	0.15	0.07
NG	17	0.09	0.03
SG	14	0.13	0.05
NJ	17	0.23	0.09

A=	all samples
AN=	all northern samples
AS=	all southern samples
ND=	northern desert pavement
SD=	southern desert pavement
NG=	northern grasses and cacti
SG=	southern grasses and cacti
NJ=	northern juniper tree

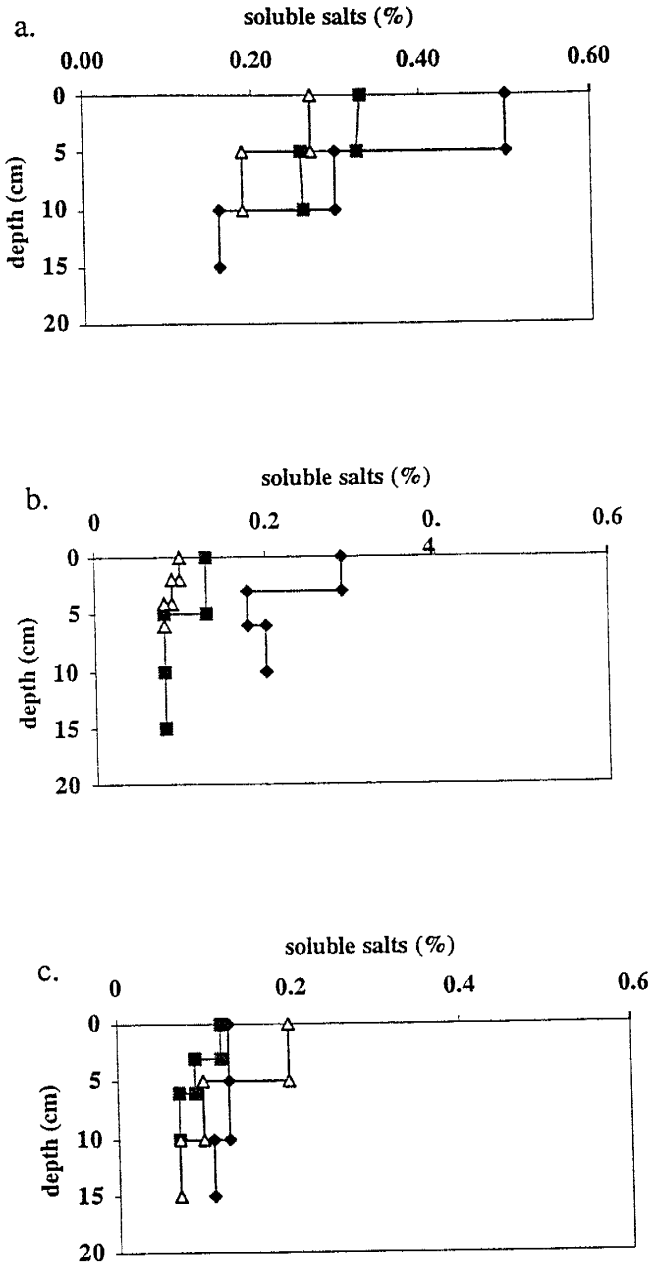

Figure 9. Soluble salt concentration with depth in (a) juniper tree catchments; (b) southern desert pavement catchments; and (c) southern grasses and cacti catchments. Highest concentrations are found in the near surface samples of juniper tree, and southern desert pavement and grasses and cacti catchments. In northern desert pavement catchments, the highest concentration is found deeper in the soil profile (not shown).

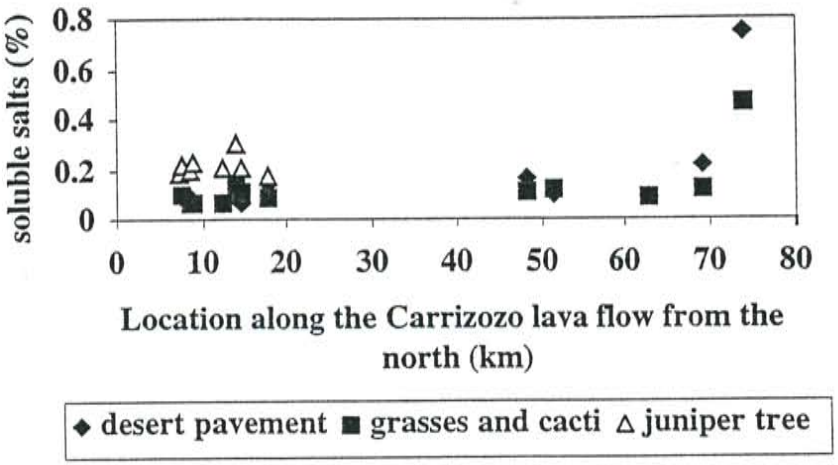

Figure 10. Soluble salt concentration along the Carrizozo lava flow, New Mexico. Zero represents the northernmost edge of the lava flow and seventy-five represents the southernmost edge. Increased concentration of soluble salts are observed in the south, and greater concentrations are within the northern juniper tree catchments.

deposits along the Carrizozo lava flow, with slight increasing concentrations to the south (Figure 12).

5.4.3. Calcium Carbonate

Calcium carbonate concentration was determined using the Chittick method (Appendix 9.2.7.) on sixty-six incremental and bulk samples (Table 8; Appendix 9.3.7.). Calcium carbonate concentrations vary significantly with depth in each surface cover type. However, no concentration trends are apparent.

The calcium carbonate concentrations do not vary significantly with surface cover types. However, variations are observed with location on the lava flow. Calcium carbonate concentrations are greater in the south with an average of 3.45 wt% $CaCO_3$ as compared to the northern average of 1.05 wt% $CaCO_3$ (Figure 13).

5.4.4. Elemental Composition

Major element chemical analysis was conducted on twelve sand and twelve silt size fractions, all obtained from the particle size analysis (Table 9; Appendix 9.3.8.). When analyses are normalized on a $CaCO_3$ and LOI-free basis (discussed later), there are no significant major element differences between the sand and silt fractions. However, there is a tendency for the silt fractions to have higher concentrations of Al_2O_3 and Fe_2O_3, than the sand size fraction (Figure 14). Thus, possibly suggesting a higher magnetite content (Table 9).

One hundred and nine incremental and bulk loess samples (Appendix 9.3.9.) were analyzed for major elements using x-ray fluorescence spectrometry (Appendix 9.2.8.).

Table 7. Chloride concentration in the loess deposits on the Carrizozo lava flow, New Mexico. Analytical data is presented in Appendix 9.3.6.

	n=	Chloride (ppm)	
		average	stdev
A	48	5.7	12.2
AN	21	3.2	2.9
AS	27	7.7	15.9
ND	6	1.6	0.1
SD	12	14.7	20.4
NG	7	1.7	0.1
SG	15	2.1	0.3
NJ	8	5.3	1.4

A=	all samples
AN=	all northern samples
AS=	all southern samples
ND=	northern desert pavement
SD=	southern desert pavement
NG=	northern grasses and cacti
SG=	southern grasses and cacti
NJ=	northern juniper tree

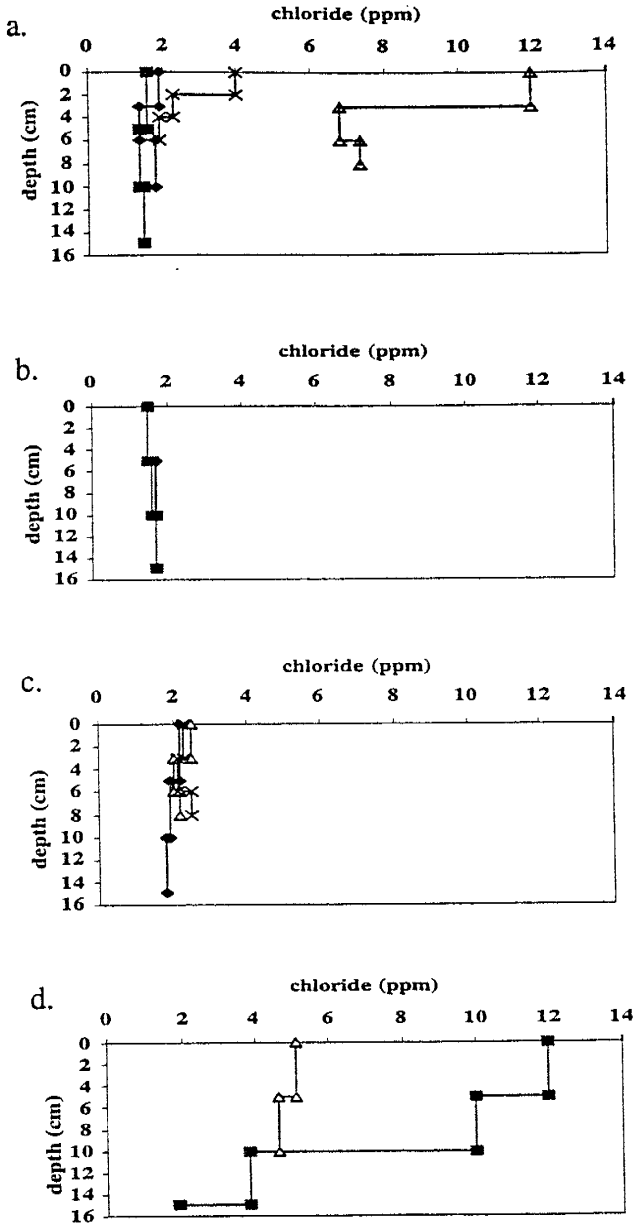

Figure 11. Chloride concentration within the soil profiles on the Carrizozo lava flow. Distribution is dependent on surface cover type: (a) all desert pavement, (b) northern grasses and cacti, (c) southern grasses and cacti, and (d) juniper tree. All desert pavement catchments have the highest concentration in near surface sample. The northern grasses and cacti catchments have the highest concentration is at the base of the soil profile, whereas the southern catchments have the highest concentrations in near surface samples. The juniper tree catchments have the highest concentrations in the near surface samples. Surface cover influences the hydrologic conditions within the profile influencing the movement of chloride with depth.

Table 8. Calcium carbonate concentration in the loess deposits on the Carrizozo lava flow, New Mexico. Samples were analyzed using the Chittick method. Analytical data presented in Appendix 9.3.7.

	n=	$CaCO_3$ (wt%)	
		average	stdev
A	65	2.03	3.36
AN	39	1.05	1.42
AS	26	3.45	4.66
ND	13	1.42	1.97
SD	12	3.3	4.03
NG	14	0.45	0.82
SG	14	3.66	5.43
NJ	12	1.36	1.13

A=	all samples
AN=	all northern samples
AS=	all southern samples
ND=	northern desert pavement
SD=	southern desert pavement
NG=	northern grasses and cacti
SG=	southern grasses and cacti
NJ=	northern juniper tree

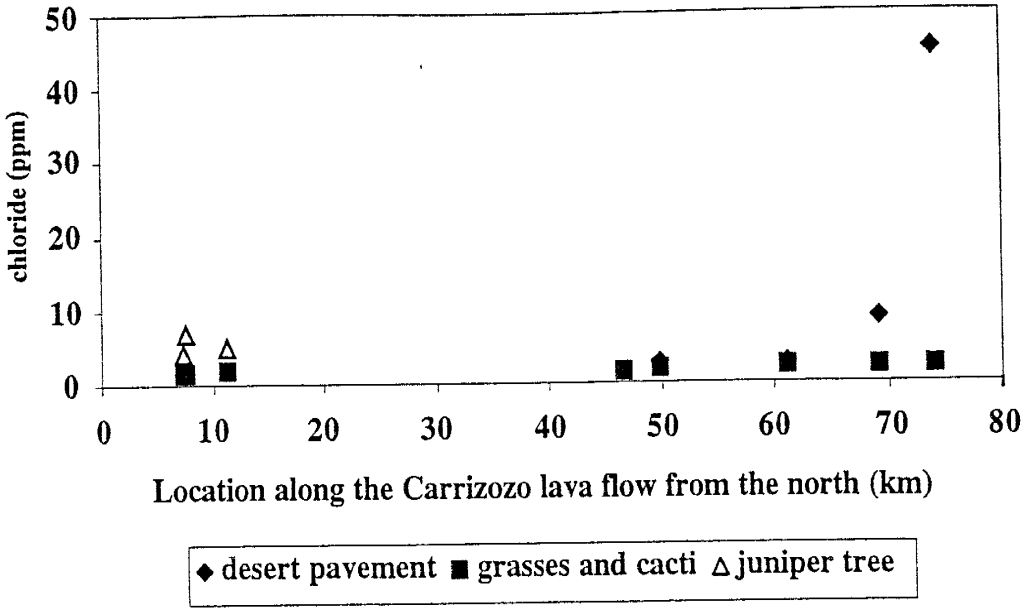

Figure 12. Chloride concentration (ppm) along the the Carrizozo lava flow, New Mexico. Zero represents the northernmost edge of the lava flow and seventy-five represents the southernmost edge. Chloride increases in the south. In the north, chloride is greatest in the juniper tree catchments.

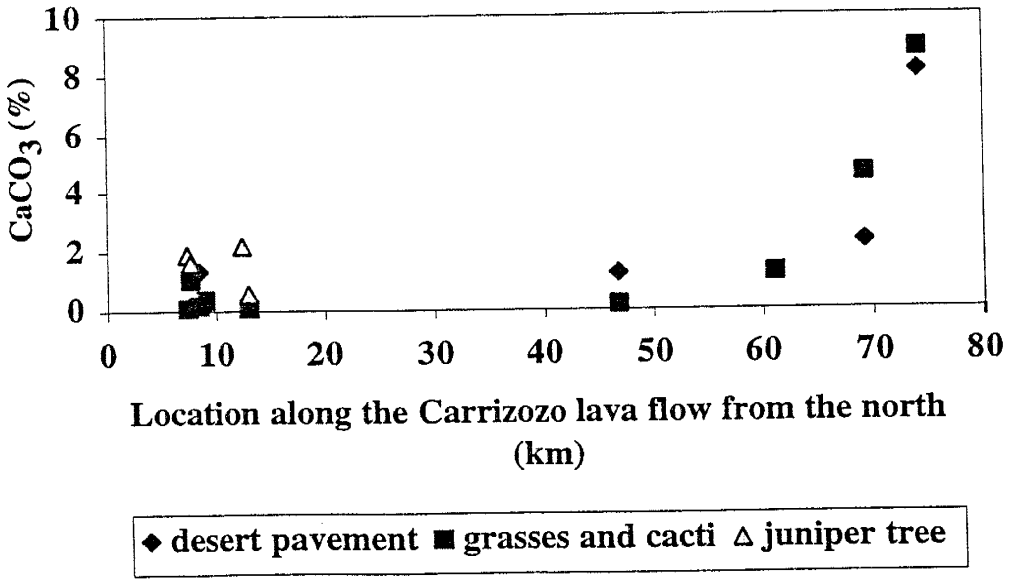

Figure 13. Calcium carbonate (%) along the Carrizozo lava flow, New Mexico. Zero represents the northernmost edge of the lava flow and seventy-five represents the southernmost edge. Calcium carbonate increases to the south, and in the northern region is greatest in juniper tree catchments.

Table 9. Summary of the major element chemistry of the particle size fractions of the loess samples from the Carrizozo lava flow, New Mexico in (wt% oxide). Samples were analyzed using x-ray fluorescence spectrometry. Normalized to 100 % on a $CaCO_3$-free and loss-free basis.Averages and standard deviations are provided. Analytical data is presented in Appendix 9.3.8.

		SiO_2		TiO_2		Al_2O_3		Fe_2O_3*		MnO	
	n=	average	std dev	average	std dev	average	std dev	average	std dev	average	std dev
A sd	12	77.69	3.41	0.61	0.12	10.34	1.19	3.30	0.98	0.070	0.026
A si	12	72.68	1.70	0.94	0.06	12.48	0.66	4.55	0.30	0.080	0.015
ND sd	2	78.89	2.30	0.54	0.04	10.21	1.15	2.92	0.46	0.070	0.040
ND si	2	72.39	2.73	0.96	0.05	12.84	1.41	4.58	0.60	0.060	0.020
SD sd	3	79.26	0.59	0.58	0.13	9.42	0.34	3.05	0.52	0.070	0.020
SD si	3	71.76	2.19	0.94	0.11	12.38	0.31	4.65	0.37	0.090	0.020
NG sd	2	76.43	1.74	0.62	0.06	11.26	0.26	3.23	0.15	0.070	0.020
NG si	2	72.31	2.06	0.97	0.01	12.95	0.74	4.64	0.22	0.080	0.010
SG sd	3	75.58	6.74	0.69	0.22	10.75	2.15	4.01	1.93	0.100	0.022
SG si	3	73.55	1.41	0.90	0.02	11.86	0.10	4.33	0.16	0.080	0.005
NJ sd	2	78.57	0.28	0.58	0.06	10.32	0.13	3.07	0.37	0.050	0.009
NJ si	2	73.44	0.20	0.98	0.00	12.75	0.16	4.56	0.31	0.060	0.008

		CaO		MgO		Na_2O		K_2O		P_2O_5	
	n=	average	std dev	average	std dev	average	std dev	average	std dev	average	std dev
A sd	12	1.46	0.09	1.63	1.01	2.27	0.18	2.31	0.15	0.32	0.32
A si	12	1.40	0.13	1.97	1.06	2.66	0.24	2.64	0.12	0.60	0.26
ND sd	2	1.50	0.00	1.10	0.19	2.18	0.11	2.34	0.19	0.25	0.12
ND si	2	1.37	0.18	1.40	0.57	2.99	0.18	2.65	0.13	0.76	0.06
SD sd	3	1.50	0.00	1.64	0.31	2.14	0.02	2.18	0.07	0.15	0.00
SD si	3	1.50	0.00	2.88	1.52	2.48	0.15	2.62	0.13	0.70	0.41
NG sd	2	1.37	0.19	1.30	0.34	2.57	0.06	2.52	0.07	0.63	0.73
NG si	2	1.40	0.14	1.44	0.41	2.83	0.12	2.76	0.16	0.63	0.28
SG sd	3	1.43	0.12	2.54	1.86	2.28	0.17	2.24	0.13	0.39	0.34
SG si	3	1.40	0.18	2.33	0.97	2.47	0.12	2.53	0.01	0.54	0.22
NJ sd	2	1.48	0.03	1.11	0.27	2.28	0.21	2.34	0.17	0.21	0.04
NJ si	2	1.30	0.09	1.17	0.10	2.70	0.19	2.69	0.03	0.34	0.07

A sd=	all sand samples
A si=	all silt samples
ND=	northern desert pavement
SD=	southern desert pavement
NG=	northern grasses and cacti
SG=	southern grasses and cacti
NJ=	northern juniper tree
* =	Total Fe as Fe_2O_3
sd=	sand fraction
si=	silt fraction

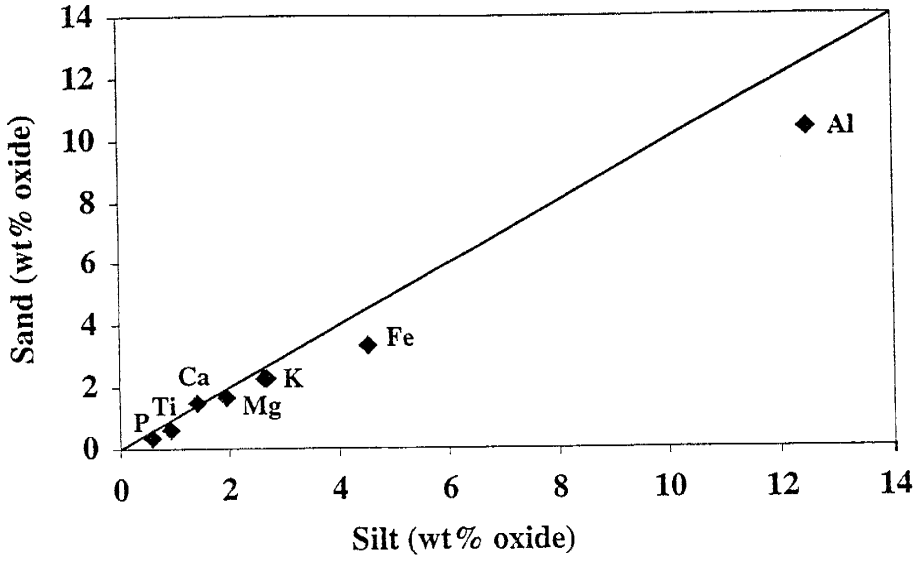

Figure 14. Average element concentrations within the sand and silt fractions. Elements presented are in oxide form. Slight tendency for the silt fraction to have higher concentrations of Al_2O_3 and Fe_2O_3.

The only oxide that varies with depth in the soil profiles is CaO and variation is dependent on the surface cover type. Juniper tree catchments, and all grasses and cacti catchments have greater concentrations of CaO in near surface samples, whereas all desert pavement catchments, have the greatest concentration deeper in the soil profile (Figure 15 a, b, c). In the desert pavement and grasses and cacti catchments of location CLF-17, the highest concentrations of CaO is found deeper in the soil profile, averaging 15.2 wt%, which are the greatest concentrations seen throughout the flow. At the location of CLF-17, high concentrations may be attributed to a greater influx of carbonate. There are slight chemical variations observed between surface cover types. CaO concentrations are the highest in juniper tree catchments (3.4 wt%) when compared to the desert pavement and grasses and cacti catchments, both averaging 1.7 wt% CaO.

The only major elements that show variations with location are CaO and MgO. In the north, CaO concentration averages 1.7 wt% in both the grasses and cacti and desert pavement catchments, whereas in the south, the concentration averages 3.8 wt% (Appendix 9.3.9.). This overall increase to the south is well illustrated in Figure 16. Magnesium oxide shows a similar trend. In the north, MgO concentrations are the same for all three surface cover types, averaging 1.4 wt%. In the south, MgO averages 2.7 wt% (Appendix 9.3.9.; Figure 17) for the two surface cover type.

Semi-arid and arid soils are influenced by the accumulation of $CaCO_3$. In order to interpret the chemical composition of the loess without the influence of secondary carbonate (pedogenic), the $CaCO_3$ (wt%) concentrations were plotted verse CaO (wt%) (Figure 18). The y-intercept is at approximately 1.5 wt% CaO indicating that at concentrations greater than 1.5 wt%, pedogenic $CaCO_3$ is influencing the soil. Therefore,

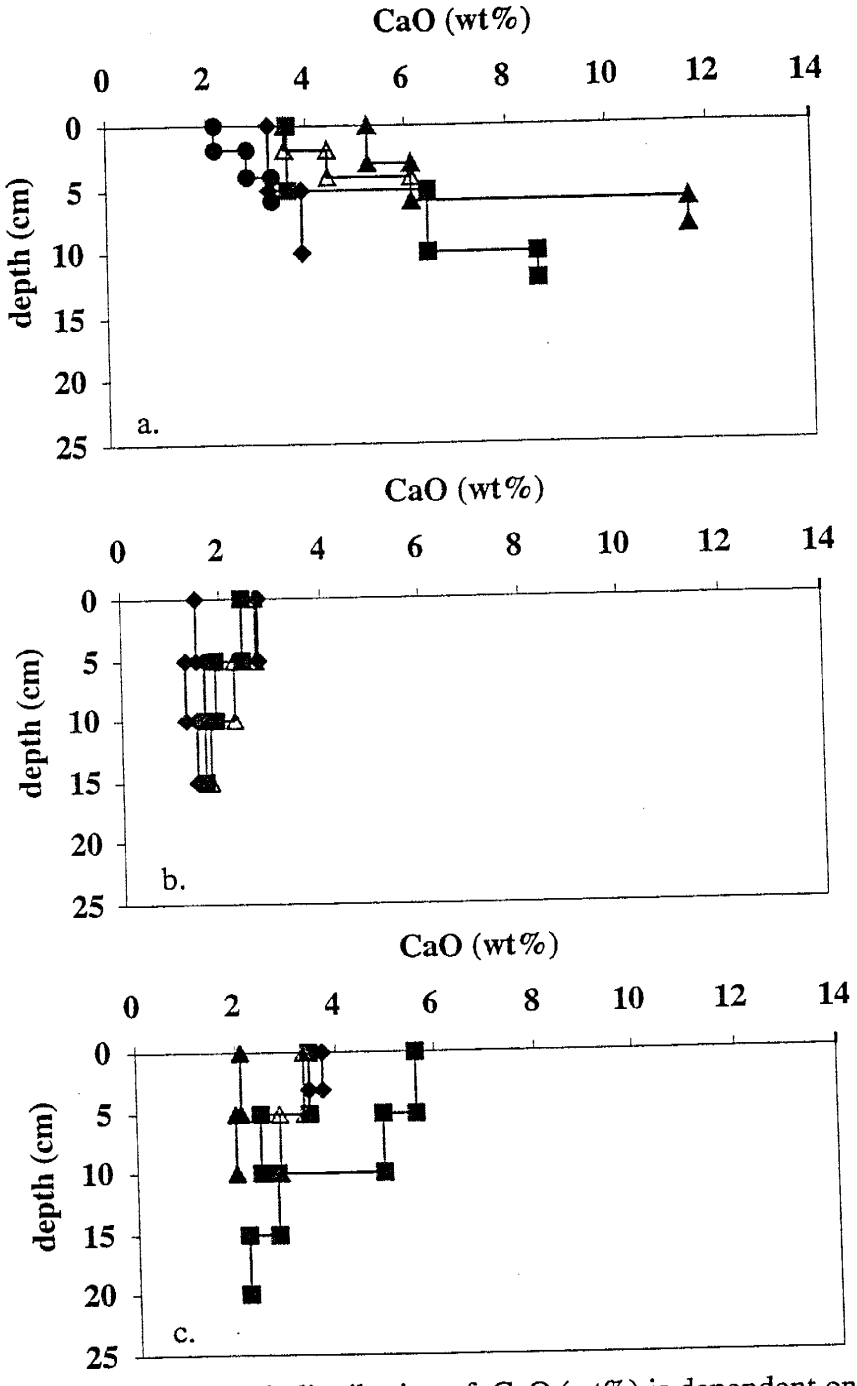

Figure 15. Depth distribution of CaO (wt%) is dependent on surface cover type: (a.) desert pavement catchments, (b) grasses and cacti catchments and (c) juniper tree catchments. In the desert pavement catchments, CaO concentration increases with depth in the soil profile, whereas in grasses and cacti and juniper tree catchments, the concentrations decrease with depth. Thus suggesting that the type of surface cover influences the distribution of CaO through the soil profile.

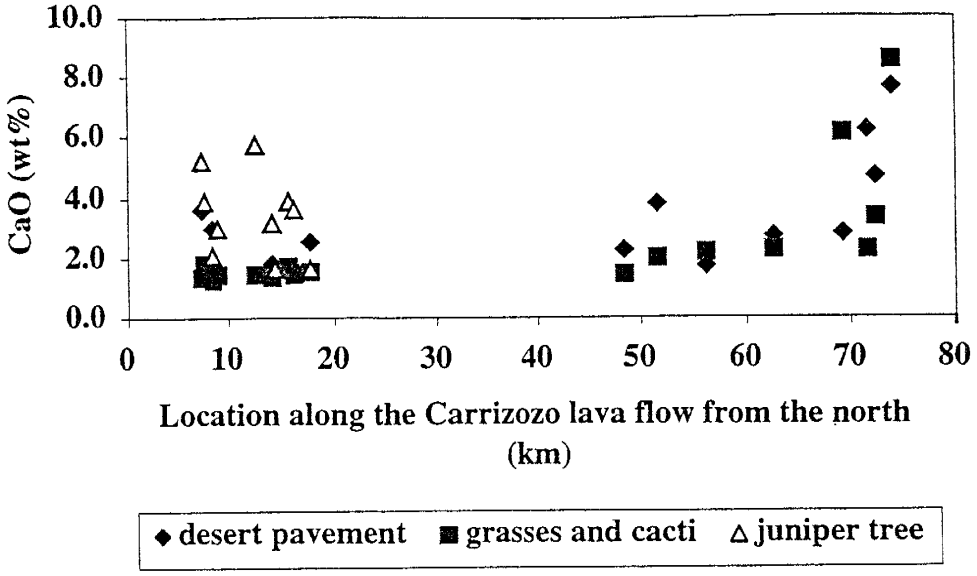

Figure 16. Variations of CaO along the Carrizozo lava flow, New Mexico. Zero represents the northernmost edge of the lava flow and seventy-five represents the southernmost edge. CaO increases to the south. In the north, the juniper tree catchments contain the highest concentration.

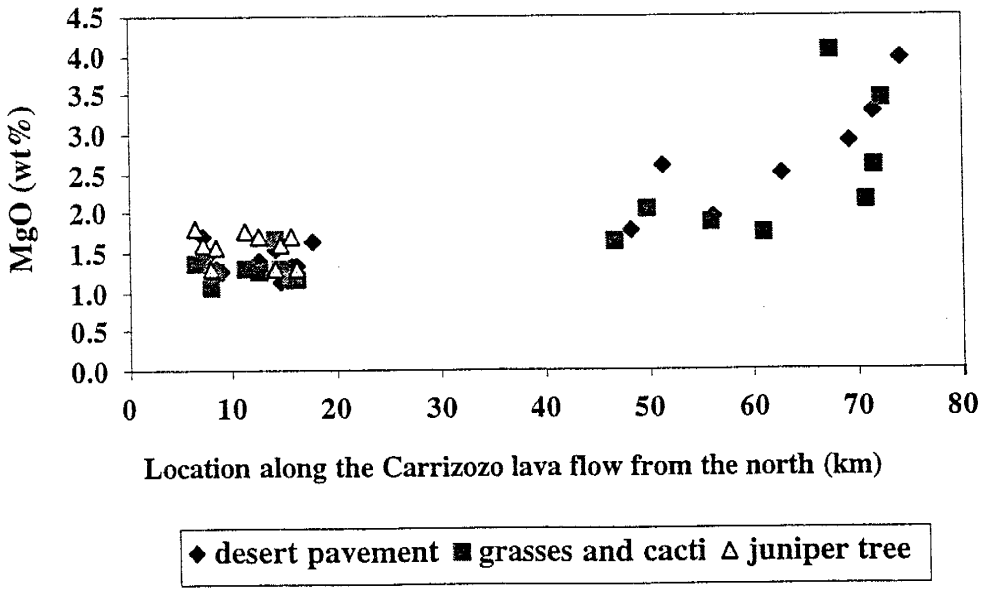

Figure 17. Variations in MgO along the Carrizozo lava flow, New Mexico. Zero represents the northernmost edge of the lava flow, and seventy-five represents the southernmost edge. MgO increases in the south, and no variation exists within surface cover types.

CaO concentrations of greater than 1.5 wt% were adjusted to the value of 1.5 wt% and re-normalized to 100%. The adjustment for the input of pedogenic carbonate produced a $CaCO_3$-free sample (Table 10, Appendix 9.3.10.).

The average composition of the $CaCO_3$-free loess is relatively uniform. Some chemical variations still are evident, as greater concentrations of CaO and MgO are present in the southern region. Comparing the concentrations of CaO and MgO (Figure 19), an increasing correlation is observed. The observed increasing correlation suggests that the loess is influenced by a mineral with both CaO and MgO. The prevailing wind direction and the local geology indicates that the loess could be influenced by dolomites from the San Andres Mountains.

One hundred and five samples were analyzed for trace elements (Appendix 9.3.11.) using x-ray fluorescence spectrometry (Appendix 9.2.8.). There is no variability in concentrations between surface cover types. The average $CaCO_3$-free trace element composition of the loess is uniform over most of the flow, except for the element sulfur (Table 11). Sulfur increases in the southern region from 247 ppm to 379 ppm (Figure 20).

A good correlation also exists between the CaO and S concentrations (Figure 21). This correlation suggests that the loess is influenced by trace amounts of gypsum. Southwestern prevailing winds and the White Sands gypsum deposit located to the south of the lava flow, could be the source for the higher S concentrations.

Twenty-nine bulk northern samples (Appendix 9.3.12.) were analyzed for trace and rare earth elements using instrumental neutron activation analysis (Appendix 9.2.9.). There is no significant variation in trace element content for the twenty-nine samples

(Table 12). High standard deviations are observed and could be attributed to calcium carbonate and LOI.

Table 10. Summary of the major element chemistry of the loess samples from the Carrizozo lava flow, New Mexico. Samples were analyzed using x-ray fluorescence spectrometry. Normalized to 100% on a $CaCO_3$-free and loss-free basis. Averages and standard deviations are provided. Analytical data is presented in Appendix 9.3.10.

		SiO_2		TiO_2		Al_2O_3		Fe_2O_3*		MnO	
	n=	average	std dev	average	std dev	average	std dev	average	std dev	average	std dev
A	109	73.69	1.81	0.80	0.06	12.81	0.76	4.40	0.44	0.100	0.013
AN	62	74.51	1.27	0.80	0.05	12.79	0.60	4.27	0.33	0.090	0.012
AS	47	72.60	1.86	0.81	0.07	12.82	0.93	4.57	0.52	0.100	0.014
ND	19	74.37	0.98	0.81	0.00	12.86	0.50	4.42	0.30	0.090	0.010
SD	22	72.19	1.30	0.84	0.10	12.85	0.80	4.69	0.40	0.100	0.010
NG	23	75.28	1.26	0.77	0.00	12.48	0.63	4.13	0.30	0.090	0.010
SG	25	72.97	2.21	0.79	0.10	12.80	1.05	4.46	0.60	0.100	0.020
NJ	20	73.75	1.03	0.81	0.00	13.08	0.48	4.29	0.40	0.100	0.010

		CaO		MgO		Na_2O		K_2O		P_2O_5	
	n=	average	std dev	average	std dev	average	std dev	average	std dev	average	std dev
A	109	1.46	0.09	1.99	0.90	1.82	0.13	2.71	0.13	0.23	0.14
AN	62	1.43	0.01	1.43	0.10	1.77	0.14	2.72	0.12	0.19	0.10
AS	47	1.50	0.02	2.74	0.90	1.88	0.11	2.70	0.15	0.28	0.17
ND	19	1.42	0.10	1.40	0.20	1.78	0.10	2.70	0.10	0.15	0.10
SD	22	1.50	0.00	2.99	0.80	1.85	0.10	2.72	0.20	0.28	0.10
NG	23	1.39	0.10	1.28	0.20	1.80	0.10	2.66	0.10	0.13	0.00
SG	25	1.49	0.00	2.52	0.90	1.90	0.10	2.68	0.10	0.28	0.20
NJ	20	1.50	0.00	1.63	0.20	1.75	0.10	2.80	0.10	0.28	0.10

A=	all samples
AN=	all northern samples
AS=	all southern samples
ND=	northern desert pavement
SD=	southern desert pavement
NG=	northern grasses and cacti
SG=	southern grasses and cacti
NJ=	northern juniper tree
* =	Total Fe as Fe_2O_3

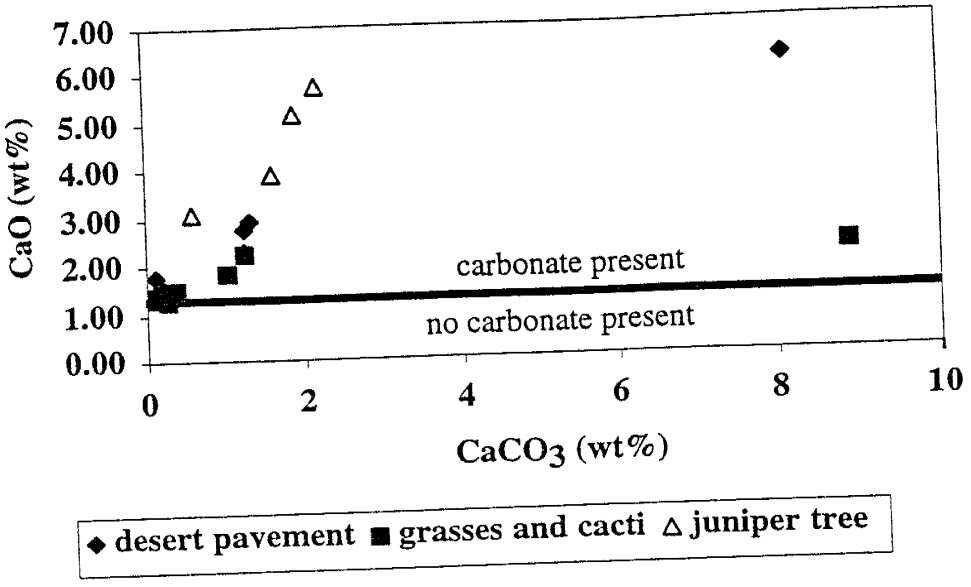

Figure 18. Distribution of $CaCO_3$ with respect to CaO. $CaCO_3$ correlates well with CaO. The y-intercept value of 1.5 wt % CaO was used in determining the $CaCO_3$-free composition of the loess on the Carrizozo lava flow, New Mexico.

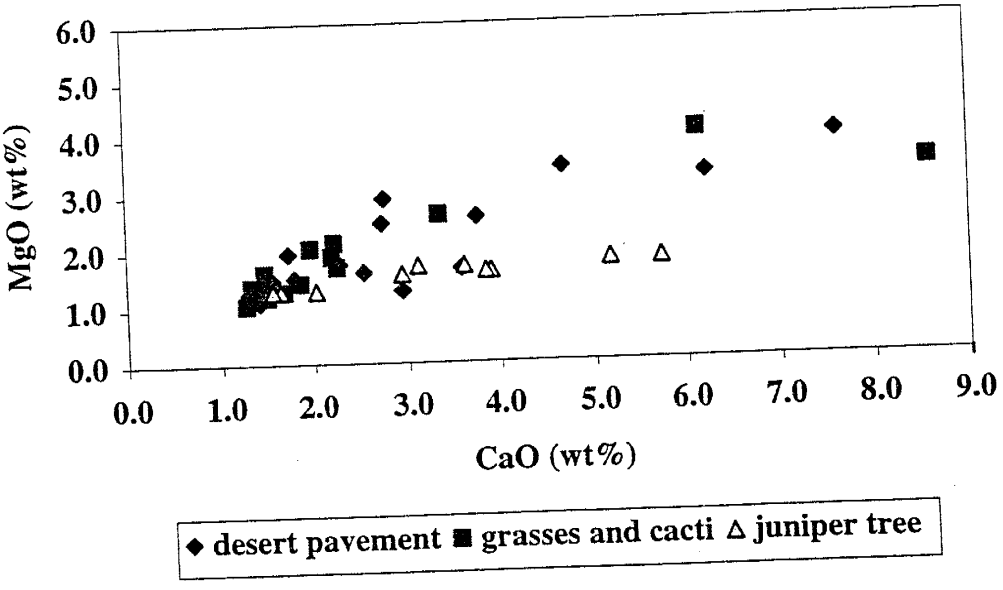

Figure 19. Correlation diagram of major oxide elements CaO (wt %) and MgO (wt%) for all analyzed loess samples on the Carrizozo lava flow, New Mexico. The observed correlation implies that CaO and MgO both influence the loess composition with the addition of dolomite from the San Andres Mountains.

Table 11. Summary of the trace element chemistry of the loess samples from the Carrizozo lava flow, New Mexico. Samples were analyzed using x-ray fluorescence spectrometry. Normalized on a $CaCO_3$-free and loss-free basis. Averages and standard deviations are provided. Averages are presented in ppm. Analytical data is presented in Appendix 9.3.11.

		S		Cr		V		Ni		Cu		Zn	
	n=	average	std dev	average	std dev	average	std dev	average	std dev	average	std dev	average	std dev
A	105	357	167	57	8	73	9	21	4	35	7	92	14
AN	60	247	46	56	7	69	8	19	2	35	6	93	12
AS	45	379	175	58	9	78	7	24	4	35	7	90	16
ND	19	295	1	58	5	71	8	19	1	33	3	91	6
SD	21	462	199	62	7	81	6	24	3	34	5	89	10
NG	22	232	42	55	9	66	10	18	2	30	3	89	11
SG	24	305	108	55	9	75	7	23	5	36	9	91	19
NJ	19	236	52	56	5	71	7	20	2	40	7	101	14

		Ga		As		Rb		Sr		Nb		Y	
	n=	average	std dev	average	std dev	average	std dev	average	std dev	average	std dev	average	std dev
A	101	15	1	5	1	129	17	293	71	13	2	29	2
AN	60	15	1	5	2	129	16	279	58	14	1	29	2
AS	41	14	1	5	1	129	19	312	82	13	1	29	3
ND	19	15	1	5	1	127	14	257	29	16	0	30	1
SD	21	14	1	5	1	133	20	309	54	13	1	30	2
NG	22	14	1	4	1	126	15	242	23	15	1	28	2
SG	24	14	1	5	1	125	17	316	102	12	1	28	3
NJ	19	16	1	7	1	134	17	343	54	13	1	28	2

		Zr		Mo		Ba		Pb		Th		U	
	n=	average	std dev	average	std dev	average	std dev	average	std dev	average	std dev	average	std dev
A	101	361	37	3	0	567	39	27	9	12	1	3	1
AN	60	368	26	3	0	559	44	26	6	12	2	3	1
AS	41	351	47	0	0	579	28	28	12	4	1	4	1
ND	19	380	31	2	0	563	46	24	5	12	2	3	1
SD	21	385	44	n.r.	n.r.	573	27	22	3	13	1	4	1
NG	22	359	21	3	0	553	43	23	3	11	1	3	1
SG	24	322	25	n.r.	n.r.	584	29	32	15	12	1	4	1
NJ	19	367	22	3	1	562	45	31	6	13	2	3	1

A=	all samples
AN=	all northern samples
AS=	all southern samples
ND=	northern desert pavement
SD=	southern desert pavement
NG=	northern grasses and cacti
SG=	southern grasses and cacti
NJ=	northern juniper tree
n.r.=	none recorded

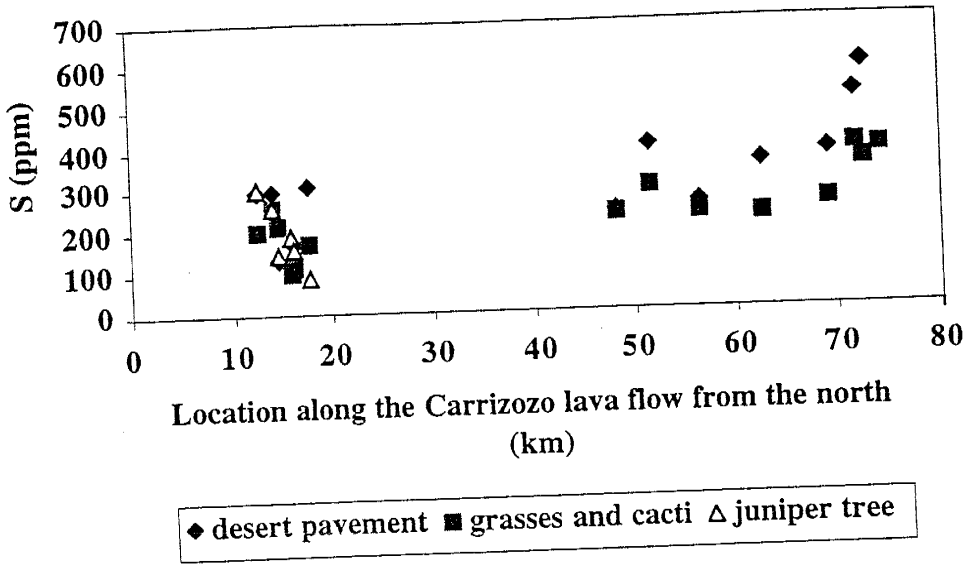

Figure 20. Sulfur (S ppm) along the Carrizozo lava flow, New Mexico. Zero represents the northernmost extreme of the lava flow and seventy-five represents the southernmost extreme. S increases in the south, toward the gypsum deposit of White Sands.

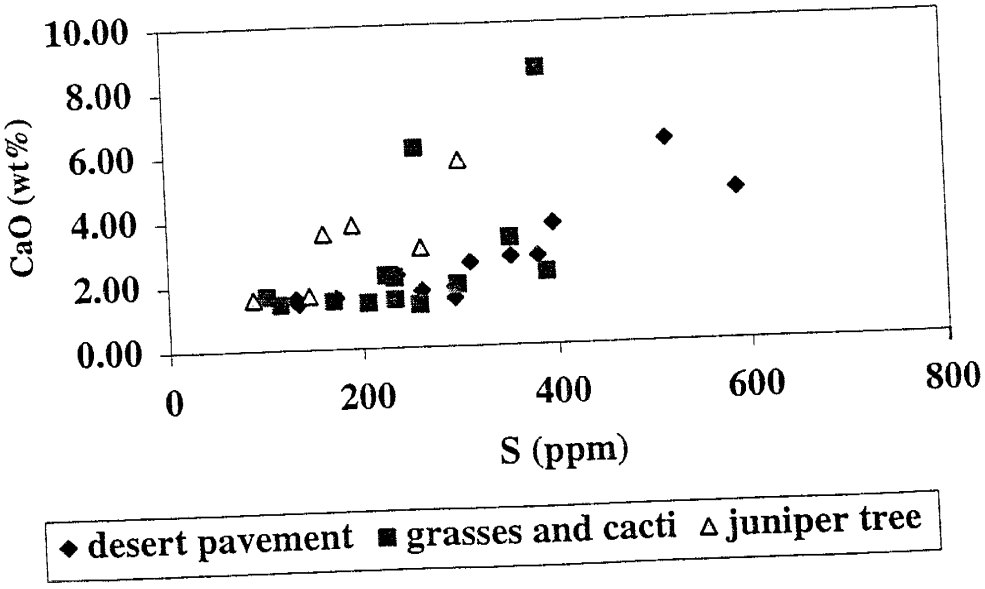

Figure 21. Correlation diagram of S (ppm) and CaO (wt%). Good correlation is exhibited. This is expected due to the evaporite gypsum in the south.

Table 12. Summary of the trace and rare earth element chemistry of the loess deposits on the Carrizozo lava flow, New Mexico. Samples were analyzed using instrumental neutron activation. Averages and standard deviations are provided. Analysis was only completed on bulk samples from the northern region.High standard deviations are attributed to $CaCO_3$ and LOI content.Averages are presented in ppm. Analytical data is presented in Appendix 9.3.12.

		Na_2O		Sc		Cr		FeO		Co		As		Br		Sb	
	n=	average	std dev	average	std dev	average	std dev	average	std dev	average	std dev	average	std dev	average	std dev	average	std dev
A	29	1.60	0.23	8.39	0.82	48	8	3.72	0.35	10.52	1.44	5.61	0.87	4.94	3.67	0.74	0.08
ND	8	1.67	0.16	9.06	0.68	52	6	3.98	0.27	11.26	1.22	5.72	0.63	3.39	1.46	0.80	0.08
NG	10	1.72	0.19	8.21	0.67	46	6	3.68	0.17	10.01	0.90	4.98	0.59	2.70	1.10	0.70	0.09
NJ	11	1.45	0.23	8.07	0.81	48	11	3.57	0.43	10.44	1.82	6.10	0.93	8.10	4.15	0.74	0.06

		Cs		Ba		La		Ce		Nd		Sm		Eu		Tb	
	n=	average	std dev	average	std dev	average	std dev	average	std dev	average	std dev	average	std dev	average	std dev	average	std dev
A	29	4.43	0.52	550	73	31.79	3.65	64.3	6.7	25.2	3.2	5.36	0.54	1.15	0.12	0.72	0.07
ND	8	4.90	0.47	572	52	34.38	3.13	69.4	5.0	27.2	3.0	5.84	0.41	1.24	0.09	0.80	0.04
NG	10	4.39	0.49	595	60	32.69	2.18	660.1	4.0	26.4	2.8	5.44	0.31	1.17	0.06	0.73	0.05
NJ	11	4.13	0.34	493	62	29.10	3.48	59.1	6.2	22.8	2.2	4.94	0.47	1.05	0.12	0.67	0.07

		Yb		Lu		Hf		Ta		W		Th		U	
	n=	average	std dev	average	std dev	average	std dev	average	std dev	average	std dev	average	std dev	average	std dev
A	29	2.77	0.33	0.42	0.05	9.83	1.24	1.16	0.17	1.13	0.34	9.36	1.00	2.62	0.39
ND	8	3.09	0.16	0.47	0.03	10.55	1.18	1.25	0.10	1.31	0.47	10.16	0.75	2.98	0.19
NG	10	2.83	0.18	0.43	0.03	10.13	0.80	1.22	0.10	1.10	0.20	9.57	0.67	2.69	0.26
NJ	11	2.50	0.31	0.39	0.04	9.04	1.25	1.03	0.20	1.02	0.30	8.59	0.88	2.31	0.36

A=	all samples
ND=	northern desert pavement
NG=	northern grasses and cacti
NJ=	northern juniper tree

6. DISCUSSION

6.1. Dust flux interpretations and comparisons:

Eolian dust transport involves three stages: entrainment, dispersion, and deposition. The nature of sediment transport by wind is controlled both by the nature of the airflow near the ground and by the properties of the ground surface over which the flow occurs (Pye, 1987). The deposition of eolian sediment is influenced by four processes: (1) wind velocity reduction, (2) particle trapping due to collision with rough, moist, or electrically charged surfaces, (3) formation of charged or aggregates which settle back to the ground, and (4) particles being washed out of atmospheric suspension by precipitation (Pye, 1987). The natural topographic variations of the Carrizozo lava flow surface provide an opportunity to evaluate the sources of these processes.

Depressions on the basalt flow surface act as catchments or basins for dust and water to accumulate in. As precipitation falls, dust and dissolved chemical constituents are carried out of atmospheric suspension onto the lava flow surface. The dust and dissolved chemical constituents are transported and deposited in the depressions by surface water flow. The dust accumulates and the water filters the dissolved chemical constituents through the existing accretionary mantle, leaching and re-depositing the dissolved chemical constituents into the existing soil profile.

Dust accumulation (loess) and thus soil development in the individual catchments varies as a function of time, shape, total surface area of the catchment, total surface area of the accumulation and depth. Eppes (1996) investigated the affect of shape and surface area of the catchment, on the thickness of the accumulation over a given time and constant dust flux. Given two depressions with similar shapes but different surface areas,

different thickness of eolian material will result. However, given three catchments with equal surface areas, dramatically different thickness of eolian material will occur depending on the catchment shape (Figure 22). The thickness of the eolian material affects the infiltration potential and thus the soil development.

For these reasons, the dust fluxes presented should be interpreted with caution. The catchments on the Carrizozo lava flow are natural, irregular in size and shape, and affected by surface cover and vegetation. To constrain the variability catchment to catchment, sampling was constrained to 2-6 m^2 area catchments and a conical shaped depression was assumed due to lava flow morphology. The dust flux values are valid approximations based on field measurements and the assumption of constant dust flux over 5,000 years. In addition, the methods of measuring the dust flux on the Carrizozo lava flow were obtained using different methods than previously published data, and should be taken into consideration when comparing data. The natural catchments are at ground level and probably yield higher dust flux values than those studies using elevated dust traps.

Using a constant dust flux based on field interpretations and constraining the sampling to 2-6 m^2 catchments, variability in dust flux is seen with different surface cover types. Average dust flux is highest in catchments containing the greater surface cover (i.e. juniper tree vs. desert pavement). In theory, dust deposition occurs as the airflow crosses a roughness boundary (Pye, 1987), in this case between bare lava flow surface and a juniper tree. At this roughness boundary, the roughness height (z_o= thin layer just above the surface in which the wind velocity is 0) is increased and may be

displaced upwards by a distance (d= the height of the juniper tree) (Tsoar and Pye, 1987; Figure 23). This reduces the wind velocity gradient above the juniper tree, and the critical value for re-suspension of settling grains is reduced. Therefore, it would be expected that the juniper tree is more efficient in trapping dust than the desert pavement. Reheis and Kihl (1995) also observed this phenomenon, where tall vegetation acted as a natural wind baffle, decreasing the wind velocity, increasing the dust deposition rate in dust traps in Southern Nevada and California.

For the purposes of comparison, all dust fluxes include the sand size fraction. The dust flux on the Carrizozo lava flow, in south-central New Mexico, ranges from 0.19 to 0.94 g/cm^2/ka (19 to 94 g/m^2/yr), averaging 0.54 g/cm^2/ka (54 g/m^2/yr). These values are very comparable to the dust fluxes observed in the southwestern United States and in similar desert climate environments around the world. Gile et al. (1981) collected dust in marbled traps elevated 30 to 90 cm above the ground, near Las Cruces, New Mexico. The dust flux ranged from 9.3 to 125.8 g/m^2/yr. In the lower Sonoran desert of Central Arizona, Pewe et al. (1981) estimated a flux of 54 g/m^2/yr. from periodic rooftop sampling over one year. In Israel, a similar desert environment, Yaalon and Dan (1974) estimated a loess accumulation rate of 50 to 200 g/m^2/yr. The dust flux on the Carrizozo lava flow are within the range of these three modern measurements, implying that there is no significant variation in dust fall in the last 5,000 years. However, these ranges are approximations and dust flux can be affected by seasonal influences of precipitation and temperature (Reheis and Kihl, 1995).

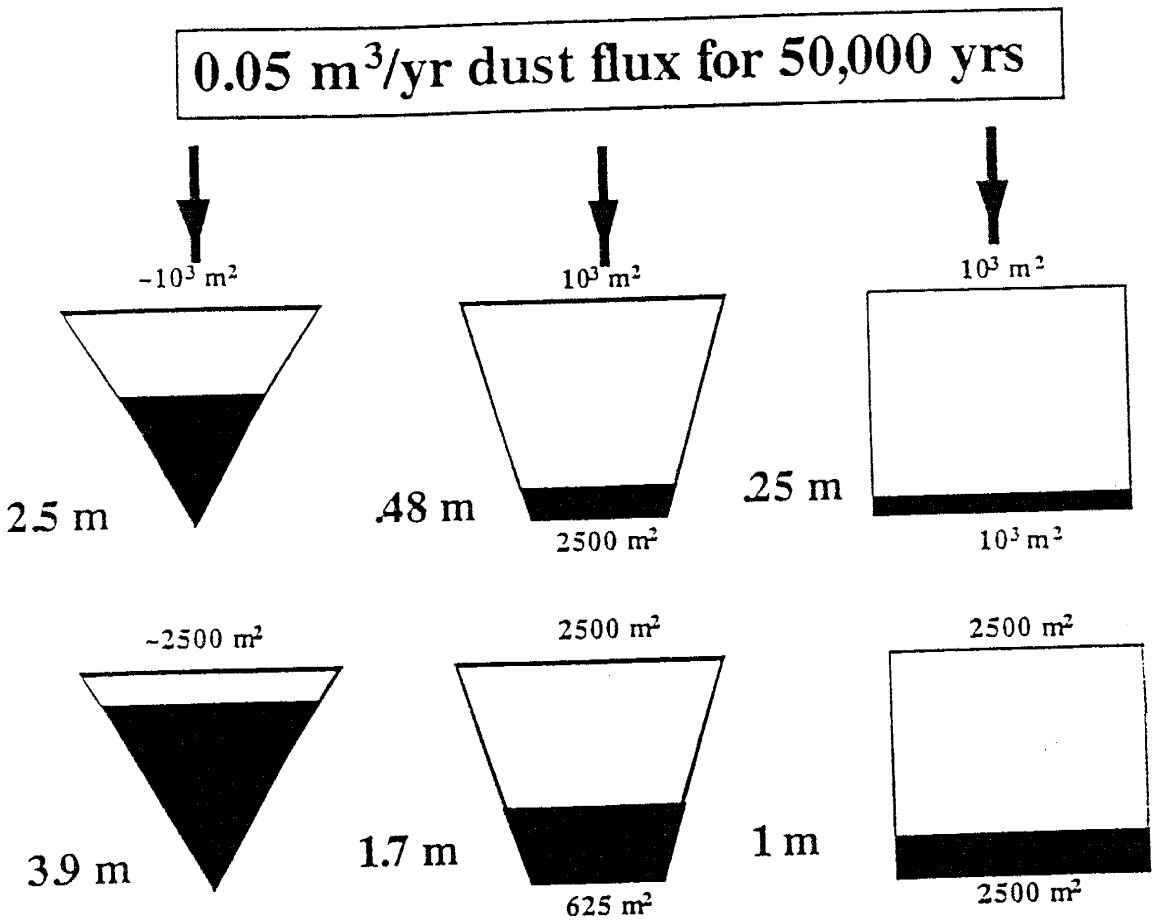

Figure 22. Differences in the depth of eolian mantle accumulated in depressions with different surface areas and shape. The rate of dust accumulation was assumed constant at 0.05 m^3 over a period of 5,000 years. Catchment areas for all depressions are equal. Figure taken from Eppes (1996).

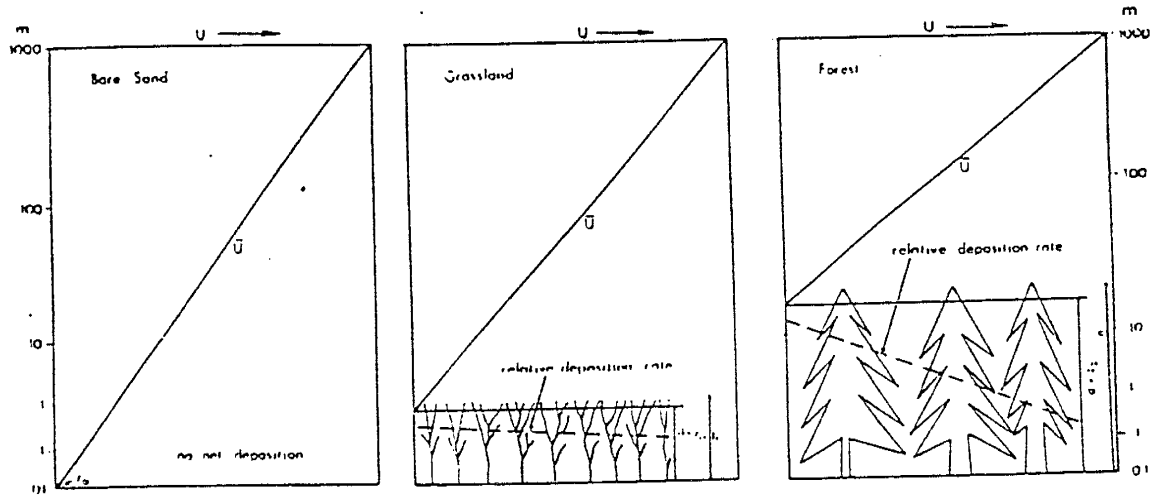

Figure 23. Character of the wind profile and schematic dust deposition pattern during passage of a dust cloud over bareground, grassland and forest. Taken from Tsoar and Pye (1987).

6.2. Pedogenesis in the Carrizozo loess deposits:

An important aspect of the loess deposits on the Carrizozo lava flow is the initial development of vesicular A horizons and the accumulation of organic matter. The vesicular A horizons were found only in southern desert pavement catchments, whereas the organic accumulations were found only in northern juniper tree catchments. The formation and development of these horizons influences the moisture content within soil profiles.

The formation of the vesicular A horizons results from the entrapment and incorporation of eolian dust beneath a stone pavement that affects infiltration and moisture content through the soil profile, with the production of large-sized pores (vesicles) (McFadden et al., 1986). The large pores allow the soil to take in large amounts of rainwater and runoff over a short period of time, facilitating the movement of water, clay, fine silt and soluble materials to deeper in the soil profile (Birkeland, 1984). Thus, the development of vesicular A horizons may increase the overall rate of leaching of material to below the vesicular A horizon into subjacent horizons, in this case the C horizon.

Organic matter is found in varying amounts in mineral soils and is composed of decomposed plant material (Birkeland, 1987). The organic accumulations are important to many soil properties such as the formation of soil structures and to the reactions that undergo during pedogenesis (Birkeland, 1984). During the formation of soil organic matter, large amounts of CO_2 and organic acids are produced, which increase the solubility of some ions in the soil environment. Organic matter also increases the water holding capacity of the soil (Birkeland, 1984).

This leaching and accumulation phenomenon influenced by the vesicular A horizons and organic accumulations can be evident in the concentrations of soluble salts, chloride, calcium carbonate, and calcium oxide with depth in the soil profile. The movement of the chemical constituents is dependent on mobility. Under "normal" soil environments the mobility would rank as the following: chloride > soluble salts > calcium carbonate > calcium oxide.

Chloride, in particular, is a hydrologically very mobile and chemically inert tracer used in evaluating soil water movement (Liu et al., 1995). As soils develop, the soil structure will change, as discussed previously, with the development of vesicular A horizons and the accumulation of organic matter. The development of these structures alters the movement of soil water and solutes within the soil profile. Chloride concentrations reflect soil-moisture content, as chloride concentrations increase when moisture decreases (Scanlon, 1991). In the soil environment, it would be typical to see the greatest chloride concentrations in the deeper portion of the soil profile, as chloride would move readily through the profile.

The chemical constituents within the soil profiles in the Carrizozo loess deposits do not behave according to their mobilities. Chemical variability with depth is seen to be dependent on surface cover type and location. The surface cover type influences the moisture regime within that soil profile and the location influences the influx of constituents. Therefore, affecting the resultant accumulations within each profile. The chloride concentrations are very low in concentration and discussion should be interpreted with caution. The movement of calcium carbonate through the soil profile is

evident, however high variability with depth occurs throughout all catchments and no trends are apparent.

6.2.1. Northern catchments:

In the desert pavement catchments, the highest soluble salt and CaO concentrations are found deepest in the soil profile, whereas the highest chloride concentration is found in the near surface samples. It is apparent through soluble salt and CaO accumulation, that the vesicular A horizons beneath the desert pavement surface cover facilitates the movement of the chemical constituents within the soil profile. However, one would also expect higher concentrations of chloride to be concentrated deeper in the soil profile. The high concentrations of chloride in near surface samples suggest a local change in hydrologic conditions within the catchment, influencing the chloride accumulation.

In catchments containing greater vegetation (juniper tree), the concentrations of soluble salts, chloride, and CaO are highest in the near surface of the soil profile. Thus, indicating that the height of the juniper tree preferentially traps material providing a greater influx of loess to the surface or a local change in hydrologic conditions within the profile due to the juniper tree, reduces the amount of moisture influx through the sol profile.

6.2.2. Southern catchments:

In the desert pavement catchments, the highest concentrations of soluble salts and chloride are found closest to the surface, whereas the highest CaO concentrations are

found in the deepest soils of the profiles. The high CaO concentrations deep in the soil profile suggests that movement of material down through the soil profile is occurring. However, a secondary imprinting is occurring with the higher concentrations of chloride and soluble salts in the near surface, possibly due to a local change in hydrologic conditions within the profile.

The overall chloride concentrations of the Carrizozo loess were compared to concentrations obtained from a study in the semi-arid, Sevilleta National Wildlife Refuge (SNWR), about 25 km north of Socorro, NM (Moore, 1997). Concentrations of chloride were determined from three different collectors over a six-month period: (1) dust collectors designed from Reheis and Kihl (1995), (2) wet-dry precipitation collectors and (3) soil columns designed of plastic piping. Chloride concentrations averaged 110 mg $Cl/m^2/yr$ within the dust collectors, 24 mg $Cl/m^2/yr$ within the precipitation collectors, and 29 mg $Cl/m^2/yr$ within the soil columns. The chloride concentrations from the SNWR are much higher than the average 7 mg $Cl/m^2/yr$ determined in the Carrizozo loess. The lower chloride concentrations in the Carrizozo loess suggests that chloride has moved through the soil profiles over the last 5,000 years.

However, the chloride concentration distributions within the soil columns of the SNWR study exhibit similar trends as the soil profiles in the Carrizozo loess. Similar trends with higher concentrations of chloride in near surface samples suggest an influx of chloride to the profile or column. Thus, the Carrizozo loess has undergone a temporal change in the hydrologic properties within the soil profiles over the last 5,000 years.

6.3. Effects of surface cover type on the physical and chemical nature of the loess deposits:

The texture of the Carrizozo lava flow loess deposits and the soluble salt and CaO concentrations are affected by surface cover type. Sand abundance, soluble salts and CaO concentrations are highest in the catchments containing greater surface cover (i.e. juniper tree vs. desert pavement). This is in part due to the height of the juniper tree, as previously discussed, and/or the organic litter trapping the saltating sand grains.

6.4. Spatial variability of loess deposits on the Carrizozo lava flow:

The chemical composition of the loess deposits varies spatially with location on the Carrizozo lava flow. Higher concentrations of soluble salts, chloride, $CaCO_3$, CaO, MgO, and S are observed in the south. These high concentrations differ with respect to proximity of source and are indicative of provenance effects. Differences in concentrations have been attributed to the influence of the local gypsum evaporite dune deposit of White Sands as well as influence of local dolomitic rocks in the San Andres Mountains due to dust transport by the southwestern prevailing winds.

6.5. The overall physical and chemical composition of the Carrizozo lava flow loess and comparisons:

The physical composition of the loess deposits are uniform over the Carrizozo lava flow. The grain-size distribution of the loess on the Carrizozo lava flow, however, varies compared to studies in the southwestern United States and around the world, and is dependent on the source of the material and the distance transported.

The texture of the soils on the three lava flows (Afton, Aden, and Little Black Mountain) of the Potrillo volcanic field (Eppes, 1996) varies with proximity to the Rio Grande River. The soils on the Little Black Mountain lava flow have higher sand content, averaging 71 %, as compared to the Afton (39%) and Aden (26%) lava flows, as well as within the deposits on the Carrizozo lava flow (28%). The Little Black Mountain lava flow is closest in proximity to the Rio Grande, and the grain size distribution is clearly affected by the influence of the river. The overall sand, silt, and clay content of the loess deposits on the Carrizozo lava flow, closely resemble the grain-size distribution found in the soils on the Aden lava flow of the Potrillo volcanic field.

The dust deposits in central Arizona contains lower sand values at about 8% and silt 78%, and clay 14% (Pewe et al., 1981). The lower sand values may be attributed to the sampling design. Samples collected from the rooftops of houses may not be influenced as much by the saltating sand grains commonly found on lower ground surfaces. Therefore, the sand content in the deposits would be lower in content.

Even though the chemical composition of the loess spatially varies along the Carrizozo lava flow, when the secondary calcium carbonate due to pedogenic processes is removed, the overall chemical composition of the loess is remarkably uniform. The averaged $CaCO_3$-free chemical compositions for the major elements were normalized to the North American Shale Composite standard [NASC] (Gromet et al., 1984), local crustal composition (Watrus, 1998), and the Carrizozo basalt (Renault, 1951) (Appendix 9.3.12.). A good correlation exists between the loess composition and the NASC and local crustal composition. However there is high deviation from the composition of the

basalt (Figure 24). Therefore, the loess must be derived from regional sources with the influence of local crustal sources, and not derived from the basalt itself.

The average major elements $CaCO_3$-free chemical composition of the loess deposits on the Carrizozo lava flow were compared to three soils developed on various aged lava flows in the Potrillo volcanic field in southwestern New Mexico (Figure 25, Appendix 9.3.8.). The soils were on the Aden (AD), Afton (AF) and Little Black Mountain (LBM) lava flows of 19 ka, 94 ka, and 184 ka age, respectively. The compositions were obtained from Eppes (1996) and were normalized to 100% on a $CaCO_3$-free basis. The soils developing on the Potrillo volcanic field are very similar in compositions to those on the Carrizozo lava flow. The Aden and Afton soils are the most similar in composition with positive deviations in CaO and MgO, and the older Little Black Mountain soils show slightly greater variability. The dust composition from locale to locale is remarkably uniform, indicating that the dust composition is of regional composition, but local sources due influence the composition.

The average $CaCO_3$-free loess composition for the trace and rare earth elements was normalized to the North American Shale Composite [NASC] (Gromet et al., 1984), and the local crustal composition (Watrus, 1998) (Appendix 9.3.13.). The rare earth chemistry is unavailable for the local crustal composition. A good correlation is exhibited with the NASC and slightly better correlation with the local crustal composition. Slight deviations are observed in the sulfur, zirconium, and halfnium (Figure 26) and may be attributed to the local volcanic rocks in the north. The trace and rare earth element chemistry, therefore suggests that the loess is derived from regional sources with the influence of local sources.

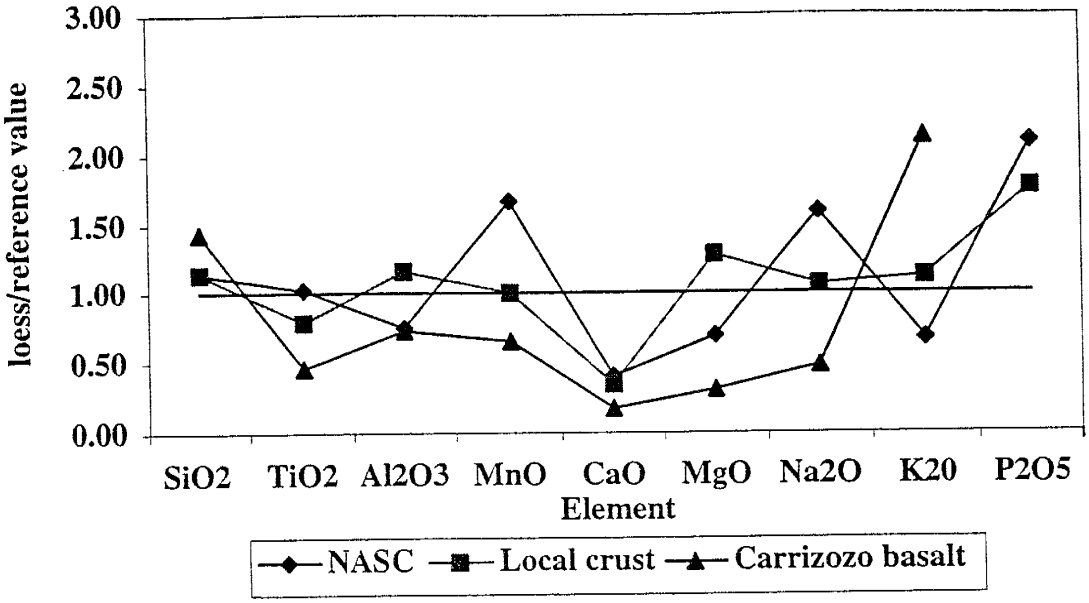

Figure 24. Loess chemistry normalized to the North American Shale Composite (Gromet et al., 1984), local crustal composition (Watrus, 1998), and the Carrizozo basalt (Renault, 1951). Good correlation is observed between the loess and NASC and local crustal composition. Greater deviation occurs between the loess and the composition of the Carrizozo basalt. Therefore, indicating the loess is of regional composition and not derived from the basalt.

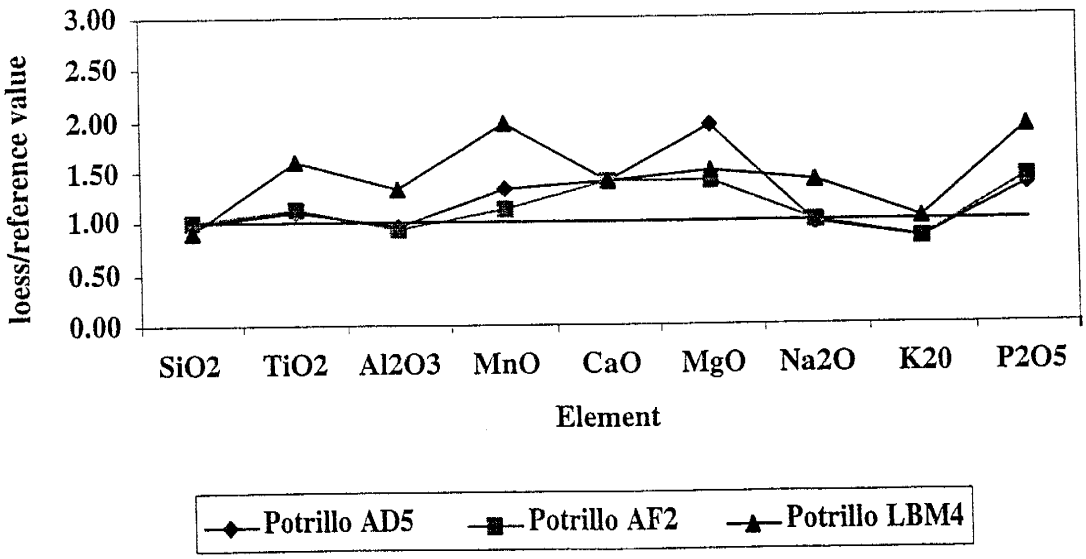

Figure 25. Loess chemistry normalized to the soils developing in eolian material on the Potrillo volcanic field. Good correlation is indicated with slight positive deviation in the the CaO and MgO, suggesting that the Carrizozo loess is influenced by local geology.

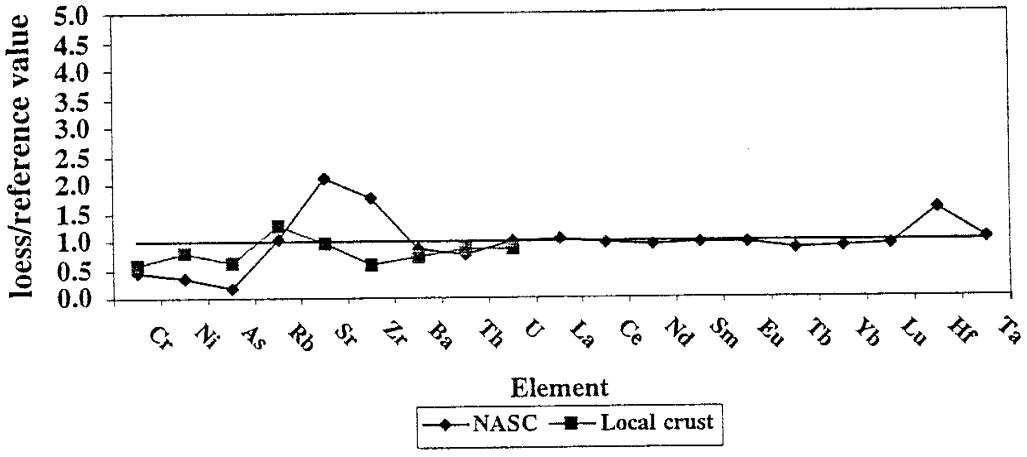

Figure 26. Loess chemistry normalized to the reference values of the North American Shale Composite and local crustal composition. Rare earth element chemistry is unavailable for the local crustal composition. Strong correlations exist, with only slight deviations in Zr and Hf from the NASC, however less variation exists with local crust.

7. CONCLUSION

Natural topographic variations in surface topography, southwestern prevailing winds, various local lithologies and the age constraint of 5,000 years, makes the Carrizozo lava flow an excellent setting for studying eolian dust deposits. The Carrizozo lava flow has provided the opportunity to evaluate abundance, physical and chemical composition of soils developing in the loess deposits over the last 5,000 years. Surface cover, provenance, and wind direction influences the physical and chemical composition and abundance of the loess deposits and these factors influence the degree of soil development.

On a small scale, chemical variability is observed with depth in the soil profiles as a function of surface cover type. Surface cover type influences the hydrologic conditions and thus the movement and accumulation of dissolved chemical constituent through the soil profile. It was observed that concentrations of soluble salts, chloride, $CaCO_3$ and CaO vary to some degree in the soil profiles. One would expect the solute (chloride), with greatest mobility, to be accumulated deepest in the soil profile. However, higher concentrations were found in near surface samples of all catchments, with the accumulation of less mobile solutes deeper in the soil profile. Thus, indicating an imprinting or change in the hydrologic conditions within the catchments is occuring.

Surface cover types not only affect the infiltration and movement of material but the influx of material as well. The greater the vegetative cover (i.e. juniper tree vs. desert pavement), the greater the concentrations of material and chemical constituents. As observed, the height of the juniper tree plays a role in decreasing the wind velocity,

subsequently increasing the deposition of material. The greater accumulation of tree litter effectively traps saltating grains, increasing surface concentrations.

On a large scale, the loess deposits spatially vary within the boundaries of the Carrizozo lava flow. Increased concentrations of MgO, CaO, S, soluble salts, chloride and $CaCO_3$ in the south are a result of the southwestern prevailing winds influencing the transportation of the evaporite gypsum dune deposit of White Sands and the erosional products of dolomitic rocks from the San Andres Mountains.

Overall, the abundance, physical and chemical composition of the loess deposits on the Carrizozo lava flow are remarkably uniform and comparable to local and regional studies. The eolian deposits do not show evidence of a change in dust flux. The average dust flux is very comparable to those found in the southwestern United States and in similar desert environments. The non-pedogenic chemical composition of the loess is very comparable to the regional shale standard, the local crustal composition, and to the soils developing in the eolian material on the Potrillo volcanic field. The chemistry varies significantly from the composition of the Carrizozo basalt, indicating indeed the material is not of basaltic origin.

This study has provided an initial baseline of the physical and chemical composition and abundance of young soils developing in loess deposits. The Carrizozo lava flow has provided an opportunity to investigate the spatial variability and remarkable uniformity of material that has been deposited and developed over 5,000 years and the affects and influences of surface cover type on the composition.

8. REFERENCES

Allen, K. 1951. The Carrizozo Malpais: Roswell Geological Society, Fifth Field Conference.Guidebook of Capitan-Carrizozo-Chupadera Mesa Region, Lincoln and Socorro Counties, New Mexico. 11pp.

Anthony, E., Hoffer, J. Williams, W. Poths, J., and Penn, B. 1998. Geochemistry and geochronology of Quaternary mafic volcanic rocks in the vicinity of Carrizozo, New Mexico. New Mexico Geological Society Guidebook, 49th Field Conference, Las Cruces. 117-122.

Bachman, G. and Machette, M. 1977. Calcic soils and calcretes in the southwestern United States. U.S. Geological Survey Open File Report. 77- 794. 163pp.

Berner, R. and Holdren, G, Jr. 1977. Mechanism of feldspar weathering: Some observational evidence. Geology. 5: 369-372.

Birkeland, P. 1987. Soils and Geomorphology. Oxford University Press, New York. 372pp.

Budding, A. 1964. Geologic outline of the Jicarilla Mountains, Lincoln County, New Mexico. New Mexico Geological Society, Fifteenth Field Conference, Ruidoso County. 82-86.

Dunbar, N. 1999. Cosmogenic 36-Cl determined age of the Carrizozo lava flows, south-central New Mexico. New Mexico Geology. in press.

Eppes, M. 1996. A spatial variability and chronosequence study of soils developing on basalt flows in the Potrillo volcanic field, southern New Mexico. M.S. Geology Thesis (unpublished). New Mexico Institute of Mining and Technology. 95pp

Eschrich, D. personal communication. White Sands Meterological Team-Forecast Station. White Sands Missile Range.

Faris, K. 1980. A geochemical model for the magmatic history of the Carrizozo basalt field, south-central New Mexico. MS Thesis (unpublished). New Mexico Institute of Mining and Technology. 168pp.

Gile, L. 1975. Holocene soils and soil geomorphic relations in an arid region of southern New Mexico. Quaternary Research. 5:321-360.

Gile, L. and Grossman, R. 1979. The desert soil project monograph: U.S. Department of Agriculture, Soil Conservation Service. 984pp.

Gile, L., Hawley, J., and Grossman, R. 1981. Soils and geomorphology in the Basin and Range area of New Mexico-Guidebook to the desert project. New Mexico Bureau of Mines and Mineral Resources Memoir. 39: 222.

Gromet, L., Dymek, R., Haskin, L., and Korotov, R. 1984. The North American Shale Composite: Its compilation, major and trace element characteristics. Geochimica et Cosmochimica Acta. 48: 2469-2482.

Hallett, R. and Kyle, P. 1993. XRF and INAA determinations of major and trace elements in Geological Survey of Japan Igneous and Sedimentary rock standards. Geostandards Newsletter. 17/1:127-133.

Harrison, J., McFadden, L., Weldon, R.1990. Spatial soil variability in the Cajon Pass chronosequence: Implications for the use of soils as a geomorphic tool. Geomorphology. 3:399-416.

Jacobs, J., Korotev, R., Blanchard, D., and Haskins, L. 1977. A well tested procedure for instrumental neutron activation analysis of silicate rocks and minerals. Journal of Radioanalytical Chemistry. 40:93-114.

Keszthelyi, L. and Pieri, D. 1993. Emplacement of the 75-km long Carrizozo lava flow field, south-central New Mexico. Journal of Volcanology and Geothermal Research. 59: 59- 75.

Kottlowski, F. 1955. Geology of the San Andres Mountains. New Mexico Geological Society, Sixth Field Conference, south-central New Mexico. 137-145.

Lattman, L. 1973. Calcium carbonate cementation of alluvial fans in southern Nevada. Geological Society of America Bulletin. 84: 3013- 3028.

Liu, B., Phillips, F., Hoines, S., Campbell, A., Sharma, P. 1995. Water movement in desert soil traced by hydrogen and oxygen isotopes, chloride, and chlorine-36, southern Arizona. Journal of Hydrology. 168:91-110.

Machette, M. 1985. Calcic soils of the southwestern United States *.In* Weide, D. (ed.): Soils and Quaternary geology of the southwestern United States. Geological Society of America Special Paper. 203: 23- 42.

McFadden, L. and Tinsley, J. 1985. The rate and depth of accumulation of pedogenic carbonate accumulation in soils: Formation and testing of a compartment model. *In* Weide, D. (ed.): Soils and Quaternary geology of the southwestern United States. Geological Society of America Special Paper. 203: 23- 42.

McFadden, L., Wells, S., and Dohrenwend, J. 1986. Influence of Quaternary climate changes on processes of soil development on desert loess deposits on the Cima volcanic filed, California. Catena. 13: 361- 389.

Moore, J.W. 1997. Monitoring infiltration of atmospheric chloride across the land surface in Central New Mexico. MS Hydrology Independent Study (unpublished). New Mexico Institute of Mining and Technology.pp

New Mexico Bureau of Mines and Mineral Resources (NMBMMR). 1982. New Mexico highway geologic map. Socorro, New Mexico.

Norrish, K. and Chappell, B. 1977. An accurate x-ray fluorescence spectrographic method for the analysis of a wide range of geologic samples. Geochimica Cosmochimica Acta. 33:67-76.

Norrish, K. and Hutton, J. 1969. X-ray fluorescence spectrometry : *in* Zussman (ed.) Physical methods in determinative mineralogy (2nd ed.) Academic Press. London.

Perhac, R. 1964. Resume of the geology of the Gallinas Mountains. New Mexico Geological Society, Fifteenth Field Conference, Ruidoso County. 87-91.

Pewe, T., Pewe, E., Pewe, R., Journaux, A., and Slatt, R. 1981. Desert dust; origin, characteristics, and effect on man. Geological Society of America Special Paper 186: 169-190.

Phillips, F., Dunbar, N., and Zreda, M. 1997. A test of chlorine-36 for dating of late Quaternary basaltic volcanos. EOS, Transactions of the American Geophysical Union. 78:F760.

Pye, K. 1987. Aeolian dust and dust deposits. Academic Press. London. 334pp

Reheis, M. 1990. Influence of climate and eolian dust on soil formation. Catena. 17: 219-248.

Reheis, M. and Kihl, R. 1995. Dust deposition in southern Nevada and California, 1984-1989: Relations to climate, source area, and source lithology. Journal of Geophysical Research. 100 (D5): 8893- 8918.

Reheis, M.,Goodmacher, J., Harden, J., McFadden, L., Rockwell, T., Shroba, R., Sowers, J., and Taylor, E. 1995. Quaternary soils and dust deposition in southern Nevada and California. Geological Society of America Bulletin. 107 (9): 1003-1022.

Renault, J. 1970. Major element variations in the Potrillo, Carrizozo and McCarty's Basalt fields, New Mexico. New Mexico Bureau of Mines and Mineral Resources Circular. 113:1-22.

Ruhe, R. 1984. Loess-derived soils, Mississippian Valley Region. Soil Science Society of America Journal. 48/4:864-867.

Salyards, S. 1991. A possible mid-Holocene age of the Carrizozo malpais from paleomagnetics using secular variation magnetostatigraphy. New Mexico Geological Society Guidebook, 42nd Field Conference, Sierra Blanca, Sacramento, Capitan Ranges. 153-157.

Scanlon, B. 1991. Evaluation of moisture flux from chloride data in desert soils. Journal of Hydrology. 128:137-156.

Shield, L. and Crispin, J. 1956. Vascular vegetation of a recent volcanic area in New Mexico. Ecology. 37(2): 341-351.

Shields, L. 1956 Zonation of vegetation within the Tularosa Basin, New Mexico. The Southwest Naturalist. 1(2): 49-68.

Singer, M. and Janitzky, P. (Eds). 1986. Field laboratory procedures used in a soil chronosequence study. Bulletin 1648. United States Geological Survey. Denver, Colorado.

Slate, J., Bull, W., Ku, T., Shatiqullah, M., Lynch, D., Huang, V. 1991. Soil- carbonate genesis in the Pinacate volcanic field, northwestern Sonora, Mexico. Quaternary Research. 35:400-416.

Smalley, I. 1966. The properties of glacial loess and the formation of loess deposits. Journal of Sedimentary Petrology. 36:669-676.

Soil Survey Staff. 1951. Soil Survey manual: Washington, D.C. U.S. Department of Agriculture. U.S. Government Printing Office, Agricultural Handbook 18.

Soil Survey Staff. 1975. Soil taxonomy: Washington, D.C. U.S. Department of Agriculture. U.S. Government Printing Office, Agricultural Handbook 436.

Thompson, T. 1964. A stratigraphic section of the Sierra Blanca volcanics in the Nogel Peak area, Lincoln County. New Mexico Geological Society, Fifteenth Field Conference, Ruidoso County. 76-78.

Tsoar, H. and Pye, K. 1987. Dust transport and the question of desert loess formation. Sedimentology. 34:139-153.

U.S. Department of Agriculture, Weather Bureau. Climatic summary of the United States, Section 29, southern New Mexico. Government Printing Office, Washington D.C.

Watrus, J. 1998. A regional geochemical atlas for part of Socorro County, New Mexico. MS Thesis (unpublished). New Mexico Institute of Mining and Technology. 123pp.

Weber, R. 1964. Geology of the Carrizozo quadrangle, New Mexico. New Mexico Geological Society, Fifteenth Field Conference, Ruidoso County. 100-104.

Weber, R. 1979. Valley of Fires. New Mexico Geology. 1/2:27.

Wells, S., Dohrenwend, J., McFadden, L., Turrin, B., Mahrer, K. 1985. Late Cenozoic landscape evolution on the lava flow surfaces of the Cima volcanic field, Mojave Desert, California. Geological Society of America Bulletin. 96:1518-1529.

Yaalon, D. and Dan, J. 1974. Accumulation and distribution of loess-derived deposits in the semi desert and desert fringe areas of Israel. Zeitschrift fur Geomorphologie, Supplement 20: 91-105.

Yaalon, D. and Ganor, E. 1973. The influence of dust on soils during the Quaternary. Soil Science. 116: 146- 155.

9. APPENDIX
9.1 Catchment types

9.1.1. Desert pavement

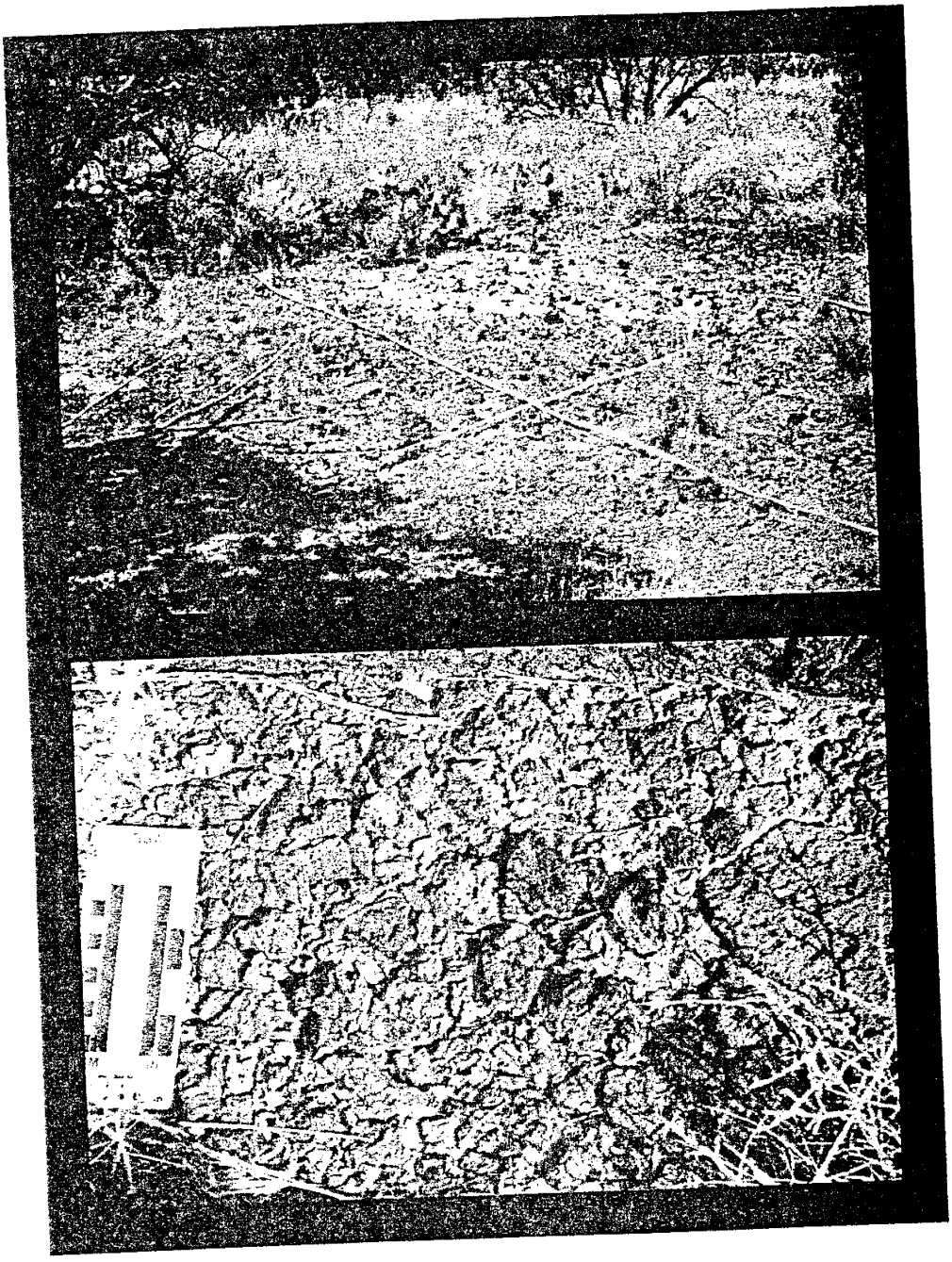

9.1.2. Grasses and cacti

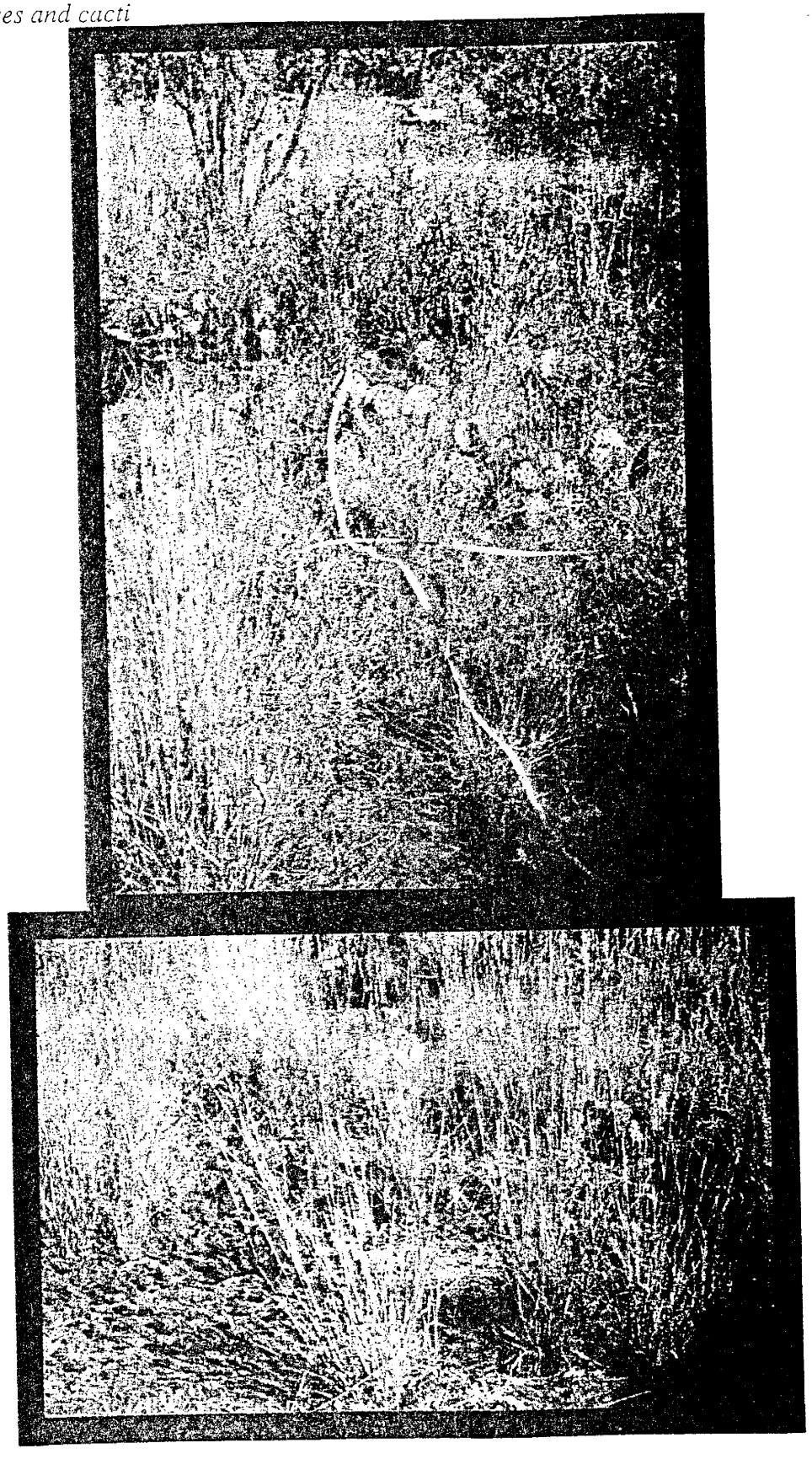

9.1.3. Juniper tree

9.2 Analytical Methods

9.2.1. Dust flux calculations

Dust flux was calculated using field measurements of catchment area, surface area, depth and bulk density. Factors of (1) constant flux over 5 ka and (2) a conical shaped depression was applied. Volume of accumulation was determined using the equation $V=1/3\prod r^2h$ (cm^3), where r= radius of accumulation and h= depth and then converted to grams using bulk density calculations ($g.cm^{-3}$). Area of catchment was taken into account by $\prod r^2$ (cm^2), where r= radius of catchment. Volume with respect to area and 1 ka was used to determine the dust flux ($g.cm^{-2}.ka^{-1}$).

9.2.2. Particle Size Settling Tube Method

Prior to the particle size procedure, organic matter from the northern samples was removed by the organic matter digestion method (Singer and Janitzky, 1986). Approximately 25 g of soil sample was placed in a 250 ml beaker and put into suspension. Approximately 5 ml of 30% hydrogen peroxide (H_2O_2) was added until the reaction subsided and organic matter with binded soil particles was removed. Excess hydrogen peroxide was removed by heating for approximately 1 hr. after final addition of peroxide. Sample was dried in oven.

20 g of dried digested sample was placed into a 125 ml Erlenmeyer flask. 50 ml of 10% sodium pyrophosphate and 30 ml of deionized water (DI-H_2O) was added to the flask, capped and shaken on a mechanical shaker for 4 hrs. A blank was prepared following the same procedure.

The clay and silt fractions were wt sieved using DI-H_2O through a 63 um sieve into 1200 ml fleakers. Sand fraction was washed into known weight beaker and dried.

Fleakers were filled to 1200 ml, capped and shaken vigorously for 30-45 seconds at distinct 2 minute intervals. Fleakers were allowed to settle for 8-9 hr depending on room temperature in order to allow the greater than 2 um material to settle below the 10 cm depth. 25 ml aliquot of clay suspension was collected at the 10 cm depth and placed in appropriate weighed dish for drying.

9.2.3. Electron Microprobe Analysis

Homogeneous unconsolidated samples were attached to a 1 inch round disc by carbon tape. Sample discs were carbon-coated and run on the SX-100 electron microprobe using backscatter electron and scanning electron modes. Images were taken of grain morphology.

9.2.4. X-ray Diffractometry

Two oriented clay slides of each sample was prepared for analysis of clay minerals on the x-ray diffractometer. 20-25g of homogeneous sample was placed into suspension with di H_2O for 5 minutes and remixed. Di H_2O was added and removed until clay was in a dispersed state. The less than 2 um fraction was decanted from the surface of the suspension and placed onto a glass slide and allowed to air dry. The air-dried slides were first analyzed at 2° 2Θ/minute from 2° to 38° 2Θ with Cu Kα radiation. The slides were then placed in a closed dessicator with ethylene glycol for 24 hrs. The slides were analyzed from 2° to 15° 2Θ. Thirdly, the clay slides were heated at 350° for 30 minutes. The heated slide was analyzed twice, (1) from 8.5° to 9.8° 2Θ and (2) 2° to 15° 2Θ.

Bulk mineralogy was preformed on the same samples using the random oriented sample. The whole sample was packed into a sample holder to achieve a non-oriented sample. Samples were analyzed from 5° to 70° 2Θ for bulk mineralogy.

The basal spacing (2Θ) used for the various clay mineral groups are as follows:

chlorite	6.2-6.3
kaolinite	12.4
gypsum	11.5
calcite	29.4
feldspar	27-28
quartz	26.6-26.8
Ca smectite	5.7
Na smectite	7.1

9.2.5. Electrical Conductivity

Sample preparation followed the procedures of Singer and Janitzky (1986). Approximately 10 g of air-dried soil and 50 ml of deionized water (diH_2O) was placed into a plastic test tube with cap and shaken on a mechanical shaker for 30 minutes. Solution was filtered in a Buchner funnel over a vacuum flask and extract was saved in another plastic test tube. Conductivity was measured on the extract using the conductivity meter.

9.2.6. Chittick Method

Sample preparation followed the procedures of Singer and Janitzky (1986). Approximately 7.5- 10 g of powdered (80 mesh) oven-dry sample was placed in a flask with a magnetic stirring rod and attached to the Chittick apparatus. While agitating the flask contents, 10 ml of 6 N hydrochloric acid (HCl) was introduced to the sample. Gas that is liberated during a 5 minute interval is measured by leveling a bulb on the

apparatus. Calcium carbonate is calculated from the volume of evolved gas, dry sample weight, and the molecular weight of the carbonate mineral.

9.2.7. X-ray fluorescence spectrometry

Fused glass discs and pressed powdered pellets were made for analysis of major and trace element chemistry by x-ray fluorescence spectrometry on the Philips' PW2400 WD-XRF spectrometer. Preparation methods followed Norrish and Hutton (1969).

The first procedure was to determine flux loss in order to ensure high quality analysis. Approximately 2 to 4 g of flux was placed into a known weight Pt (95%Pt/ 5% Au) crucible and fused on the Spartan Fusion Instrument. Flux loss was determined by the flux weight loss divided by the weight of the flux times 100 to achieve a percentage.

Preparation of glass fusion discs included combining 1.0 g of sample with approximately 6 g of flux (adjusted for flux loss), 0.05 g of LiBr, and 0.05 g of NH_4NO_3 ($LiNO_3$ for southern samples) into the Pt crucibles. The mixture is heated and fused on the fusion instrument and cooled in a casting dish. An in-house standard and a personal standard were prepared for each analytical run.

The pressed powdered pellets were prepared following the methods of Norrish and Chappell (1977). Approximately 7 g of samples and 7 drops of binder (2% polyvinyl alcohol) were pressed at 10 tons with a boric acid backing.

Loss on ignition was also conducted (Hallett and Kyle, 1993). Approximately 2-4 g of sample was placed into a ceramic crucible. The crucibles were placed in a high temperature furnace and were heated to 1000^{0}C for approximately 4 to 5 hours. Loss on ignition was calculated by the weight of crucible and sample minus the weight after 1000^{0}C divided by the weight of the sample times 100.

9.2.8. Instrumental Neutron Activation Analysis

Approximately 80 to 100 g of sample were loaded into clean, high-purity silica (suprasil) vials, sealed and washed in acetone. (Jacobs et al., 1977). The vials were packed and wrapped in aluminum foil and aligned along the inside wall of a 3.35 inch irradiation container and sent for irradiation at the University of Missouri research reactor. Samples were counted on two coaxial, p-type, high Ge detector at New Mexico Institute of Mining and Technology.

Appendix 9.3.1. Soil descriptions of the loess deposits on the Carrizozo lava flow, New Mexico

Northern Samples #	Color (dry) hue value/chroma	Color (moist) hue value/chroma
CLF-8-D (0-3)	7.5 YR 4/4	7.5 YR 3/4
CLF-8-D(3-6)	7.5 YR 4/6	7.5 YR 3/4
CLF-8-D(6+)	7.5 YR 4/4	7.5 YR 3/4
CLF-8-G(0-5)	7.5 YR 4/4	7.5 YR 3/4
CLF-8-G(5-10)	7.5 YR 4/4	7.5 YR 3/3
CLF-8-J(0-2)	7.5 YR 3/2	7.5 YR 2.5/2
CLF-8-J(2-5)	7.5 YR 3/2	7.5 YR 2.5/2
CLF-7-D(0-5)	7.5 YR 4/4	7.5 YR 3/4
CLF-7-D(5-10)	7.5 YR 4/4	7.5 YR 3/3
CLF-7-D(10+)	7.5 YR 4/4	7.5 YR 3/4
CLF-7-G(0-5)	7.5 YR 4/4	7.5 YR 3/3
CLF-7-G(5-10)	7.5 YR 4/4	7.5 YR 3/3
CLF-7-G(10-15)	7.5 YR 4/4	7.5 YR 3/3
CLF-7-G(15+)	7.5 YR 4/4	7.5 YR 3/3
CLF-7-J(0-5)	7.5 YR 3/2	7.5 YR 2.5/2
CLF-7-J(5-10)	7.5 YR 3/2	7.5 YR 2.5/2
CLF-7-J(10-15)	7.5 YR 3/4	7.5 YR 2.5/3
CLF-6-D(0-3)	7.5 YR 4/4	7.5 YR 3/3
CLF-6-D(3-5)	7.5 YR 4/4	7.5 YR 3/4
CLF-6-G(0-4)	7.5 YR 5/4	7.5 YR 3/4
CLF-6-G(4-10)	7.5 YR 5/4	7.5 YR 3/4
CLF-6-G(10+)	7.5 YR 4/4	7.5 YR 3/3
CLF-6-J(0-5)	7.5 YR 3/3	7.5 YR 2.5/2
CLF-6-J(5-10)	7.5 YR 3/4	7.5 YR 2.5/2
CLF-5-D(0-5)	7.5 YR 4/6	7.5 YR 3/4
CLF-5-D(5-10)	7.5 YR 4/4	7.5 YR 2.5/3
CLF-5-D(10+)	7.5 YR 4/4	7.5 YR 2.5/3
CLF-5-G(0-5)	7.5 YR 4/4	7.5 YR 3/3
CLF-5-G(5-10)	7.5 YR 4/4	7.5 YR 2.5/3
CLF-5-G(10+)	7.5 YR 3/4	7.5 YR 2.5/3
CLF-5-J(0-5)	7.5 YR 3/1	7.5 YR 2.5/1
CLF-5-J(5-10)	7.5 YR 3/2	7.5 YR 2.5/2
CLF-11-D	7.5 YR 4/6	7.5 YR 3/4
CLF-11-G(0-5)	7.5 YR 4/4	7.5 YR 3/3
CLF-11-G(5-10)	7.5 YR 4/4	7.5 YR 3/4
CLF-11-J(0-5)	7.5 YR 3/3	7.5 YR 2.5/3
CLF-11-J(5-10)	7.5 YR 3/4	7.5 YR 2.5/3
CLF-10-D	7.5 YR 4/4	7.5 YR 3/2
CLF-10-G(0-5)	7.5 YR 4/4	7.5 YR 3/2
CLF-10-G(5-10)	7.5 YR 4/4	7.5 YR 3/4
CLF-10-J(0-5)	7.5 YR 2.5/3	7.5 YR 2.5/1
CLF-10-J(5-10)	7.5 YR 2.5/3	7.5 YR 2.5/2
CLF-1-D	7.5 YR 3/2	7.5 YR 2.5/2
CLF-1-G	7.5 YR 4/4	7.5 YR 3/4
CLF-1-J	7.5 YR 3/3	7.5 YR 2.5/2
CLF-2-D	7.5 YR 4/3	7.5 YR 3/2
CLF-2-G	7.5 YR 4/4	7.5 YR 3/3
CLF-2-J	7.5 YR 3/2	7.5 YR 2.5/2
CLF-3-D	7.5 YR 4/4	7.5 YR 3/4
CLF-3-G	7.5 YR 4/6	7.5 YR 3/4
CLF-3-J	7.5 YR 3/3	7.5 YR 2.5/2
CLF-4-D	7.5 YR 5/4	7.5 YR 4/4
CLF-4-G	7.5 YR 4/3	7.5 YR 3/3
CLF-4-J	7.5 YR 3/4	7.5 YR 2.5/3

Southern Samples #	Color (dry) hue value/chroma	Color (moist) hue value/chroma
CLF-12-D	7.5 YR 3/3	7.5 YR 4/4
CLF-12-G(0-5)	7.5 YR 4/4	7.5 YR 3/3
CLF-12-G(5-10)	7.5 YR 4/4	7.5 YR 2.5/3
CLF-12-G(10+)	7.5 YR 4/4	7.5 YR 2.5/3
CLF-13-D(0-5)	7.5 YR 5/4	7.5 YR 3/4
CLF-13-D(5-10)	7.5 YR 5/4	7.5 YR 3/4
CLF-13-D(10+)	7.5 YR 5/4	7.5 YR 3/4
CLF-13-G(0-5)	7.5 YR 5/4	7.5 YR 3/3
CLF-13-G(5-10)	7.5 YR 5/4	7.5 YR 3/3
CLF-13-G(10+)	7.5 YR 4/4	7.5 YR 3/3
CLF-18-D(0-2)	7.5 YR 5/6	7.5 YR 3/4
CLF-18-D(2-4)	7.5 YR 4/6	7.5 YR 3/4
CLF-18-D(4+)	7.5 YR 4/6	7.5 YR 3/4
CLF-18-G(0-2)	7.5 YR 4/4	7.5 YR 3/4
CLF-18-G(2-4)	7.5 YR 4/4	7.5 YR 3/4
CLF-18-G(4+)	7.5 YR 4/6	7.5 YR 3/3
CLF-19-D(0-2)	7.5 YR 5/6	7.5 YR 4/6
CLF-19-D(2-4)	7.5 YR 5/6	7.5 YR 4/6
CLF-19-D(4+)	7.5 YR 5/4	7.5 YR 4/4
CLF-19-G(0-3)	7.5 YR 4/6	7.5 YR 3/3
CLF-19-G(3-6)	7.5 YR 4/6	7.5 YR 3/4
CLF-19-G(6+)	7.5 YR 4/4	7.5 YR 3/4
CLF-14-D(0-3)	7.5 YR 5/4	7.5 YR 3/4
CLF-14-D(3-6)	7.5 YR 5/6	7.5 YR 3/4
CLF-14-D(6+)	7.5 YR 5/4	7.5 YR 3/4
CLF-14-G(0-5)	7.5 YR 4/3	7.5 YR 2.5/2
CLF-14-G(5-10)	7.5 YR 4/3	7.5 YR 2.5/2
CLF-14-G(10+)	7.5 YR 4/3	7.5 YR 2.5/2
CLF-15-D(0-5)	7.5 YR 5/4	7.5 YR 3/4
CLF-15-D(5-10)	7.5 YR 6/4	7.5 YR 3/4
CLF-15-D(10+)	7.5 YR 5/4	7.5 YR 3/4
CLF-15-G(0-3)	7.5 YR 4/6	7.5 YR3/4
CLF-15-G(3-6)	7.5 YR 4/6	7.5 YR 3/4
CLF-15-G(6+)	7.5 YR 4/6	7.5 YR 3/4
CLF-16-D(0-2)	7.5 YR 5/6	7.5 YR 4/6
CLF-16-D(2-4)	7.5 YR 6/4	7.5 YR 4/4
CLF-16-D(4+)	7.5 YR 6/4	7.5 YR 4/4
CLF-16-G(0-5)	7.5 YR 4/4	7.5 YR 3/4
CLF-16-G(5-10)	7.5 YR 5/4	7.5 YR 3/4
CLF-16-G(10-20)	7.5 YR 5/4	7.5 YR 3/4
CLF-16-G(20+)	7.5 YR 5/4	7.5 YR 3/4
CLF-17-D(0-3)	7.5 YR 6/4	7.5 YR 4/4
CLF-17-D(3-6)	7.5 YR 5/4	7.5 YR 4/4
CLF-17-D(6+)	7.5 YR 6/4	7.5 YR 4/4
CLF-17-G(0-3)	7.5 YR 4/4	7.5 YR 3/4
CLF-17-G(3-6)	7.5 YR 5/4	7.5 YR 4/4
CLF-17-G(6+)	7.5 YR 6/4	7.5 YR 4/4

7.5 YR 6/3-6/4	light brown
7.5 YR 5/2-5/4	brown
7.5 YR 4/2-4/4	brown
7.5 YR 3/2-3/4	dark brown
7.5 YR 2.5/2-2.5/4	very dark brown
7.5 YR 2.5/1	black
7.5 YR 5/6-5/8	strong brown
7.5 YR 4/6-4/8	strong brown
7.5 YR 3/6-3/8	strong brown
7.5 YR 2.5/6-2.5/8	strong brown

Appendix 9.3.2. Sample locations with respect to distance from the northern extreme of the Carrizozo lava flow, New Mexico. Latitude and longitude is also provided for each sample location.

Sample #	Location		Latitude	Longitude
(CLF)	(miles)	(km)		
8	4.5	7.24	N33 47.756	W105 57.784
7	4.8	7.64	N33 47.704	W105 57.532
6	5.3	8.45	N33 46.418	W105 54.531
5	5.5	8.85	N33 46.280	W105 54.209
11	7.0	11.27	N33 41.717	W105 55.604
10	7.8	12.47	N33 41.567	W105 55.604
1	8.8	14.08	N33 42.622	W105 57.142
2	9.0	14.48	N33 42.233	W105 56.623
3	9.8	15.69	N33 41.722	W105 55.996
4	10.0	16.09	N33 40.845	W105 55.116
12	29.0	46.67	N33 30.288	W106 09.410
13	31.0	49.89	N33 26.341	W106 09.457
18	34.8	55.92	N33 24. 838	W106 09.039
19	38.0	61.15	N33 23.759	W106 08.860
14	43.0	69.20	N33 20.361	W106 18.026
15	44.5	71.61	N33 19.907	W106 18.724
16	45.0	72.42	N33 15.749	W106 18.164
17	46.0	74.03	N33 18.078	W106 19.006

9.3.3. Bulk mineralogy of loess samples from the Carrizozo lava flow, New Mexico. Diffractograms illustrate bulk mineralogy.

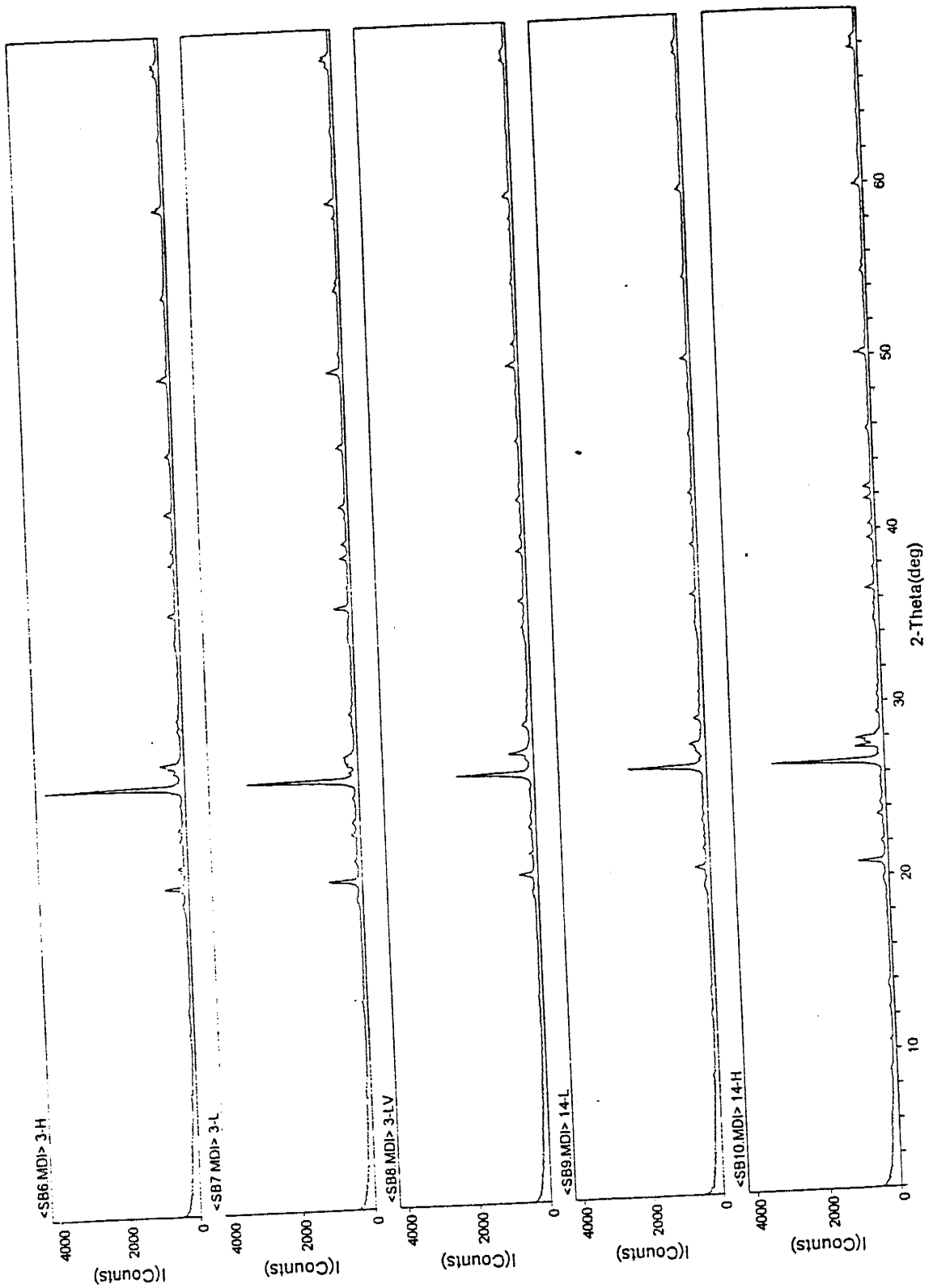
<SB6.MDI> 3-H
<SB7.MDI> 3-L
<SB8.MDI> 3-LV
<SB9.MDI> 14-L
<SB10.MDI> 14-H
I(Counts)
4000
2000
0
10
20
30
40
50
60
2-Theta(deg)

9.3.4. Clay mineralogy of the loess samples from the Carrizozo lava flow, New Mexico. Diffractograms illustrate the air, gycolated and heated experimental analyses.

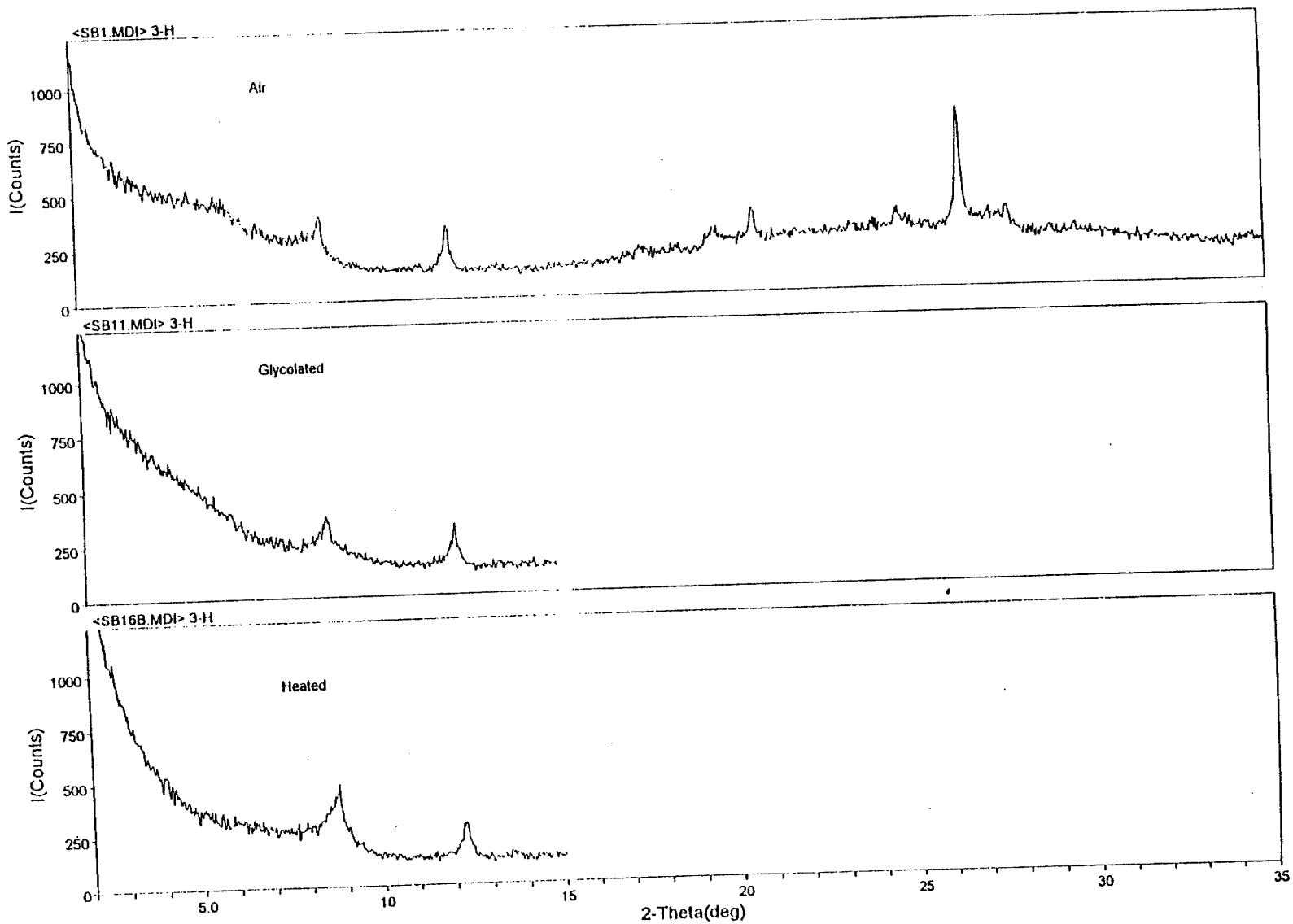
<SB1.MDI> 3-H
Air
I(Counts)
1000
750
500
250
0
<SB11.MDI> 3-H
Glycolated
I(Counts)
1000
750
500
250
0
<SB16B.MDI> 3-H
Heated
I(Counts)
1000
750
500
250
0
5.0
10
15
20
25
30
35
2-Theta(deg)

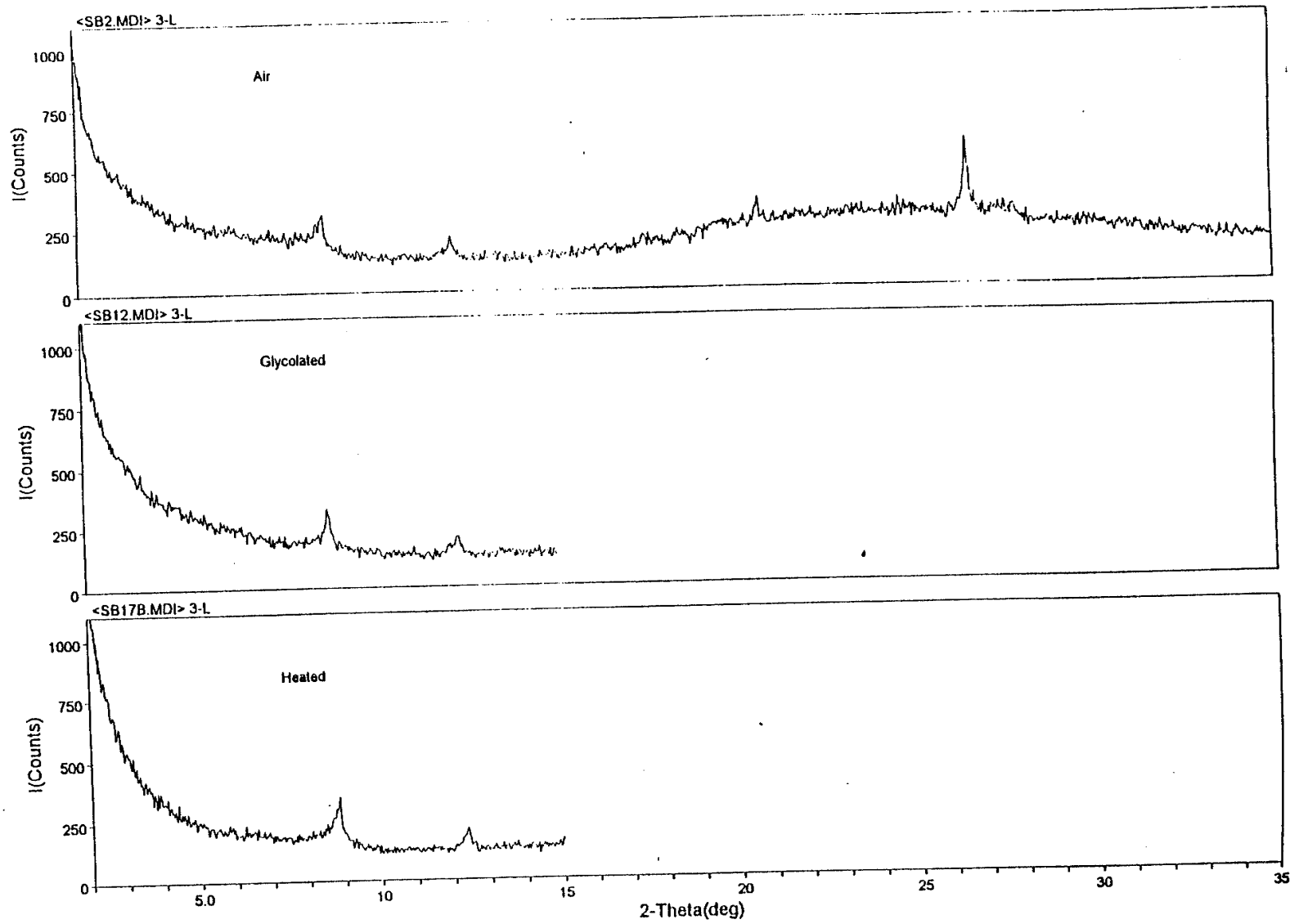
<SB2.MDI> 3-L
Air
I(Counts)
1000
750
500
250
0
<SB12.MDI> 3-L
Glycolated
I(Counts)
1000
750
500
250
0
<SB17B.MDI> 3-L
Heated
I(Counts)
1000
750
500
250
0
5.0
10
15
20
25
30
35
2-Theta(deg)

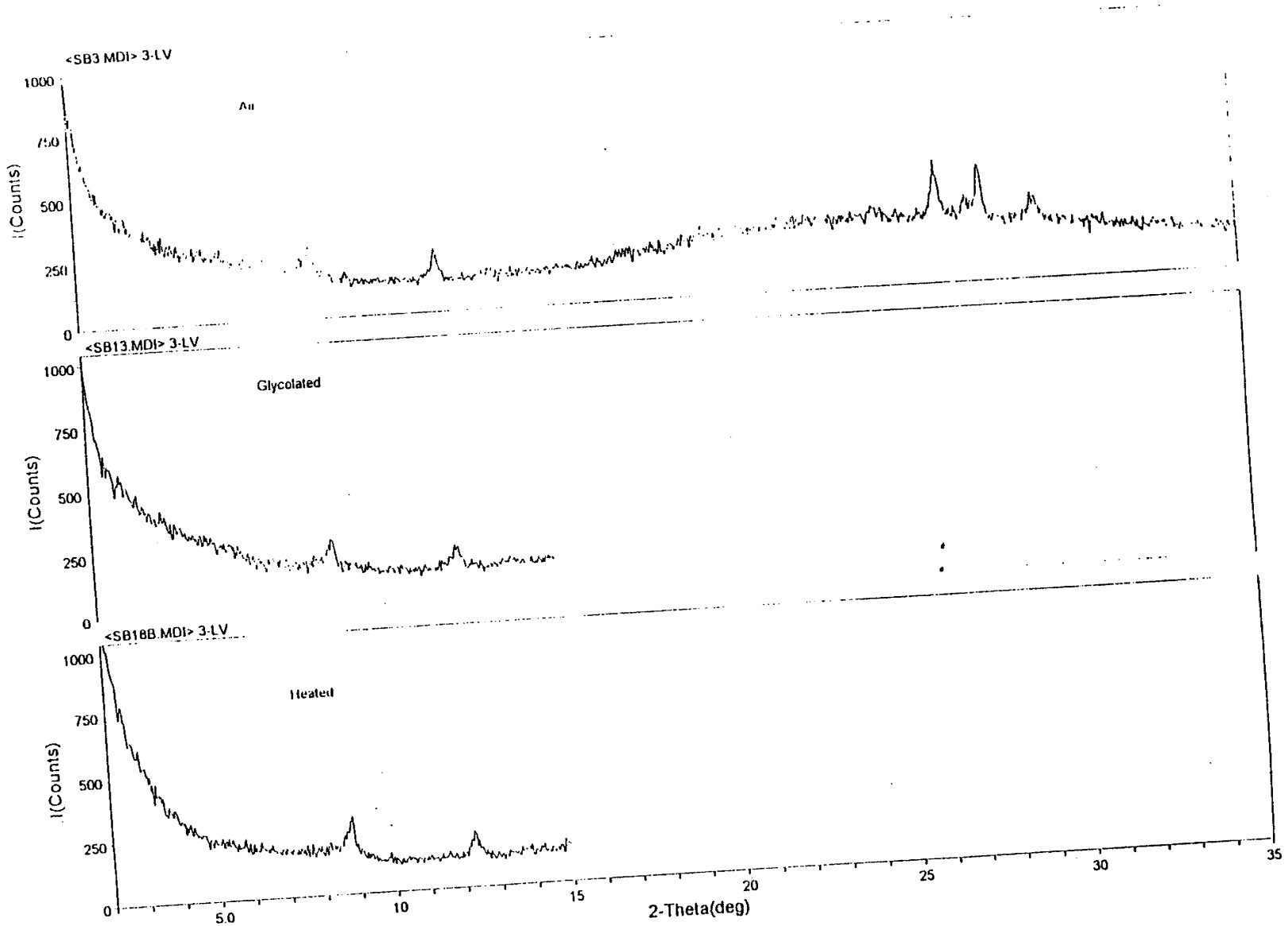
<SB3.MDI> 3-LV
Air
I(Counts)
1000
750
500
250
0
<SB13.MDI> 3-LV
Glycolated
I(Counts)
1000
750
500
250
0
<SB18B.MDI> 3-LV
Heated
I(Counts)
1000
750
500
250
0
5.0
10
15
20
25
30
35
2-Theta(deg)

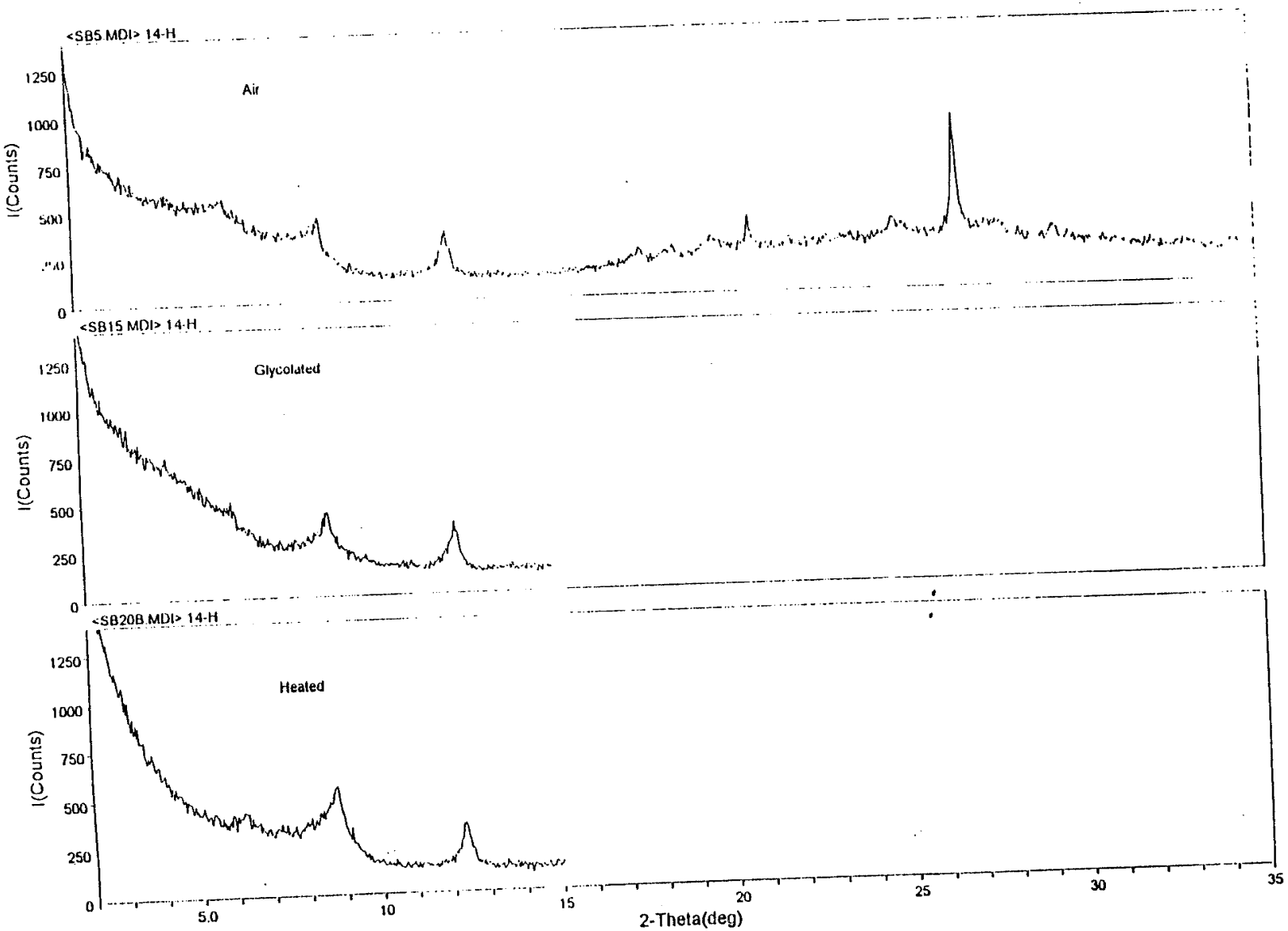
<SB5 MDI> 14-H
Air
<SB15 MDI> 14-H
Glycolated
<SB20B MDI> 14-H
Heated
I(Counts)
1250
1000
750
500
250
0
5.0
10
15
20
25
30
35
2-Theta(deg)

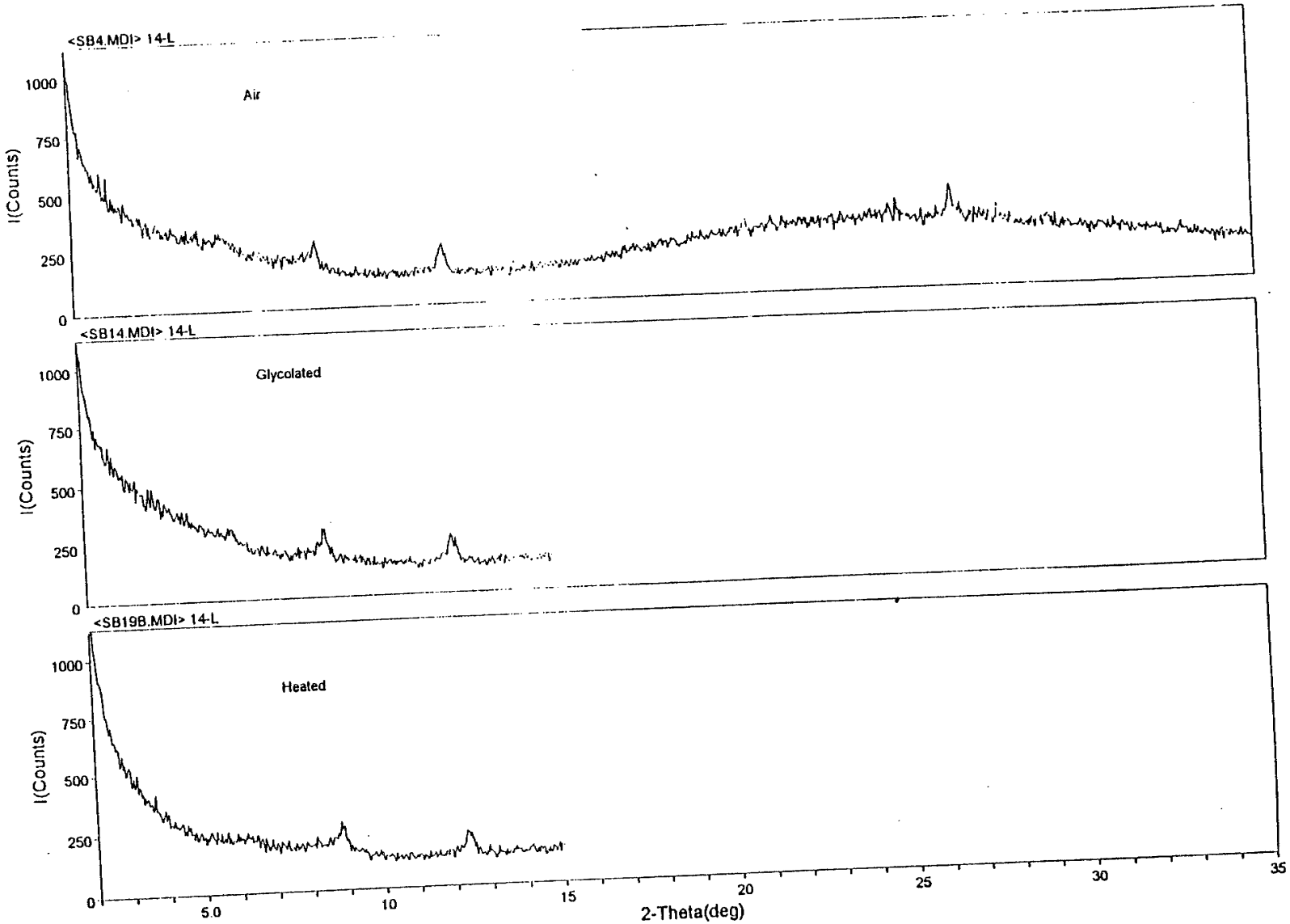
<SB4.MDI> 14-L
Air
I(Counts)
1000
750
500
250
0
<SB14.MDI> 14-L
Glycolated
I(Counts)
1000
750
500
250
0
<SB19B.MDI> 14-L
Heated
I(Counts)
1000
750
500
250
0
5.0
10
15
20
25
30
35
2-Theta(deg)

Appendix 9.3.5. Soluble Salt concentrations in the loess deposits on the Carrizozo lava flow, New Mexico.Samples were analyzed using electrical conductivity.

Northern Sample #	Soluble Salts (%)
CLF-8-J (0-2)	0.18
CLF-8-J(2-5)	0.15
CLF-7-D	0.09
CLF-7-D(0-5)	0.07
CLF-7-D(5-10)	0.06
CLF-7-D(10+)	0.08
CLF-7-G	0.10
CLF-7-G (0-5)	0.08
CLF-7-G(5-10)	0.08
CLF-7-G(10-15)	0.09
CLF-7-G(15-23)	0.09
CLF-7-J	0.22
CLF-7-J(0-5)	0.50
CLF-7-J(5-10)	0.30
CLF-7-J(10-15)	0.16
CLF-7-J(15-20)	0.14
CLF-6-D(0-3)	0.09
CLF-6-D(3-5)	0.09
CLF-6-G(0-4)	0.07
CLF-6-G(4-10)	0.06
CLF-6-G(10-14)	0.06
CLF-6-J(0-5)	0.17
CLF-6-J(5-10)	0.21
CLF-5-D(0-5)	0.06
CLF-5-D(5-10)	0.07
CLF-5-D(10-15)	0.09
CLF-5-G(0-5)	0.05
CLF-5-G(5-10)	0.07
CLF-5-G(10-15)	0.10
CLF-5-J(0-5)	0.27
CLF-5-J(5-10)	0.19
CLF-11-D	0.06
CLF-11-G(0-5)	0.14
CLF-11-G(5-10)	0.09
CLF-11-J(0-5)	0.21
CLF-11-J(5-10)	0.21
CLF-10-G(0-5)	0.19
CLF-10-G(5-10)	0.10
CLF-10-J(0-5)	0.33
CLF-10-J(5-10)	0.26
CLF-1-D	0.06
CLF-1-G	0.11
CLF-1-J	0.21
CLF-4-D	0.14
CLF-4-G	0.09
CLF-4-J	0.17

Southern Sample #	Soluble Salts (%)
CLF-12-D	0.16
CLF-12-G(0-5)	0.18
CLF-12-G(5-10)	0.09
CLF-12-G(10+)	0.07
CLF-13-D(0-5)	0.13
CLF-13-D(5-10)	0.08
CLF-13-D(10+)	0.08
CLF-13-G(0-5)	0.20
CLF-13-G(5-10)	0.10
CLF-13-G10+)	0.07
CLF-19-D(0-2)	0.10
CLF-19-D(2-4)	0.09
CLF-19-D(4+)	0.08
CLF-19-G(0-3)	0.12
CLF-19-G(3-6)	0.09
CLF-19-G(6+)	0.07
CLF-14-D(0-3)	0.29
CLF-14-D(3-6)	0.18
CLF-14-D(6+)	0.20
CLF-14-G(0-5)	0.13
CLF-14-G(5-10)	0.13
CLF-14-G(10+)	0.11
CLF-17-D(0-3)	0.75
CLF-17-D(3-6)	0.25
CLF-17-D(6+)	1.25
CLF-17-G(0-3)	0.25
CLF-17-G(3-6)	0.15
CLF-17-G(6+)	1.00

D= desert pavement
G= grasses and cacti
J= juniper tree

	n=	Soluble salts (%) average	std dev
A	74	0.17	0.19
AN	46	0.14	0.09
AS	28	0.23	0.29
ND	12	0.08	0.02
SD	13	0.28	0.34
NG	17	0.09	0.03
SG	15	0.18	0.23
NJ	17	0.23	0.09

A= all samples
AN= all northern samples
AS= all southern samples
ND= northern desert pavement
SD= southern desert pavement
NG= northern grasses and cacti
SG= southern grasses and cacti
NJ= northern juniper tree

Appendix 9.3.6. Chloride concentration in the loess deposits on the Carrizozo lava flow, New Mexico.

Northern Sample #	Chloride (ppm)
CLF-8-D (0-3)	1.9
CLF-8-D (3-6)	1.4
CLF-8-D (6+)	1.8
CLF-8-G(0-5)	1.5
CLF-8-G(5-10)	1.7
CLF-8-J(0-2)	3.6
CLF-8-J(2-5)	4.7
CLF-7-D(0-5)	1.6
CLF-7-D(5-10)	1.4
CLF-7-D(10+)	1.5
CLF-7-G(0-5)	1.5
CLF-7-G(5-10)	1.6
CLF-7-G (10+)	1.7
CLF-7-J(0-5)	12
CLF-7-J(5-10)	10
CLF-7-J(10-15)	3.8
CLF-7-J(15-23)	1.9
CLF-11-G(0-5)	2
CLF-11-G(5-10)	1.6
CLF-11-J(0-5)	5.1
CLF-11-J(5-10)	4.6

D= desert pavement
G= grasses and cacti
J= juniper tree

Southern Sample #	Chloride (ppm)
CLF-12-G(0-5)	1.6
CLF-12-G(5-10)	1.6
CLF-12-G(10+)	1.9
CLF-13-D(0-5)	2
CLF-13-D(5-10)	3.8
CLF-13-D(10+)	1.6
CLF-13-G(0-5)	2.2
CLF-13-G(5-10)	1.9
CLF-13-G(10+)	1.8
CLF-19-D (0-2)	4
CLF-19-D(2-4)	2.3
CLF-19-D(4+)	1.9
CLF-19-G(0-3)	2.5
CLF-19-G(3-6)	2
CLF-19-G(6+)	2.2
CLF-14-D(0-3)	12
CLF-14-D(3-6)	6.8
CLF-14-D(6+)	7.3
CLF-14-G(0-5)	2.3
CLF-14-G(5-10)	2.3
CLF-14-G(10+)	2.4
CLF-17-D(0-3)	79
CLF-17-D(3-6)	24
CLF-17-D(6+)	32
CLF-17-G(0-3)	2.3
CLF-17-G(3-6)	2.1
CLF-17-G(6+)	2.5

Appendix 9.3.7. Calcium carbonate concentrations in the loess deposits on the Carrizozo lava flow, New Mexico. Samples were analyzed using the Chittick method.

Northern Sample #	$CaCO_3$ (%)
CLF-8-D(0-3)	3.41
CLF-8-D(3-6)	5.64
CLF-8-D(6-15)	4.99
CLF-8-G(0-5)	0.06
CLF-8-G(5-10)	0.17
CLF-8-J(0-2)	2.47
CLF-8-J(2-4)	3.15
CLF-7-D(0-5)	0.16
CLF-7-D(5-10)	0.27
CLF-7-D(10+)	0.28
CLF-7-G(0-5)	3.26
CLF-7-G(5-10)	0.58
CLF-7-G(10-15)	0.16
CLF-7-G(15-23)	0.17
CLF-7-J(0-5)	2.43
CLF-7-J(5-10)	2.68
CLF-7-J(10-15)	0.91
CLF-7-J(15-20)	0.45
CLF-6-D(0-3)	1.72
CLF-6-D(3-5)	0.95
CLF-6-G(0-4)	0.24
CLF-6-G(4-10)	0.16
CLF-6-G(10-14)	0.33
CLF-5-D(0-5)	0.26
CLF-5-D(5-10)	0.17
CLF-5-D(10-15)	0.16
CLF-5-G(0-5)A	0.23
CLF-5-G(5-10)A	0.26
CLF-5-G(10-15)A	0.56
CLF-5-J(0-5)	0.14
CLF-5-J(5-10)	0.15
CLF-5-J(10-15)	0.48
CLF-11-J(5-10)	2.24
CLF-10-D #1	0.13
CLF-10-D #2	0.31
CLF-10-G(0-5)	0.13
CLF-10-G(5-10)	0.05
CLF-10-J(0-5)	0.50
CLF-10-J(5-10)	0.71

Southern Sample #	$CaCO_3$ (%)
CLF-12-D	0.44
CLF-12-G(0-5)	0.23
CLF-12-G(5-10)	0.15
CLF-12-G(10+)	0.12
CLF-19-D BULK	1.22
CLF-19-D(0-2)	0.85
CLF-19-D(2-4)	1.97
CLF-19-D(4+)	2.15
CLF-19-G BULK	1.25
CLF-19-G(0-3)	2.05
CLF-19-G(3-6)	0.96
CLF-19-G(6+)	0.41
CLF-14-D BULK	2.29
CLF-14-D(0-3)	1.74
CLF-14-D(3-6)	1.21
CLF-14-D(6+)	4.40
CLF-14-G BULK	4.59
CLF-14-G(0-5)	2.91
CLF-14-G(5-10)	4.28
CLF-14-G(10+)	7.69
CLF-17-D(0-3)	5.85
CLF-17-D(3-6)	3.35
CLF-17-D(6+)	15.07
CLF-17-G(0-3)	2.49
CLF-17-G(3-6)	3.14
CLF-17-G(6+)	21.01

D= desert pavement
G= grasses and cacti
J= juniper tree

Appendix 9.3.8. Major element chemistry of the particle size fractions of the loess deposits on the Carrizozo lava flow, New Mexico. Samples were analyzed using x-ray fluorescence spectrometry. Normalized on a loss-free basis and to 100 %. Analytical total is also provided.

Sample #	SiO_2	TiO_2	Al_2O_3	Fe_2O_3*	MnO	CaO	MgO	Na_2O	K_2O	P_2O_5	LOI	Analytical
	%	%	%	%	%	%	%	%	%	%		Total %
CLF-1-D sd	80.41	0.51	9.39	2.60	0.042	1.49	0.96	2.10	2.20	0.17	4.87	99.27
CLF-1-Dsi	74.18	0.93	11.83	4.14	0.053	1.24	0.99	3.11	2.55	0.80	4.58	99.71
CLF-4-D sd	76.63	0.56	10.93	3.22	0.104	2.13	1.22	2.24	2.45	0.33	4.44	100.17
CLF-4-Dsi	69.08	0.97	13.57	4.90	0.076	3.25	1.76	2.80	2.70	0.70	6.11	98.47
CLF-12-D sd	78.28	0.71	9.76	3.46	0.064	1.85	1.29	2.15	2.13	0.15	4.9	98.78
CLF-12-Dsi	73.53	0.93	11.93	4.45	0.075	2.00	1.52	2.47	2.47	0.43	4.44	97.87
CLF-14-D sd	78.61	0.56	9.20	3.16	0.094	2.15	1.71	2.10	2.13	0.15	2.85	98.72
CLF-14-Dsi	70.60	1.03	12.42	5.00	0.086	2.65	2.54	2.29	2.70	0.48	6	99.32
CLF-17-D sd	78.32	0.46	9.00	2.42	0.064	3.24	1.87	2.09	2.22	0.14	5.36	98.99
CLF-17-Dsi	65.43	0.78	11.76	4.14	0.102	7.28	4.25	2.46	2.48	1.10	10.11	98.31
CLF-1-G sd	70.63	0.63	10.75	3.13	0.078	7.31	1.45	2.45	2.32	1.08	21.28	98.00
CLF-1-Gsi	68.19	0.92	12.97	4.62	0.080	5.01	1.67	2.80	2.77	0.79	11.38	98.45
CLF-4-G sd	77.54	0.58	11.06	3.12	0.054	1.23	1.06	2.52	2.56	0.12	6.1	99.42
CLF-4-Gsi	73.64	0.97	12.41	4.48	0.075	1.30	1.15	2.74	2.64	0.43	4.54	97.97
CLF-12-G sd	79.89	0.64	9.40	3.13	0.094	1.30	1.11	2.10	2.09	0.10	4.27	99.76
CLF-12-Gsi	75.02	0.87	11.93	4.19	0.075	1.19	1.26	2.47	2.53	0.30	3.43	97.22
CLF-14-G sd	64.39	0.88	12.56	5.90	0.116	6.32	4.41	2.32	2.20	0.73	12.08	98.45
CLF-14-Gsi	70.97	0.90	11.55	4.38	0.077	4.12	2.49	2.29	2.46	0.57	6.43	97.89
CLF-17-G sd	76.57	0.48	9.32	2.58	0.076	4.27	1.81	2.21	2.24	0.28	6.85	98.68
CLF-17-Gsi	67.00	0.84	10.87	3.97	0.079	8.70	2.91	2.40	2.33	0.69	12.97	101.87
CLF-1-J sd	78.03	0.62	10.18	3.32	0.054	1.79	1.29	2.13	2.21	0.24	6.99	99.13
CLF-1-Jsi	73.16	0.98	12.84	4.78	0.065	1.24	1.24	2.56	2.66	0.29	6.98	99.72
CLF-4-J sd	78.67	0.53	10.40	2.81	0.042	1.46	0.92	2.42	2.45	0.18	3.43	99.58
CLF-4-Jsi	73.46	0.98	12.62	4.34	0.053	1.36	1.11	2.83	2.71	0.39	3.74	97.82

	n=	SiO_2		TiO_2		Al_2O_3		Fe_2O_3*		MnO	
		average	std dev	average	std dev	average	std dev	average	std dev	average	std dev
A sd	12	76.87	4.54	0.60	0.10	10.19	1.04	3.20	0.90	0.068	0.000
A si	12	71.61	3.14	0.90	0.10	12.32	0.73	4.47	0.32	0.071	0.000
ND sd	2	78.52	2.67	0.54	0.04	10.16	1.09	2.91	0.44	0.070	0.040
ND si	2	71.63	3.61	0.95	0.03	12.70	1.23	4.52	0.54	0.060	0.020
SD sd	3	78.40	0.18	0.58	0.13	9.32	0.39	3.02	0.53	0.074	0.020
SD si	3	69.85	4.10	0.91	0.12	12.04	0.34	4.53	0.44	0.088	0.010
NG sd	2	74.09	4.88	0.60	0.00	10.91	0.22	3.12	0.01	0.066	0.017
NG si	2	70.91	3.85	0.95	0.00	12.69	0.40	4.55	0.09	0.078	0.004
SG sd	3	73.61	8.16	0.67	0.20	10.43	1.85	3.87	1.78	0.095	0.020
SG si	3	71.00	4.01	0.87	0.00	11.45	0.54	4.18	0.21	0.077	0.002
NJ sd	2	78.35	0.45	0.57	0.10	10.29	0.16	3.06	0.36	0.048	0.009
NJ si	2	73.31	0.21	0.98	0.00	12.73	0.16	4.56	0.31	0.059	0.001

	n=	CaO		MgO		Na_2O		K_2O		P_2O_5	
		average	std dev	average	std dev	average	std dev	average	std dev	average	std dev
A sd	12	2.60	2.00	1.50	0.90	2.20	0.20	2.30	0.10	0.29	0.30
A si	12	2.50	2.50	1.80	1.00	2.60	0.30	2.60	0.10	0.53	0.24
ND sd	2	1.81	0.45	1.09	0.18	2.17	0.10	2.33	0.18	0.25	0.12
ND si	2	2.24	1.42	1.38	0.55	2.96	0.22	2.63	0.10	0.75	0.07
SD sd	3	2.41	0.73	1.62	0.30	2.11	0.03	2.16	0.05	0.14	0.01
SD si	3	3.98	2.88	2.77	1.38	2.41	0.10	2.55	0.13	0.67	0.37
NG sd	2	4.27	4.30	1.25	0.30	2.48	0.00	2.44	0.20	0.60	0.68
NG si	2	3.15	2.63	1.41	0.40	2.77	0.00	2.71	0.10	0.61	0.26
SG sd	3	3.96	2.53	2.44	1.70	2.21	0.10	2.18	0.10	0.37	0.32
SG si	3	4.67	3.78	2.22	0.90	2.38	0.10	2.44	0.10	0.52	0.20
NJ sd	2	1.62	0.24	1.10	0.30	2.28	0.20	2.33	0.20	0.21	0.04
NJ si	2	1.30	0.09	1.17	0.10	2.69	0.20	2.69	0.00	0.34	0.07

sd= sand fraction
si= silt fraction
* = Total Fe as Fe_2O_3
D= desert pavement
G= grasses and cacti
J= juniper tree

Appendix 9.3.9. Major element chemistry of the loess deposits on the Carrizozo lava flow, New Mexico.
Total element chemistry of the loess deposits on the Carrizozo lava flow, New Mexico. Samples were analyzed using x-ray fluorescence spectrometry. Normalized on a loss-free basis and to 100 %. Analytical total is also provided.

Sample #	SiO_2 %	TiO_2 %	Al_2O_3 %	Fe_2O_3* %	MnO %	CaO %	MgO %	Na_2O %	K_2O %	P_2O_5 %	LOI	Analytical Total %
CLF-8-D(0-3)	73.91	0.75	12.17	4.09	0.093	2.82	1.65	1.61	2.75	0.16	7.04	97.82
CLF-8-D(3-6)	72.35	0.74	12.41	4.18	0.092	4.08	1.71	1.53	2.74	0.15	8.78	98.06
CLF-8-D(6-10)	72.60	0.74	12.37	4.19	0.092	3.89	1.70	1.53	2.73	0.15	8.54	97.90
CLF-8-G(0-5)	76.36	0.76	11.82	3.98	0.079	1.26	1.33	1.66	2.65	0.11	6.47	97.95
CLF-8-G(5-10)	75.70	0.76	12.23	4.02	0.087	1.41	1.42	1.67	2.59	0.12	5.98	97.02
CLF-8-J(0-2)	70.29	0.75	12.63	4.62	0.124	5.18	1.84	1.46	2.57	0.52	22.93	99.56
CLF-8-J(2-5)	71.38	0.73	12.31	3.90	0.107	5.19	1.76	1.53	2.61	0.47	19.14	96.80
CLF-7-D(0-5)	74.47	0.77	12.87	4.42	0.094	1.42	1.41	1.68	2.74	0.12	5.95	98.02
CLF-7-D(5-10)	73.86	0.78	13.28	4.52	0.101	1.47	1.47	1.63	2.78	0.12	6.66	97.39
CLF-7-D(10-17)	72.97	0.82	13.58	4.79	0.100	1.77	1.50	1.59	2.77	0.12	7.53	97.58
CLF-7-G(0-5)	74.36	0.74	12.14	3.97	0.092	2.73	1.50	1.69	2.65	0.14	7.58	97.09
CLF-7-G(5-10)	74.98	0.74	12.47	4.08	0.093	1.67	1.45	1.69	2.69	0.12	6.93	96.79
CLF-7-G(10-15)	74.85	0.75	12.74	4.14	0.097	1.49	1.41	1.69	2.69	0.13	7.41	97.26
CLF-7-G(15-23)	74.98	0.76	12.68	4.20	0.096	1.49	1.35	1.66	2.65	0.14	7.72	96.55
CLF-7-J(0-5)	72.13	0.75	11.88	3.32	0.082	5.61	1.69	1.57	2.66	0.30	33.66	98.03
CLF-7-J(5-10)	71.35	0.75	12.59	3.95	0.094	4.94	1.78	1.55	2.71	0.29	24.87	98.66
CLF-7-J(10-15)	73.52	0.77	12.43	4.30	0.093	2.82	1.54	1.59	2.68	0.25	15.3	98.27
CLF-7-J(15-23)	74.43	0.77	12.29	4.28	0.087	2.21	1.45	1.61	2.65	0.22	11.88	97.48
CLF-6-D(0-3)	73.64	0.78	11.73	4.13	0.078	3.97	1.34	1.72	2.50	0.11	7.67	98.75
CLF-6-D(3-5)	74.87	0.78	12.46	4.13	0.086	1.93	1.24	1.78	2.63	0.10	6.07	97.19
CLF-6-G(0-4)	77.89	0.72	11.06	3.48	0.090	1.26	1.01	1.87	2.53	0.10	5.06	97.15
CLF-6-G(4-10)	77.51	0.74	11.31	3.68	0.083	1.24	1.03	1.82	2.51	0.08	5.26	97.82
CLF-6-G(10-14)	75.36	0.78	12.70	4.22	0.088	1.36	1.15	1.73	2.51	0.10	7.55	98.28
CLF-6-J(0-5)	74.14	0.80	12.71	4.36	0.103	2.09	1.31	1.67	2.65	0.18	11.65	99.31
CLF-6-J(5-15)	74.06	0.82	12.84	4.37	0.100	1.99	1.29	1.69	2.66	0.18	10.63	98.23
CLF-5-D(0-5)	75.91	0.76	12.31	3.94	0.083	1.24	1.15	1.83	2.67	0.11	5.1	97.50
CLF-5-D(5-10)	74.61	0.78	13.08	4.28	0.094	1.33	1.28	1.72	2.72	0.11	6.37	98.22
CLF-5-D(10-15)	74.27	0.81	13.22	4.42	0.092	1.37	1.31	1.69	2.70	0.12	7.5	98.66
CLF-5-G(0-5)	76.72	0.69	11.82	3.62	0.092	1.33	1.17	1.80	2.64	0.12	7.03	97.55
CLF-5-G(5-10)	75.45	0.75	12.44	4.03	0.102	1.42	1.30	1.71	2.68	0.13	8.04	98.82
CLF-5-G(10-15)	75.06	0.74	12.53	4.06	0.105	1.65	1.33	1.70	2.69	0.14	8.43	97.78
CLF-5-J(0-5)	73.14	0.78	12.62	3.55	0.093	3.45	1.62	1.67	2.76	0.33	20.36	96.52
CLF-5-J(5-10)	74.26	0.79	12.17	3.95	0.089	2.45	1.54	1.74	2.75	0.27	13.58	97.74
CLF-11-D	72.58	0.91	13.75	4.90	0.092	1.46	1.38	1.89	2.70	0.18	7.42	97.92
CLF-11-G(0-5)	73.16	0.87	13.38	4.60	0.103	1.54	1.34	1.91	2.79	0.15	13.59	98.87
CLF-11-G(5-10)	73.43	0.88	13.47	4.66	0.100	1.32	1.28	1.92	2.68	0.12	10.02	98.02
CLF-11-J(0-5)	66.22	0.78	12.93	4.30	0.099	8.71	2.03	1.72	2.73	0.28	25.73	97.17
CLF-11-J(5-10)	71.58	0.83	13.49	4.73	0.092	2.77	1.55	1.75	2.89	0.16	14.38	98.91
CLF-10-D	73.33	0.88	12.61	4.61	0.089	1.81	1.54	2.03	2.73	0.20	7.54	97.80
CLF-10-G(0-5)	74.06	0.82	12.95	4.38	0.102	1.46	1.27	1.90	2.75	0.13	12.01	98.84
CLF-10-G(5-10)	73.84	0.82	13.44	4.39	0.101	1.27	1.25	1.94	2.68	0.11	9.21	95.92
CLF-10-J(0-5)	70.60	0.85	13.47	4.47	0.121	3.35	1.80	1.86	2.95	0.33	26.22	100.24
CLF-10-J(5-10)	71.43	0.83	13.44	4.40	0.117	2.88	1.63	1.88	2.95	0.27	18.39	98.16
CLF-1-D	75.28	0.80	12.58	4.13	0.080	1.43	1.11	1.87	2.59	0.12	7.38	98.87
CLF-1-G	68.29	0.73	12.02	4.16	0.102	8.41	1.66	1.70	2.67	0.27	15.39	93.79
CLF-1-J	74.30	0.83	12.88	4.42	0.089	1.66	1.29	1.76	2.62	0.15	9.56	98.74
CLF-2-D	74.05	0.86	12.95	4.47	0.091	1.61	1.33	1.88	2.61	0.15	6.45	99.71
CLF-2-G	73.84	0.81	13.05	4.56	0.088	1.67	1.30	1.85	2.69	0.14	8.49	99.45
CLF-2-J	71.93	0.77	12.97	4.04	0.104	3.84	1.61	1.71	2.74	0.28	19.81	99.33
CLF-3-D	74.24	0.83	12.65	4.41	0.082	1.59	1.34	1.94	2.68	0.23	5.67	99.26
CLF-3-G	74.71	0.80	12.73	4.37	0.087	1.40	1.17	1.93	2.68	0.13	7.09	99.39
CLF-3-J	71.07	0.82	13.16	4.53	0.116	3.62	1.71	1.81	2.89	0.29	15.62	99.15
CLF-4-D	71.33	0.89	13.58	4.75	0.089	2.55	1.63	2.03	2.81	0.32	6.4	99.37
CLF-4-G	74.76	0.79	12.52	4.12	0.088	1.50	1.17	2.14	2.74	0.16	6.21	98.45
CLF-4-J	73.36	0.81	13.33	4.44	0.089	1.58	1.30	2.11	2.76	0.22	8.55	100.52
CLF-1-D(0-2)	75.59	0.84	12.32	4.54	0.058	1.11	1.11	1.83	2.51	0.12	5.64	99.75
CLF-1-D(2-5)	74.65	0.85	13.07	4.53	0.068	1.13	1.22	1.75	2.60	0.12	6.35	98.89
CLF-1-G(0-5)	76.65	0.70	11.94	3.78	0.088	1.26	1.13	1.76	2.58	0.10	7.5	97.08
CLF-1-G(5-10)	76.52	0.73	12.01	3.92	0.088	1.23	1.11	1.74	2.54	0.09	6.99	97.76
CLF-1-G(10-15)	76.07	0.74	12.27	4.06	0.093	1.29	1.15	1.70	2.54	0.09	7.25	97.73
CLF-1-J(0-3)	72.08	0.78	12.95	3.92	0.098	3.76	1.59	1.74	2.82	0.28	17.44	98.39
CLF-1-J(3-5)	72.30	0.79	12.89	4.16	0.096	3.44	1.50	1.75	2.80	0.26	14.66	97.75
CLF-12-D	72.79	0.86	12.59	4.69	0.088	2.29	1.78	1.88	2.59	0.28	6.34	99.10
CLF-12-G(0-5)	72.50	0.82	13.54	4.68	0.108	1.62	1.77	1.86	2.73	0.20	7.26	96.28
CLF-12-G(5-10)	73.37	0.82	13.18	4.65	0.108	1.44	1.62	1.84	2.66	0.14	9.02	97.74
CLF-12-G(10+)	73.94	0.83	13.08	4.61	0.101	1.36	1.46	1.79	2.56	0.11	6.91	98.41
CLF-13-D(0-5)	70.96	0.84	12.68	4.59	0.089	3.25	2.46	1.86	2.77	0.30	7.78	97.93
CLF-13-D(5-10)	69.71	0.82	13.13	4.66	0.090	3.87	2.68	1.79	2.78	0.31	7.66	96.49
CLF-13-D(10+)	69.44	0.82	13.11	4.79	0.085	4.19	2.59	1.73	2.83	0.24	7.3	97.41
CLF-13-G(0-5)	71.86	0.83	12.93	4.64	0.100	2.40	2.17	1.86	2.80	0.24	8.88	97.76
CLF-13-G(5-10)	72.25	0.82	13.32	4.63	0.100	1.86	2.06	1.86	2.76	0.17	8.42	95.64

Appendix 9.3.9. (continued) Major element chemistry

Sample #	SiO_2 %	TiO_2 %	Al_2O_3 %	Fe_2O_3* %	MnO %	CaO %	MgO %	Na_2O %	K_2O %	P_2O_5 %	LOI	Analytical Total %
CLF-13-G(10+)	73.02	0.84	12.97	4.66	0.099	1.62	1.90	1.85	2.75	0.13	8.68	98.23
CLF-18-D(0-2)	73.90	0.90	11.81	4.64	0.085	1.87	1.88	2.05	2.50	0.20	4.33	96.98
CLF-18-D(2-4)	73.43	0.92	12.43	4.78	0.091	1.66	1.81	1.94	2.59	0.16	4.66	98.38
CLF-18-D(4+)	71.84	0.94	13.40	5.19	0.090	1.68	2.12	1.80	2.63	0.13	5.55	96.51
CLF-18-G(0-2)	72.86	0.81	12.50	4.43	0.118	2.27	1.91	1.94	2.77	0.21	12.06	100.23
CLF-18-G(2-4)	73.09	0.81	12.41	4.51	0.119	2.19	1.86	1.95	2.72	0.18	9.14	98.59
CLF-18-G(4+)	72.69	0.83	12.80	4.53	0.117	2.10	1.89	1.99	2.74	0.16	8.18	96.94
CLF-19-D(0-2)	72.33	0.84	12.81	4.54	0.093	2.14	1.98	2.01	2.82	0.26	4.96	97.45
CLF-19-D(2-4)	69.58	0.83	13.80	5.01	0.110	2.79	2.59	1.75	3.01	0.35	7.08	99.06
CLF-19-D(4+)	67.92	0.80	14.44	5.25	0.111	3.28	2.89	1.64	3.09	0.39	7.78	98.04
CLF-19-G(0-3)	71.63	0.81	13.14	4.48	0.101	2.90	1.80	1.95	2.80	0.21	9.37	97.68
CLF-19-G(3-6)	71.41	0.81	13.95	4.70	0.104	2.19	1.79	1.98	2.74	0.16	8.18	95.11
CLF-19-G(6+)	71.97	0.82	14.03	4.77	0.106	1.71	1.61	1.91	2.79	0.12	8.58	97.02
CLF-14-D(0-3)	70.93	0.90	12.88	4.92	0.105	2.42	2.91	1.85	2.65	0.27	6.13	95.88
CLF-14-D(3-6)	71.94	0.83	13.14	4.67	0.092	1.96	2.70	1.70	2.57	0.24	5.52	101.01
CLF-14-D(6+)	69.51	0.84	12.80	4.86	0.099	3.92	3.08	1.69	2.71	0.29	8.32	98.06
CLF-14-G(0-5)	66.51	0.80	13.87	5.23	0.117	4.48	3.80	1.56	2.73	0.74	15.4	97.49
CLF-14-G(5-10)	64.77	0.80	13.52	5.18	0.125	6.24	4.00	1.60	2.69	0.88	15.63	97.72
CLF-14-G(10+)	62.94	0.82	13.41	5.40	0.128	7.72	4.34	1.66	2.52	0.89	17.39	98.01
CLF-15-D(0-5)	72.44	0.84	11.33	4.27	0.087	3.61	2.57	1.95	2.45	0.24	5.93	97.02
CLF-15-D(5-10)	67.26	0.82	12.34	4.60	0.100	6.43	3.71	1.67	2.57	0.30	9.98	96.67
CLF-15-D(10+)	65.20	0.79	12.49	4.61	0.094	8.62	3.54	1.62	2.57	0.25	12.26	94.26
CLF-15-G(0-3)	72.93	0.77	12.18	4.20	0.091	2.67	2.30	1.91	2.58	0.20	8.18	96.50
CLF-15-G(3-6)	73.01	0.77	12.49	4.35	0.094	2.26	2.15	1.94	2.59	0.17	7.01	95.65
CLF-15-G(6+)	73.34	0.79	12.52	4.51	0.100	1.78	2.04	1.90	2.71	0.14	6.81	97.57
CLF-16-D(0-2)	72.70	0.75	11.10	3.82	0.076	3.57	3.06	1.99	2.42	0.32	6.13	97.12
CLF-16-D(2-4)	70.12	0.74	11.81	4.16	0.087	4.44	3.75	1.79	2.52	0.39	7.78	97.64
CLF-16-D(4+)	68.49	0.75	12.00	4.32	0.080	6.09	3.53	1.72	2.51	0.30	10.47	97.19
CLF-16-G(0-5)	74.59	0.64	10.65	3.40	0.078	3.39	2.43	1.95	2.43	0.26	11.02	97.18
CLF-16-G(5-10)	74.28	0.65	10.84	3.34	0.073	3.52	2.45	2.03	2.39	0.24	8.34	96.59
CLF-16-G(10-20)	75.07	0.61	10.49	3.24	0.073	3.30	2.48	2.00	2.36	0.23	8.52	94.97
CLF-16-G(20+)	73.75	0.65	10.97	3.53	0.086	3.21	3.05	1.90	2.44	0.25	12.15	98.94
CLF-17-D(0-3)	69.66	0.73	11.36	3.94	0.089	5.20	4.20	1.82	2.48	0.27	9.08	97.69
CLF-17-D(3-6)	68.18	0.69	11.91	3.95	0.099	6.07	4.39	1.71	2.50	0.27	10.58	95.82
CLF-17-D(6+)	64.14	0.67	11.20	3.92	0.093	11.61	3.27	1.62	2.47	0.25	15.38	96.70
CLF-17-G(0-3)	71.34	0.72	12.23	3.91	0.087	3.20	3.61	1.90	2.56	0.26	8.75	95.11
CLF-17-G(3-6)	71.80	0.71	11.93	3.88	0.089	3.07	3.69	1.88	2.55	0.23	8.08	96.42
CLF-17-G(6+)	59.11	0.63	9.99	3.50	0.090	19.41	2.99	1.52	2.17	0.30	20.1	97.59

	n=	SiO_2		TiO_2		Al_2O_3		Fe_2O_3*		MnO	
		average	std dev	average	std dev	average	std dev	average	std dev	average	std dev
A	109	72.47	3.06	0.79	0.06	12.59	0.79	4.32	0.43	0.095	0.012
AN	62	73.75	2.07	0.79	0.05	12.66	0.57	4.22	0.33	0.093	0.011
AS	47	70.78	3.35	0.79	0.08	12.50	1.01	4.45	0.52	0.097	0.013
ND	19	73.67	1.17	0.83	0.06	12.86	0.53	4.43	0.28	0.089	0.006
SD	22	70.34	1.97	0.82	0.07	12.49	0.74	4.57	0.37	0.092	0.007
NG	23	74.23	2.36	0.78	0.05	12.54	0.56	4.20	0.28	0.093	0.007
SG	25	71.23	3.35	0.77	0.07	12.59	1.06	4.40	0.59	0.101	0.015
NJ	20	72.21	1.75	0.80	0.03	12.89	0.41	4.27	0.26	0.101	0.012

	n=	CaO		MgO		Na_2O		K_2O		P_2O_5	
		average	std dev	average	std dev	average	std dev	average	std dev	average	std dev
A	109	3.02	2.47	1.95	0.83	1.79	0.14	2.66	0.14	0.22	0.13
AN	62	2.42	1.62	1.41	0.22	1.76	0.14	2.69	0.10	0.18	0.09
AS	47	3.81	3.11	2.65	0.82	1.83	0.13	2.63	0.17	0.27	0.16
ND	19	1.99	0.77	1.40	0.18	1.83	0.16	2.69	0.08	0.17	0.07
SD	22	3.98	2.06	2.79	0.75	1.81	0.07	2.63	0.17	0.27	0.05
NG	23	1.33	0.18	1.30	0.16	1.83	0.15	2.67	0.07	0.14	0.05
SG	25	3.52	2.51	2.44	0.87	1.86	0.12	2.63	0.14	0.17	0.04
NJ	20	3.36	1.40	1.57	0.20	1.75	0.17	2.74	0.11	0.27	0.09

D= desert pavement
G= grasses and cacti
J= juniper tree
*= Total Fe as Fe_2O_3

Appendix 9.3.10. Major element chemistry of loess deposits from the Carrizozo lava flow, New Mexico. Samples were analyzed using x-ray fluorescence spectrometry. Normalized on a CaCO3- free and loss-free basis and to 100%.

Sample #	SiO_2 %	TiO_2 %	Al_2O_3 %	Fe_2O_3* %	MnO %	CaO %	MgO %	Na_2O %	K_2O %	P_2O_5 %
CLF-8-D(0-3)	74.91	0.76	12.34	4.14	0.094	1.50	1.67	1.63	2.79	0.16
CLF-8-D(3-6)	74.30	0.76	12.74	4.29	0.094	1.50	1.76	1.58	2.82	0.16
CLF-8-D(6-10)	74.41	0.76	12.67	4.29	0.094	1.50	1.74	1.57	2.80	0.15
CLF-8-G(0-5)	76.36	0.76	11.82	3.98	0.079	1.26	1.33	1.66	2.65	0.11
CLF-8-G(5-10)	75.70	0.76	12.23	4.02	0.087	1.41	1.42	1.67	2.59	0.12
CLF-8-J(0-2)	73.02	0.78	13.12	4.80	0.129	1.50	1.91	1.52	2.67	0.54
CLF-8-J(2-5)	74.16	0.76	12.79	4.05	0.111	1.50	1.83	1.59	2.72	0.49
CLF-7-D(0-5)	74.47	0.77	12.87	4.42	0.094	1.42	1.41	1.68	2.74	0.12
CLF-7-D(5-10)	73.86	0.78	13.28	4.52	0.101	1.47	1.47	1.63	2.78	0.12
CLF-7-D(10-17)	73.17	0.82	13.62	4.80	0.100	1.50	1.50	1.59	2.77	0.12
CLF-7-G(0-5)	75.29	0.75	12.30	4.02	0.093	1.50	1.52	1.71	2.68	0.15
CLF-7-G(5-10)	75.11	0.74	12.50	4.09	0.094	1.50	1.45	1.69	2.70	0.12
CLF-7-G(10-15)	74.85	0.75	12.74	4.14	0.097	1.49	1.41	1.69	2.69	0.13
CLF-7-G(15-23)	74.98	0.76	12.68	4.20	0.096	1.49	1.35	1.66	2.65	0.14
CLF-7-J(0-5)	75.27	0.78	12.40	3.47	0.086	1.50	1.77	1.64	2.77	0.32
CLF-7-J(5-10)	73.93	0.77	13.05	4.09	0.097	1.50	1.84	1.60	2.81	0.30
CLF-7-J(10-15)	74.52	0.78	12.60	4.36	0.094	1.50	1.56	1.61	2.71	0.26
CLF-7-J(15-23)	74.97	0.77	12.38	4.31	0.087	1.50	1.46	1.63	2.67	0.22
CLF-6-D(0-3)	75.53	0.80	12.03	4.23	0.080	1.50	1.37	1.77	2.57	0.11
CLF-6-D(3-5)	75.20	0.78	12.51	4.14	0.086	1.50	1.25	1.79	2.65	0.10
CLF-6-G(0-4)	77.89	0.72	11.06	3.48	0.090	1.26	1.01	1.87	2.53	0.10
CLF-6-G(4-10)	77.51	0.74	11.31	3.68	0.083	1.24	1.03	1.82	2.51	0.08
CLF-6-G(10-14)	75.36	0.78	12.70	4.22	0.088	1.36	1.15	1.73	2.51	0.10
CLF-6-J(0-5)	74.58	0.81	12.78	4.38	0.103	1.50	1.32	1.68	2.66	0.18
CLF-6-J(5-15)	74.43	0.82	12.91	4.39	0.101	1.50	1.30	1.70	2.67	0.18
CLF-5-D(0-5)	75.91	0.76	12.31	3.94	0.083	1.24	1.15	1.83	2.67	0.11
CLF-5-D(5-10)	74.61	0.78	13.08	4.28	0.094	1.33	1.28	1.72	2.72	0.11
CLF-5-D(10-15)	74.27	0.81	13.22	4.42	0.092	1.37	1.31	1.69	2.70	0.12
CLF-5-G(0-5)	76.72	0.69	11.82	3.62	0.092	1.33	1.17	1.80	2.64	0.12
CLF-5-G(5-10)	75.45	0.75	12.44	4.03	0.102	1.42	1.30	1.71	2.68	0.13
CLF-5-G(10-15)	75.17	0.74	12.55	4.07	0.105	1.50	1.33	1.70	2.69	0.14
CLF-5-J(0-5)	74.62	0.80	12.87	3.62	0.095	1.50	1.65	1.70	2.81	0.34
CLF-5-J(5-10)	74.99	0.80	12.29	3.98	0.090	1.50	1.56	1.75	2.77	0.27
CLF-11-D	72.70	0.92	13.77	4.90	0.092	1.46	1.38	1.89	2.70	0.18
CLF-11-G(0-5)	73.31	0.87	13.41	4.61	0.103	1.50	1.34	1.92	2.80	0.15
CLF-11-G(5-10)	73.54	0.88	13.49	4.67	0.100	1.32	1.29	1.92	2.69	0.12
CLF-11-J(0-5)	71.61	0.85	13.99	4.65	0.107	1.50	2.19	1.86	2.95	0.30
CLF-11-J(5-10)	72.64	0.84	13.69	4.80	0.094	1.50	1.57	1.78	2.93	0.16
CLF-10-D	73.69	0.89	12.67	4.63	0.089	1.50	1.55	2.04	2.74	0.20
CLF-10-G(0-5)	74.18	0.83	12.97	4.39	0.102	1.47	1.28	1.91	2.76	0.13
CLF-10-G(5-10)	73.96	0.82	13.46	4.40	0.101	1.27	1.25	1.94	2.69	0.11
CLF-10-J(0-5)	72.10	0.87	13.76	4.57	0.123	1.50	1.83	1.90	3.01	0.34
CLF-10-J(5-10)	72.58	0.84	13.65	4.47	0.118	1.50	1.66	1.91	2.99	0.28
CLF-1-D	75.28	0.80	12.58	4.13	0.080	1.43	1.11	1.87	2.59	0.12
CLF-1-G	73.44	0.79	12.92	4.47	0.110	1.50	1.78	1.82	2.87	0.29
CLF-1-J	74.42	0.83	12.90	4.42	0.089	1.50	1.29	1.76	2.63	0.15
CLF-2-D	74.14	0.86	12.97	4.48	0.091	1.50	1.33	1.88	2.61	0.15
CLF-2-G	73.96	0.82	13.07	4.57	0.088	1.50	1.30	1.85	2.70	0.14
CLF-2-J	73.68	0.79	13.28	4.14	0.107	1.50	1.65	1.75	2.81	0.29
CLF-3-D	74.31	0.83	12.66	4.42	0.082	1.50	1.34	1.95	2.68	0.23
CLF-3-G	74.71	0.80	12.73	4.37	0.087	1.40	1.17	1.93	2.68	0.13
CLF-3-J	72.63	0.84	13.45	4.62	0.119	1.50	1.75	1.85	2.95	0.30
CLF-4-D	72.10	0.90	13.73	4.81	0.090	1.50	1.65	2.05	2.84	0.33
CLF-4-G	74.76	0.79	12.52	4.12	0.088	1.50	1.17	2.14	2.74	0.16
CLF-4-J	73.42	0.81	13.34	4.44	0.089	1.50	1.31	2.11	2.76	0.22
CLF-1-D(0-2)	75.59	0.84	12.32	4.54	0.058	1.11	1.11	1.83	2.51	0.12
CLF-1-D(2-5)	74.65	0.85	13.07	4.53	0.068	1.13	1.22	1.75	2.60	0.12

Appendix 9.3.10. (continued) Major element chemistry

Sample #	SiO_2 %	TiO_2 %	Al_2O_3 %	Fe_2O_3* %	MnO %	CaO %	MgO %	Na_2O %	K_2O %	P_2O_5 %
CLF-1-G(0-5)	76.65	0.70	11.94	3.78	0.088	1.26	1.13	1.76	2.58	0.10
CLF-1-G(5-10)	76.52	0.73	12.01	3.92	0.088	1.23	1.11	1.74	2.54	0.09
CLF-1-G(10-15)	76.07	0.74	12.27	4.06	0.093	1.29	1.15	1.70	2.54	0.09
CLF-1-J(0-3)	73.77	0.80	13.25	4.01	0.100	1.50	1.63	1.78	2.88	0.28
CLF-1-J(3-5)	73.76	0.81	13.15	4.25	0.098	1.50	1.53	1.78	2.86	0.26
CLF-12-D	73.50	0.87	12.72	4.74	0.089	1.50	1.80	1.89	2.61	0.28
CLF-12-G(0-5)	72.71	0.82	13.58	4.70	0.108	1.50	1.78	1.87	2.74	0.20
CLF-12-G(5-10)	73.49	0.82	13.20	4.66	0.108	1.44	1.63	1.84	2.66	0.14
CLF-12-G(10+)	74.06	0.83	13.10	4.62	0.101	1.36	1.47	1.80	2.56	0.11
CLF-13-D(0-5)	72.39	0.86	12.93	4.68	0.091	1.50	2.51	1.90	2.83	0.30
CLF-13-D(5-10)	71.55	0.84	13.47	4.78	0.092	1.50	2.75	1.84	2.85	0.31
CLF-13-D(10+)	71.52	0.85	13.50	4.94	0.088	1.50	2.66	1.78	2.91	0.25
CLF-13-G(0-5)	72.65	0.84	13.07	4.69	0.101	1.50	2.20	1.88	2.83	0.24
CLF-13-G(5-10)	72.63	0.83	13.39	4.66	0.100	1.50	2.07	1.87	2.78	0.17
CLF-13-G(10+)	73.24	0.84	13.00	4.67	0.100	1.50	1.90	1.86	2.76	0.13
CLF-18-D(0-2)	74.30	0.91	11.87	4.67	0.086	1.50	1.89	2.06	2.52	0.20
CLF-18-D(2-4)	73.68	0.92	12.47	4.80	0.091	1.50	1.82	1.95	2.60	0.16
CLF-18-D(4+)	72.10	0.94	13.45	5.21	0.090	1.50	2.13	1.81	2.64	0.13
CLF-18-G(0-2)	73.57	0.82	12.62	4.48	0.119	1.50	1.92	1.96	2.79	0.21
CLF-18-G(2-4)	73.74	0.82	12.52	4.55	0.120	1.50	1.87	1.96	2.74	0.18
CLF-18-G(4+)	73.25	0.84	12.90	4.56	0.118	1.50	1.91	2.01	2.76	0.16
CLF-19-D(0-2)	72.93	0.85	12.92	4.58	0.094	1.50	1.99	2.03	2.85	0.26
CLF-19-D(2-4)	70.63	0.85	14.01	5.09	0.111	1.50	2.63	1.78	3.06	0.35
CLF-19-D(4+)	69.30	0.82	14.73	5.36	0.113	1.50	2.95	1.67	3.15	0.40
CLF-19-G(0-3)	72.80	0.83	13.35	4.56	0.102	1.50	1.83	1.98	2.84	0.22
CLF-19-G(3-6)	72.03	0.82	14.07	4.75	0.104	1.50	1.81	2.00	2.76	0.16
CLF-19-G(6+)	72.24	0.82	14.09	4.79	0.107	1.50	1.61	1.92	2.80	0.12
CLF-14-D(0-3)	71.72	0.91	13.02	4.98	0.106	1.50	2.94	1.87	2.68	0.27
CLF-14-D(3-6)	72.40	0.84	13.23	4.70	0.093	1.50	2.72	1.71	2.58	0.24
CLF-14-D(6+)	71.41	0.86	13.15	4.99	0.102	1.50	3.16	1.74	2.78	0.30
CLF-14-G(0-5)	68.70	0.83	14.33	5.40	0.121	1.50	3.93	1.61	2.82	0.76
CLF-14-G(5-10)	68.19	0.85	14.24	5.45	0.132	1.50	4.21	1.68	2.83	0.92
CLF-14-G(10+)	67.31	0.88	14.34	5.77	0.137	1.50	4.64	1.78	2.69	0.95
CLF-15-D(0-5)	74.18	0.86	11.60	4.37	0.089	1.50	2.63	2.00	2.51	0.25
CLF-15-D(5-10)	70.94	0.87	13.02	4.85	0.106	1.50	3.92	1.76	2.71	0.32
CLF-15-D(10+)	70.45	0.85	13.49	4.98	0.101	1.50	3.82	1.75	2.78	0.27
CLF-15-G(0-3)	73.93	0.78	12.35	4.26	0.092	1.50	2.33	1.94	2.62	0.20
CLF-15-G(3-6)	73.69	0.78	12.61	4.40	0.095	1.50	2.18	1.96	2.62	0.18
CLF-15-G(6+)	73.68	0.80	12.58	4.53	0.101	1.50	2.05	1.90	2.72	0.14
CLF-16-D(0-2)	74.41	0.77	11.36	3.91	0.078	1.50	3.13	2.04	2.47	0.33
CLF-16-D(2-4)	72.43	0.76	12.20	4.30	0.090	1.50	3.87	1.85	2.60	0.40
CLF-16-D(4+)	71.99	0.79	12.62	4.54	0.084	1.50	3.71	1.81	2.64	0.32
CLF-16-G(0-5)	76.20	0.65	10.88	3.47	0.079	1.50	2.48	1.99	2.48	0.26
CLF-16-G(5-10)	75.98	0.67	11.09	3.42	0.074	1.50	2.50	2.07	2.45	0.25
CLF-16-G(10-20)	76.59	0.62	10.70	3.30	0.074	1.50	2.53	2.04	2.41	0.24
CLF-16-G(20+)	75.18	0.66	11.18	3.59	0.088	1.50	3.11	1.94	2.49	0.25
CLF-17-D(0-3)	72.57	0.76	11.84	4.10	0.093	1.50	4.37	1.89	2.59	0.28
CLF-17-D(3-6)	71.68	0.72	12.52	4.16	0.104	1.50	4.61	1.80	2.63	0.28
CLF-17-D(6+)	72.09	0.76	12.59	4.41	0.105	1.50	3.68	1.82	2.78	0.28
CLF-17-G(0-3)	72.73	0.73	12.47	3.99	0.089	1.50	3.68	1.94	2.61	0.26
CLF-17-G(3-6)	73.10	0.72	12.15	3.95	0.091	1.50	3.76	1.91	2.59	0.23
CLF-17-G(6+)	72.50	0.78	12.25	4.29	0.111	1.50	3.67	1.87	2.66	0.37

D= desert pavement
G= grasses and cacti
J= juniper tree
*= Total Fe as Fe_2O_3

Appendix 9.3.11. Trace element chemistry of the loess deposits from the Carrizozo lava flow, New Mexico. Samples were analyzed using x-ray fluorescence spectrometry. Normalized on a $CaCO_3$-free and loss-free basis and to 100 %.

Sample #	S	Cr	V	Ni	Cu	Zn	Ga	As	Rb	Sr	Nb	Y	Zr	Mo	Ba	Pb	Th	U
	ppm	ppm	ppm	ppm	ppm	ppm	ppm	ppm	ppm	ppm	ppm	ppm	ppm	ppm	ppm	ppm	ppm	ppm
CLF-8-D(0-3)	n.r	68	64	21	n.r	86	14	4	121	250	n.r.	28	376	3	508	22	11	3
CLF-8-D(3-6)	n.r	55	64	19	n.r	86	15	4	117	264	n.r.	32	364	3	505	23	16	3
CLF-8-D(6-10)	n.r	56	64	21	n.r	87	16	5	129	273	n.r.	29	360	2	503	20	12	3
CLF-8-G(0-5)	n.r	53	59	17	n.r	84	14	3	108	194	n.r.	26	385	3	502	22	11	2
CLF-8-G(5-10)	n.r	70	61	19	n.r	83	15	5	111	217	n.r.	27	373	3	521	21	11	3
CLF-8-J(0-2)	n.r	57	65	23	n.r	116	16	9	121	336	n.r.	30	349	4	564	41	15	2
CLF-8-J(2-5)	n.r	53	66	21	n.r	103	15	7	114	322	n.r.	29	403	3	539	35	12	3
CLF-7-D(0-5)	n.r	59	63	19	n.r	94	15	4	125	229	n.r.	30	347	2	542	21	13	3
CLF-7-D(5-10)	n.r	60	69	20	n.r	98	15	4	131	231	n.r.	30	326	2	547	21	13	2
CLF-7-D(10-17)	n.r	60	76	21	n.r	100	16	4	137	249	n.r.	31	326	2	542	20	14	2
CLF-7-G(0-5)	n.r	59	65	19	n.r	102	14	3	115	274	n.r.	27	366	2	549	25	12	2
CLF-7-G(5-10)	n.r	79	63	21	n.r	94	15	3	119	238	n.r.	26	337	2	541	24	12	3
CLF-7-G(10-15)	n.r	59	64	18	n.r	93	15	3	126	229	n.r.	27	342	2	540	21	12	4
CLF-7-G(15-23)	n.r	59	70	20	n.r	91	15	3	130	224	n.r.	29	348	2	520	19	13	3
CLF-7-J(0-5)	n.r	55	63	20	n.r	114	16	6	116	483	n.r.	27	323	2	523	38	15	4
CLF-7-J(5-10)	n.r	61	70	22	n.r	106	16	6	125	406	n.r.	28	341	2	549	37	14	2
CLF-7-J(10-15)	n.r	54	67	19	n.r	84	15	7	121	292	n.r.	26	394	2	516	22	15	4
CLF-7-J(15-23)	n.r	69	63	20	n.r	77	15	5	121	268	n.r.	27	377	3	508	19	13	2
CLF-6-D(0-3)	n.r	54	60	18	n.r	81	14	5	122	331	n.r.	30	393	2	562	23	10	2
CLF-6-D(3-5)	n.r	56	67	18	n.r	79	15	4	130	257	n.r.	28	381	2	549	22	13	3
CLF-6-G(0-4)	n.r	43	54	16	n.r	74	12	3	110	232	n.r.	27	384	3	530	23	10	3
CLF-6-G(4-10)	n.r	48	58	15	n.r	73	14	3	118	233	n.r.	26	377	3	517	21	12	2
CLF-6-G(10-14)	n.r	58	65	19	n.r	83	15	5	134	232	n.r.	31	345	3	537	19	12	4
CLF-6-J(0-5)	n.r	65	69	20	n.r	102	16	8	133	295	n.r.	28	401	2	539	28	15	3
CLF-6-J(5-15)	n.r	59	74	21	n.r	94	15	6	134	290	n.r.	28	366	3	525	25	14	3
CLF-5-D(0-5)	n.r	54	63	17	n.r	88	14	3	141	232	n.r.	28	378	2	534	21	13	2
CLF-5-D(5-10)	n.r	60	66	19	n.r	95	15	3	153	237	n.r.	29	346	3	556	22	13	3
CLF-5-D(10-15)	n.r	64	70	21	n.r	100	15	6	160	232	n.r.	31	344	3	531	19	11	3
CLF-5-G(0-5)	n.r	53	53	16	n.r	96	14	3	127	235	n.r.	25	357	3	538	24	11	3
CLF-5-G(5-10)	n.r	61	57	19	n.r	108	14	4	153	235	n.r.	28	335	2	528	22	13	3
CLF-5-G(10-15)	n.r	54	59	18	n.r	107	14	4	145	243	n.r.	30	341	3	529	21	10	2
CLF-5-J(0-5)	n.r	51	66	18	n.r	106	16	6	144	379	n.r.	25	348	2	523	36	15	4
CLF-5-J(5-10)	n.r	54	63	19	n.r	103	14	5	145	314	n.r.	27	390	3	506	26	13	3
CLF-11-D	294	53	85	19	31	92	14	8	126	266	16	30	406	n.r.	627	28	12	3
CLF-11-G(0-5)	237	57	84	20	35	99	16	5	144	281	15	30	375	n.r.	624	32	13	4
CLF-11-G(5-10)	172	54	84	20	32	86	15	6	138	261	15	31	380	n.r.	622	27	12	4
CLF-11-J(5-10)	176	57	88	22	35	76	15	7	154	362	13	29	355	n.r.	564	23	11	4
CLF-10-D	296	67	83	19	38	95	13	6	122	289	16	28	430	n.r.	617	37	12	3
CLF-10-G(0-5)	271	50	80	18	31	89	15	5	140	261	14	28	350	n.r.	607	28	12	2
CLF-10-G(5-10)	247	53	82	18	29	75	15	5	146	251	14	29	359	n.r.	607	21	11	4
CLF-10-J(0-5)	265	53	84	22	51	131	16	7	151	387	12	31	366	n.r.	641	37	13	4
CLF-10-J(5-10)	266	57	85	21	41	110	16	7	147	345	13	28	346	n.r.	628	31	13	3
CLF-1-D	n.r.	57	68	18	32	88	14	6	135	252	n.r.	29	394	2	589	30	9	4
CLF-1-J	n.r.	57	72	20	34	92	16	7	150	266	n.r.	31	395	2	578	23	9	4
CLF-2-D	n.r.	60	74	19	31	89	16	5	110	263	n.r.	30	409	2	619	28	11	3
CLF-2-G	n.r.	53	71	19	34	91	15	7	131	269	n.r.	32	380	2	597	24	11	4
CLF-2-J	n.r.	54	68	18	34	108	16	7	131	385	n.r.	27	367	2	603	36	12	3
CLF-3-D	n.r.	49	75	17	32	91	15	6	111	271	n.r.	30	411	2	610	30	11	3
CLF-3-G	n.r.	43	78	15	27	71	12	7	102	228	n.r.	33	387	2	588	23	8	4
CLF-3-J	n.r.	47	76	21	48	116	16	6	178	355	n.r.	31	384	2	597	30	10	4
CLF-4-D	n.r.	53	84	19	37	94	16	6	109	311	n.r.	32	410	2	667	29	12	4
CLF-4-G	n.r.	33	64	14	26	77	14	4	99	290	n.r.	27	377	2	637	26	11	3
CLF-4-J	n.r.	49	70	18	36	91	15	5	109	306	n.r.	29	351	2	653	34	11	4

Appendix 9.3.11. (continued) Trace element chemistry

Sample #	S ppm	Cr ppm	V ppm	Ni ppm	Cu ppm	Zn ppm	Ga ppm	As ppm	Rb ppm	Sr ppm	Nb ppm	Y ppm	Zr ppm	Mo ppm	Ba ppm	Pb ppm	Th ppm	U ppm
CLF-1-D(0-2)	n.r.	56	76	16	n.r.	86	14	4	110	227	n.r.	29	408	3	539	24	12	3
CLF-1-G(5-10)	n.r.	55	63	18	n.r.	92	14	4	124	229	n.r.	27	323	3	510	25	11	3
CLF-1-G(10-15)	n.r.	53	63	18	n.r.	89	14	4	125	232	n.r.	28	340	3	519	21	10	2
CLF-1-J(0-3)	n.r.	60	72	19	n.r.	105	16	7	126	381	n.r.	29	365	4	572	34	13	3
CLF-1-J(3-5)	n.r.	58	72	19	n.r.	95	15	7	128	345	n.r.	28	362	3	552	29	13	2
CLF-12-D	239	57	85	20	32	89	14	6	117	257	13	29	357	n.r.	583	30	11	3
CLF-12-G(0-5)	292	56	80	23	35	94	14	5	129	239	13	29	313	n.r.	595	28	11	3
CLF-12-G(5-10)	251	60	80	24	34	89	15	5	134	236	13	30	330	n.r.	593	25	11	4
CLF-12-G(10+)	160	63	79	24	33	77	15	5	137	223	12	28	330	n.r.	578	20	11	4
CLF-13-D(0-5)	431	56	77	22	34	89	13	4	117	287	13	28	357	n.r.	580	27	12	3
CLF-13-D(5-10)	393	62	80	25	32	92	15	6	128	282	13	29	349	n.r.	575	22	12	3
CLF-13-D(10+)	394	67	87	26	29	88	16	5	134	275	13	29	349	n.r.	560	19	11	4
CLF-13-G(0-5)	346	59	78	23	34	96	15	5	134	268	13	29	328	n.r.	584	29	12	3
CLF-13-G(5-10)	285	59	78	24	32	89	15	5	143	257	13	28	334	n.r.	573	24	13	4
CLF-13-G(10+)	271	61	82	26	31	82	15	4	154	254	13	29	345	n.r.	560	22	12	4
CLF-18-D(0-2)	282	66	77	22	28	75	13	4	104	269	14	27	430	n.r.	579	24	12	3
CLF-18-D(2-4)	242	71	83	23	28	81	14	4	119	261	14	28	412	n.r.	589	20	12	3
CLF-18-D(4+)	262	72	89	26	34	86	15	4	133	249	15	30	410	n.r.	552	19	13	4
CLF-18-G(0-2)	232	53	73	23	38	100	14	5	131	294	12	27	338	n.r.	597	35	11	4
CLF-18-G(2-4)	211	50	77	22	34	91	14	4	134	284	12	26	313	n.r.	566	29	11	2
CLF-18-G(4+)	261	53	76	23	34	84	14	4	145	279	12	27	345	n.r.	565	23	12	3
CLF-19-D(0-2)	315	60	76	21	31	86	14	4	123	291	15	30	381	n.r.	618	25	14	5
CLF-19-D(2-4)	350	57	87	25	39	110	16	4	156	301	15	31	325	n.r.	609	23	14	4
CLF-19-D(4+)	407	60	86	27	41	113	17	6	160	300	14	31	302	n.r.	596	22	15	3
CLF-19-G(0-3)	220	51	77	21	40	105	15	5	121	306	14	28	324	n.r.	650	37	13	4
CLF-19-G(3-6)	224	54	75	20	33	96	15	6	127	283	14	28	327	n.r.	637	31	12	4
CLF-19-G(6+)	238	56	82	24	33	89	16	5	139	267	15	30	317	n.r.	641	24	13	4
CLF-14-D(0-3)	233	69	84	25	34	86	13	5	140	265	14	31	447	n.r.	555	24	14	4
CLF-14-D(3-6)	366	70	83	27	33	86	15	5	152	252	13	31	426	n.r.	546	22	12	4
CLF-14-D(6+)	561	67	88	27	37	92	15	5	166	279	12	32	429	n.r.	549	20	13	5
CLF-14-G(0-5)	94	60	79	31	55	133	16	7	135	372	11	31	279	n.r.	576	58	13	4
CLF-14-G(5-10)	472	63	80	32	57	133	16	8	135	537	11	30	280	n.r.	592	67	14	4
CLF-14-G(10+)	255	70	86	34	61	135	16	8	131	690	11	31	286	n.r.	624	81	13	4
CLF-15-D(0-5)	428	64	74	22	33	78	13	5	114	293	13	32	471	n.r.	552	25	12	4
CLF-15-D(5-10)	489	60	84	28	40	99	14	5	149	324	13	32	408	n.r.	546	21	13	5
CLF-15-D(10+)	722	67	88	30	48	107	16	4	174	364	12	33	412	n.r.	584	21	15	4
CLF-15-G(0-3)	359	60	76	23	34	85	14	4	116	283	11	28	359	n.r.	568	30	12	4
CLF-15-G(3-6)	448	60	71	22	33	78	14	4	120	269	11	30	353	n.r.	578	27	11	3
CLF-15-G(6+)	374	74	75	26	36	77	14	4	134	256	13	30	344	n.r.	562	22	12	4
CLF-16-D(0-2)	610	54	71	19	29	73	13	4	103	337	12	26	382	n.r.	556	21	11	4
CLF-16-D(2-4)	517	51	77	24	32	86	14	5	125	351	12	28	352	n.r.	539	19	13	4
CLF-16-D(4+)	703	57	83	26	33	85	15	5	133	407	12	29	388	n.r.	538	17	13	4
CLF-16-G(0-5)	468	36	62	17	28	72	11	5	94	339	9	22	305	n.r.	548	26	11	3
CLF-16-G(5-10)	541	43	63	18	29	68	12	4	94	338	10	23	299	n.r.	555	24	10	3
CLF-16-G(10-20	286	41	58	16	25	61	11	4	91	330	10	22	279	n.r.	558	21	9	4
CLF-16-G(20+)	251	44	66	20	28	77	13	5	104	348	10	24	298	n.r.	544	23	11	2
CLF-17-D(0-3)	891	49	69	20	37	85	14	5	115	412	11	27	375	n.r.	635	28	13	4
CLF-17-D(3-6)	874	56	70	23	40	92	14	6	131	422	12	28	326	n.r.	591	24	12	4
CLF-17-D(6+)	7033	63	75	24	49	91	15	6	146	583	10	30	337	n.r.	616	21	13	5
CLF-17-G(0-3)	420	45	74	18	38	90	14	6	107	319	12	28	359	n.r.	581	36	12	3
CLF-17-G(3-6)	364	48	73	19	35	84	13	5	113	311	11	28	347	n.r.	580	30	12	4
CLF-17-G(6+)	1426	93	69	30	70	91	14	6	133	758	7	28	351	n.r.	627	22	16	4

D= desert pavement
G= grasses and cacti
J= juniper tree
n.r.=none recorded

Appendix 9.3.12. Trace and rare earth element chemistry of the loess deposits on the Carrizozo lava flow, New Mexico.
Samples were analyzed using instrumental neutron activation analysis.

Sample #	Na_2O	Sc	Cr	FeO	Co	As	Br	Sb	Cs	Ba	La	Ce	Nd	Sm	Eu	Tb	Yb	Lu	Hf	Ta	W	Th	U
	ppm	ppm	ppm	ppm	ppm	ppm	ppm	ppm	ppm	ppm	ppm	ppm	ppm	ppm	ppm	ppm	ppm	ppm	ppm	ppm	ppm	ppm	ppm
CLF-1-D	1.85	7.99	46	3.66	9.31	5.91	2.0	0.80	4.57	571	33.40	66.0	24.3	5.39	1.13	0.72	2.97	0.44	11.86	1.25	1.40	10.20	3.01
CLF-1-G	1.48	7.65	40	3.38	8.87	4.92	4.5	0.60	4.48	520	29.12	58.7	24.1	4.76	1.06	0.66	2.42	0.38	9.39	1.04	1.39	8.32	2.32
CLF-1-J	1.64	8.43	56	3.91	11.75	5.15	4.2	0.71	4.83	574	30.20	60.2	23.4	5.13	1.11	0.71	2.80	0.43	10.81	1.13	0.74	8.71	2.74
CLF-2-D	1.80	9.49	61	4.37	12.71	6.06	3.8	0.89	4.22	620	35.40	72.9	27.8	5.95	1.29	0.79	3.09	0.49	11.21	1.32	1.23	10.52	2.86
CLF-2-G	1.74	8.96	53	3.96	10.94	5.93	2.9	0.76	4.55	584	32.30	65.1	24.7	5.54	1.21	0.75	2.94	0.43	10.20	1.23	1.21	9.61	2.97
CLF-2-J	1.25	6.78	32	2.97	7.94	5.72	7.6	0.75	3.80	490	28.77	58.9	20.7	4.60	0.94	0.61	2.09	0.34	7.98	0.94	1.48	8.37	1.96
CLF-3-D	1.76	8.93	50	4.08	10.57	6.22	2.9	0.88	4.51	624	36.50	72.2	27.7	6.01	1.26	0.80	3.19	0.49	12.06	1.32	2.34	10.73	3.15
CLF-3-G	1.78	8.52	47	3.88	10.41	5.90	2.6	0.81	4.48	592	33.70	68.5	26.8	5.56	1.24	0.77	2.98	0.47	11.33	1.30	1.12	9.95	2.83
CLF-3-J	1.52	7.94	42	3.54	9.52	5.28	5.6	0.73	4.43	457	31.30	61.9	25.1	5.22	1.12	0.69	2.71	0.41	9.34	1.10	1.56	9.24	2.78
CLF-4-D	1.81	8.93	44	4.13	10.52	6.77	2.8	0.89	4.82	629	39.40	77.1	27.3	6.41	1.36	0.85	3.00	0.47	10.74	1.50	1.40	11.19	3.27
CLF-4-G#1	2.00	7.40	37	3.61	9.06	4.90	1.6	0.69	3.74	691	34.60	67.2	28.0	5.59	1.23	0.69	2.73	0.40	11.25	1.40	1.32	10.74	2.84
CLF-4-G#2	1.95	7.42	42	3.59	9.09	4.00	1.7	0.73	3.84	620	33.30	65.4	28.0	5.29	1.18	0.69	2.77	0.41	9.91	1.34	1.00	9.75	2.73
CLF-4-G#3	1.97	7.43	40	3.57	9.02	4.50	1.9	0.69	3.83	688	34.10	67.3	27.1	5.38	1.17	0.69	2.86	0.44	9.84	1.31	1.30	9.50	2.54
CLF-4-J	1.91	8.40	40	3.92	10.55	5.60	4.0	0.77	4.45	634	36.80	71.8	24.8	5.77	1.25	0.81	2.92	0.46	10.65	1.40	0.99	10.57	2.88
CLF-5-D	1.60	9.51	56	4.05	12.22	5.30	2.9	0.73	5.64	531	36.30	72.4	33.4	6.24	1.34	0.83	3.06	0.46	9.38	1.26	1.01	10.58	3.12
CLF-5-G	1.54	8.87	48	3.78	10.68	4.92	2.5	0.75	5.39	596	35.10	72.5	31.1	5.87	1.19	0.80	2.94	0.44	8.73	1.20	1.02	10.09	2.47
CLF-5-J	1.34	7.33	45	3.20	8.94	5.69	8.2	0.79	3.99	408	25.57	52.1	18.9	4.35	0.95	0.58	2.33	0.35	8.28	0.94	0.96	7.85	2.11
CLF-6-D	1.58	8.43	52	3.64	11.33	5.30	2.3	0.80	5.04	549	31.10	65.5	26.0	5.43	1.17	0.78	2.99	0.43	10.34	1.19	1.30	9.31	2.75
CLF-6-G	1.66	8.23	47	3.58	10.52	5.19	2.3	0.73	4.62	586	34.50	70.3	28.0	5.78	1.21	0.76	2.98	0.45	10.34	1.20	0.78	9.68	3.09
CLF-6-J	1.51	8.94	72	4.15	13.42	7.84	7.1	0.73	4.25	478	32.00	66.1	25.4	5.51	1.20	0.75	2.78	0.42	9.17	1.14	0.96	8.84	2.39
CLF-7-D	1.53	10.17	59	4.16	12.73	5.30	3.9	0.69	5.33	573	33.10	67.4	27.4	5.95	1.27	0.84	3.43	0.53	8.60	1.12	1.00	9.76	2.81
CLF-7-G	1.59	9.03	50	3.79	11.23	4.58	4.8	0.50	4.50	510	30.30	63.6	20.7	5.24	1.12	0.74	2.73	0.42	9.73	1.09	0.88	8.83	2.81
CLF-7-J	1.43	8.80	53	3.71	11.37	5.57	7.4	0.66	3.87	477	26.32	55.7	22.2	4.74	1.02	0.65	2.50	0.38	9.55	0.99	0.92	8.12	2.33
CLF-7-J(5-10)	1.14	7.13	39	3.00	8.42	6.11	12.9	0.74	3.80	471	24.27	49.4	20.1	4.22	0.87	0.57	1.98	0.35	7.05	0.88	0.66	7.00	1.77
CLF-7-J(10-15)	1.44	8.44	50	3.61	11.02	6.56	7.1	0.74	3.97	453	29.15	59.2	23.6	4.93	1.04	0.66	2.45	0.37	10.07	0.97	1.07	8.46	2.26
CLF-7-J(15-20)	1.60	9.21	58	4.09	12.86	5.81	6.6	0.65	3.78	507	28.45	59.1	24.0	5.11	1.11	0.69	2.64	0.38	9.14	1.06	0.68	8.70	2.17
CLF-8-D	1.41	8.99	51	3.73	10.65	4.88	6.7	0.72	5.10	482	29.81	61.7	23.3	5.35	1.16	0.77	2.97	0.46	10.19	1.07	0.80	9.01	2.83
CLF-8-G	1.55	8.54	53	3.70	10.23	5.00	2.2	0.75	4.46	563	29.85	62.0	25.0	5.40	1.12	0.74	2.95	0.46	10.55	1.10	1.02	9.27	2.34
CLF-8-J	1.12	7.39	44	3.15	9.08	7.80	18.4	0.86	4.25	472	27.26	55.8	22.1	4.73	0.97	0.66	2.26	0.36	7.40	0.82	1.22	8.59	1.99

D= desert pavement
G= grasses and cacti
J= juniper tree

Appendix 9.3.13. Reference values and averages of total element chemistry of the loess deposits on the Carrizozo lava flow, New Mexico. North American Shale Composite values were obtained from Gromet et al. (1984). Local crustal composition values were obtained from Watrus (1998). Carrizozo basalt composition was obtained from Renault (1970), Potrillo volcanic field soil composition values were obtained from Eppes (1996) $=CaCO3-free loess samples

Element	Average loess composition Carrizozo$	NASC	Local crustal composition	Carrizozo Basalt	Average soil composition Potrillo (AD5)$	Average soil composition Potrillo (AF2)$	Average soil composition Potrillo (LBM4)$
SiO_2	73.69	64.8	64.5	51.6	74.4	73.45	80.28
TiO_2	0.8	0.78	1.005	1.714	0.73	0.7	0.5
Al_2O_3	12.81	16.9	11.04	17.205	13.45	13.75	9.58
MnO	0.1	0.06	0.1	0.152	0.075	0.088	0.051
CaO	1.46	3.56	4.08	8.257	1.05	1.05	1.05
MgO	1.99	2.85	1.55	6.295	1.03	1.42	1.33
Na_2O	1.82	1.15	1.72	3.712	1.85	1.8	1.3
K_20	2.71	3.99	2.4	1.277	3.22	3.28	2.65
P_2O_5	0.23	0.11	0.13	none available	0.17	0.16	0.12

Appendix 9.3.14. Reference values and averages of the trace and rare earth element chemistry of the loess deposits on the Carrizozo lava flow,New Mexico. North American Shale Composite values were obtained from Gromet et al. (1984). Local crustal composition values were obtained from Watrus (1998).

Element	Average loess composition	NASC	Local crust composition
Cr	56	124.50	97
Ni	21	58.00	26
As	5	28.40	8
Rb	127	125.00	100
Sr	298	142.00	312
Zr	355	200.00	619
Ba	558	636.00	756
Th	9.4	12.30	11
U	2.6	2.66	3
La	31.8	31.1	
Ce	64.3	66.7	
Nd	25.2	27.4	
Sm	5.4	5.59	
Eu	1.2	1.18	
Tb	0.7	0.85	
Yb	2.8	3.06	
Lu	0.4	0.456	
Hf	9.8	6.3	
Ta	1.2	1.12	